

**Cortical Neuromodulatory Mechanisms of Adaptations to Sound Contrast and their
Effects on Contrast-dependent Changes in Pupil Size**

by

Patrick Andrew Cody

B.A., St. Mary's College of Maryland, 2011

Submitted to the Graduate Faculty of the
Swanson School of Engineering in partial fulfillment
of the requirements for the degree of
Doctor of Philosophy

University of Pittsburgh

2022

UNIVERSITY OF PITTSBURGH

SWANSON SCHOOL OF ENGINEERING

This dissertation was presented

by

Patrick Andrew Cody

It was defended on

December 10, 2021

and approved by

Takashi Kozai, Ph.D., Associate Professor, Department of Bioengineering

Sandra Kuhlman, Ph.D., Associate Professor, Department of Biological Science,
Carnegie Mellon University

Srivatsun Sadagopan, Ph.D., Assistant Professor, Department of Neurobiology

Matthew Smith, Ph.D., Associate Professor, Biomedical Engineering and Neuroscience,
Carnegie Mellon University

Dissertation Director: Thanos Tzounopoulos, Ph.D.,
Endowed Professor and Vice Chair of Research, Department of Otolaryngology

Copyright © by Patrick Andrew Cody

2022

Cortical Neuromodulatory Mechanisms of Adaptations to Sound Contrast and their Effects on Contrast-dependent Changes in Pupil Size

Patrick Andrew Cody, Ph.D.

University of Pittsburgh, 2022

How does the brain efficiently process such a wide variety of sound environments? Sound environments can be described probabilistically by a change in sound levels across frequency (spectro-) and time (-temporal). To efficiently process sensory signals despite large changes in background noise the brain adapts neural response properties to spectrotemporal sound level statistics. With an increased range of sound levels, spectrotemporal contrast, the slope of neural input-output functions decreases. This gain reduction, termed contrast gain control (CGC), maintains dynamic range enabling cells to discriminate a wider input range. CGC is conserved among species, evident in the midbrain and throughout cortex. CGC accounts for changes in perceptual judgements in humans and mice, however, the underlying cortical neuromodulatory mechanisms remain poorly understood. Furthermore, neural sensory response properties change with internal state factors, such as wakefulness, that can be indexed by pupil-size. However, it is unknown how pupil-indexed internal state changes affect adaptation to sound contrast and whether these cortical adaptations are needed for sound evoked changes in pupil size. To address these questions, we combined pupillometry with 2-photon calcium imaging of layer 2/3 neurons of mouse primary auditory cortex (A1), along with pharmacological and genetic knockout approaches. Our work reveals that contrast-dependent neuromodulatory effects of synaptic zinc are necessary for CGC in A1 and that there are optimal pupil-indexed states for CGC. Further, we report contrast-dependent changes in pupil size that, like CGC, rely upon neuromodulatory zinc

signaling in auditory cortex. Thus, we reveal cortical neuromodulatory sensory processing that influences pupil size. In addition to its reported use as a marker for Alzheimer's disease and schizophrenia, pupil size may therefore serve as a non-invasive clinical marker for disrupted neuromodulatory cortical signaling during sensory adaptation. Understanding context specific neuromodulatory mechanisms of perceptual gain adaptations such as CGC provides insight into other fundamental aspects of perception that rely on gain modulation such as attention and compensation for peripheral hearing loss.

Table of Contents

Preface.....	xii
1.0 Introduction.....	1
1.1 Adaptations to Increasing Sound Level Variability: The Dynamic Range Problem	1
1.2 Contrast Gain Control	2
1.3 In Search of Circuit and Synaptic Mechanisms of Contrast Gain Control	4
1.4 Synaptic Zinc as a Candidate Neuromodulator of Contrast Dependent Gain Change in Auditory Cortex	5
1.5 Zinc Background	6
1.6 Pupil-indexed Neural States and Sensory Processing	7
1.7 Pupil Size and ‘Arousal’	8
1.8 Pupil and Neuromodulators	10
1.9 Sound Evoked Pupil Responses.....	11
1.10 Dissertation Aims.....	12
1.11 Dissertation Overview	13
2.0 Chapter 1: Neuromodulatory Mechanisms Underlying Contrast Gain Control in Mouse Auditory Cortex	16
2.1 Overview.....	16
2.2 Introduction	16
2.3 Results.....	19
2.3.1 2-Photon Calcium Imaging (2PCI) Assay for Adaptation to Sound Level Contrast in A1 L2/3 Principal Neurons	19

2.3.2 Contrast Gain Control in Primary Auditory Cortex Depends Upon Neuromodulatory Zinc Signaling	28
2.3.3 Zinc Signaling Does Not Have Any Contrast-dependent Effects on Either PV or SOM Cells	32
2.3.4 Zinc Signaling Suppresses Principal Neuron Responses Preceded by High, But Not Low, Sound Level Contrast	35
2.4 Discussion	38
2.4.1 2-Photon Calcium Imaging Assay for Contrast Adaptation: Strengths and Limitations	38
2.4.2 Heterogeneity in Scaling: Inclusion Criteria, Recording Depth, and Contrast Tuning	39
2.4.3 DRC Stimulus: Robustness and Comparison With Prior Studies	41
2.4.4 PV Cells and A1 Sound Contrast Adaptation	41
2.4.5 Different Cellular and Neuromodulatory Mechanisms Underlie Cortical Contrast Gain Control and Contrast Invariance.....	43
2.4.6 Zinc Signaling and Cell STRFs.....	43
2.4.7 Stimulus- and Context-dependent Effects of Zinc Signaling in Cortical Sound Processing	44
2.5 Materials and Methods	48
2.5.1 Animals	48
2.5.2 Stereotaxic AAV Injections	49
2.5.3 Acute Surgery Preparation For In Vivo Imaging	50
2.5.4 Sound Stimulus Delivery	51

2.5.5 Widefield Epifluorescence Imaging and Analysis for A1 Localization.....	51
2.5.6 DRC Stimuli.....	52
2.5.7 2-photon Calcium Imaging (2PCI)	53
2.5.8 FRA Mapping.....	54
2.5.9 Contrast Adaptation Assay	55
2.5.10 2-Photon Calcium Imaging (2PCI): Processing and Analysis	56
2.5.11 Statistical Analysis	57
3.0 Chapter 2: Pupil-indexed State Effects on Cortical Adaptation to Sound Contrast and Cortical Neuromodulatory Effects on Sound Contrast-dependent Changes in Pupil Size.....	58
3.1 Overview.....	58
3.2 Introduction	59
3.3 Results.....	61
3.3.1 Contrast Gain Control is Greatest at Intermediate Pupil Diameter	61
3.3.2 Contrast Gain Control Does Not Depend on Stimulus-dependent Pupil Responses to Contrast Sound.....	65
3.3.3 Synaptic Zinc Signaling Contributes to Increased Pupil Responses in High Contrast Sound.....	68
3.4 Discussion	76
3.4.1 Exploring the Contrast-dependent Effects of Pupil-indexed Cortical State on A1 Principal Neuron Response Properties	76
3.4.2 Exploring the Pupil-indexed Cortical State Factors That Impact Contrast Gain Control.....	77

3.4.3 Neural Activity Indexed by Pre-stimulus Pupil Size Versus That Associated With Sound Evoked Pupil Responses.....	78
3.4.4 The Role of Neuromodulatory Zinc Signaling in Contrast Adaptation.....	78
3.5 Materials and Methods	80
3.5.1 Animals	80
3.5.2 Stereotaxic AAV Injection.....	80
3.5.3 Acute Surgery Preparation For In Vivo Imaging	81
3.5.4 Sound Stimulus Delivery	81
3.5.5 Widefield Epifluorescence Imaging and Analysis for A1 Localization.....	81
3.5.6 DRC Stimuli.....	81
3.5.7 2-Photon Calcium Imaging (2PCI).....	82
3.5.8 Pupillometry: Acquisition	82
3.5.9 FRA Mapping.....	83
3.5.10 Contrast Gain Control Assay.....	83
3.5.11 2PCI Processing and Analysis.....	84
3.5.12 Pupillometry: Analysis	85
3.5.13 Statistics	87
4.0 Conclusion	88
4.1 Summary of Results	88
4.2 Future Directions.....	90
Bibliography	94

List of Figures

Figure 2-1: 2-photon calcium imaging (2PCI) assay for A1 adaptation to spectrotemporal sound level contrast.....	21
Figure 2-2: Frequency dependence of 2PCI assay for contrast gain control in A1 principal cells	27
Figure 2-3: Contrast gain control in A1 depends upon cortical ZnT3-dependent synaptic zinc signaling	30
Figure 2-4: Zinc signaling does not have any contrast-dependent effects on either A1 PV or SOM cells.....	34
Figure 2-5: Zinc signaling suppresses A1 pure tone responses preceded by high- but not low sound level contrast.....	37
Figure 3-1: Contrast dependent pupil-indexed cortical state effects on A1 principal cell response properties.....	63
Figure 3-2: High sound contrast evokes larger pupil responses that return to baseline after sound offset.....	66
Figure 3-3: Contrast-dependent changes in PD do not contribute to contrast gain control	67
Figure 3-4: Cortical zinc signaling contributes to an increase in pupil response magnitude to high contrast sound	70
Figure 3-5: Pre-stimulus pupil diameter increases throughout experiment duration, but contrast effect on pupil responses persists upon ACSF control injection.....	72
Figure 3-6: Synaptic zinc signaling enables larger pupil responses to high contrast sound	75

Figure 3-7: Sound contrast evoked pupil response magnitude correlates with pre-stimulus pupil diameter 86

Preface

I would first like to thank Dr. Xinyan Tracy Cui for her mentorship and guidance through the beginning of my graduate study. Her support and understanding had a major role in making my pursuit of this dissertation possible. Our work culminated into a publication in the journal *Biomaterials* regarding the performance tracking of Utah microelectrode neural implants with a biomimetic coating over a chronic period (Cody et al., 2018). That work was not included in this dissertation as it tackles very different questions. During my time in Dr. Cui's lab I had the pleasure of learning from memorable and charismatic graduate students including: Dr. James Eles, Dr. Noah Snyder, and Dr. Kasey Katt. I also appreciate my training and collaboration with Dr. I. Mitch Taylor. Last, but certainly not least, I'd like to thank Dr. Takashi D.Y. Kozai for his inspiring and invested mentorship. His support was crucial to the continuation and progression of my graduate study.

I thank my mentor, Dr. Thanos Tzounopoulos, for his commitment to my training, career, and scientific progress. His trust in my potential and his accommodation of my unique transition of study made this work possible. Our discussions kept me inspired and motivated to push my limits and pursue both technically and conceptually challenging questions. I thank the current and past Tzounopoulos lab members for their thoughtful discussion and support, both scientific and otherwise, that made enduring graduate study much more buoyant. I specifically thank Dr. Manoj Kumar for training me on in vivo 2-photon imaging and Stelios Kouvaros for surgery training, discussions, and genotyping.

I would like to thank my thesis committee members, Dr. Takashi D.Y. Kozai, Dr. Sandra Kuhlman, Dr. Srivatsun Sadagopan, and Dr. Matthew Smith for their guidance and feedback

through the course of my thesis. I specifically thank Dr. Srivatsun Sadagopan for sharing advice and code that made much of the pupillometry analyses in Chapter 2 possible.

I thank Dr. Ross Williamson for thoroughly helpful discussions, feedback, and critical reading of Chapter 1. I also thank faculty and trainees of the joint University of Pittsburgh and Carnegie Mellon University interest group in population imaging (Pop Coding PA) for their feedback as well as technical and conceptual advice. I also would like to thank Dr. Karl Kandler and Dr. Bill Yates as well as my peer trainees of the Auditory-Vestibular T32 training grant (T32-DC011499) for their scientific guidance and training.

I would like to thank my friends. They kept me sane during my graduate studies and made this time of my life meaningful. Finally, I'd like to thank my family for their motivation, support and understanding.

Funding: This work was supported by NIH grants T32-DC011499 (Drs. Karl Kandler and Bill Yates) and R01-DC007905 (to Thanos Tzounopoulos), as well as NSF grant NSF-IOS-1655480 (Thanos Tzounopoulos).

1.0 Introduction

1.1 Adaptations to Increasing Sound Level Variability: The Dynamic Range Problem

How does the brain encode the expansive range of sound environments that we experience every day? While the upper range of human hearing is 12 orders of magnitude higher than just audible sounds, certain environments may on average require only a certain portion of this sensitivity range and other environments may need another portion. Some environments may contain only a narrow range of sound levels, while others might demand a wider portion of this hearing range. This challenge is only partially addressed by a division of labor strategy at the auditory nerve (AN), the first step in the ascending auditory pathway from the peripheral hearing organ, the cochlea, to the brainstem, the cochlear nucleus (Dean et al., 2005; Robinson and McAlpine, 2009; Wen et al., 2009). AN fibers exhibit a sigmoid shaped rate-level function: the firing-rate of the AN fiber begins to increase at some sound level threshold, it then increases sharply with a large slope along a middle range of sound levels where it is most sensitive to sound level differences, then tapers off and saturates at an upper sound level limit (Sachs and Abbas, 1974; Watanabe et al., 1965). As the firing-rate of this AN fiber does not change below its sound level threshold nor above the sound level at which its firing-rate saturates, other AN fibers with different sound level thresholds have shifted rate-level functions and thus accommodate a different sound level range (Sachs and Abbas, 1974). However, this division of labor strategy only covers a range of about 35 dB (Dean et al., 2005; Evans and Palmer, 1980), which is insufficient for the demands of the natural world.

How then does the brain tackle this dynamic range problem, and how does it do it efficiently given that sound environments tend to be described by some probability of sound levels, sound level statistics? Beginning at the AN, cell rate-level functions shift depending on the most probable sound levels. As average sound levels increase over time, AN rate-level sigmoid functions shift rightward, resulting in higher thresholds and higher firing-rate saturation limits (Wen et al., 2009). This dynamic range adaptation continues up the auditory pathway to the inferior colliculus (IC) in the midbrain where it strengthens and enables the encoding of higher average sound levels (Wen et al., 2009). Cells in IC are also able to adapt to an increase in stimulus variance (Dean et al., 2005). When the range of sound levels increases over time, cell rate-level, or input-output, functions decrease in slope, gain, to accommodate sound levels that would have otherwise been below threshold or above saturation. Such compensation for sound level variance also increases along the auditory pathway, such that neurons in auditory cortex (ACtx) are able to change the gain of their input-output functions to a greater degree and thus accommodate greater changes in sound level variance (Rabinowitz et al., 2013).

1.2 Contrast Gain Control

Sound environments are not, however, defined solely by sound level, but also by their sound frequency content. Sound level can thus vary across time (temporally), as previously described with shifts in sound level variance over time, as well as across frequency (spectrally), sound level fluctuates across the frequency range of the environment. An increase in sound level variance across frequency and time is called an increase in spectrotemporal contrast, or simply,

contrast. How does the auditory system compensate for changes in contrast? Similar to the adaptation to sound level variance across time, cells decrease the slope (gain) of their input-output function to accommodate increases in stimulus contrast (Rabinowitz et al., 2011). This process is termed contrast gain control (CGC) and it is evident along the ascending auditory pathway from the IC, to the thalamus (ventral medial geniculate, MGBv), and into ACtx (Lohse et al., 2020). CGC is modeled by passing a cell's linear spectrotemporal tuning, its spectrotemporal receptive field (STRF), through a sigmoid nonlinearity, a function resembling aforementioned rate-level functions, that provides parameters that translate to threshold, gain, dynamic range, and baseline rate (Rabinowitz et al., 2012). The model better predicts cell firing-rates when the gain parameter is allowed to fluctuate with sound level contrast. In ACtx, cells are most sensitive to changes in contrast at the frequency range along which they are most responsive (Rabinowitz et al., 2012). Despite this contrast induced shift in the cell gain parameter of its input-output sigmoid nonlinearity (CGC), baseline firing-rates of neurons in ACtx do not change overall and are thus invariant to contrast (Lohse et al., 2020). Thus, adaptation to sound level contrast presents as two phenomena, CGC, a slope shift in the input-output nonlinearity, and contrast invariance, the invariance of cortical baseline firing-rates to contrast changes.

What implications does contrast adaptation have on behavior and human perception? This question has only recently begun to be systematically explored despite the literature introducing adaptation in the context of the 'cocktail party problem' and 'hearing in noise' in the last decade (Rabinowitz et al., 2013; Willmore et al., 2014). Human participants' sensitivity to sound level differences, the minimum difference between two sound levels to be noticeable, decreases with increasing sound level contrast (Lohse et al., 2020). Similarly, mice are less able to discriminate changes to a sound target volume when the target is in high contrast sound (Angeloni et al., 2021).

Both of these studies show solely the perceptual detriment associated with increasing contrast rather than a benefit. Novel behavioral paradigms are needed that allow for simultaneous neural recording, internal brain state markers, and pharmacological intervention that show the perceptual benefit to an increased encoding range associated with increased sound contrast. Nonetheless, Angeloni et al, 2021, do reveal that ACtx is necessary for target detection in background noise (Angeloni et al., 2021). This suggests that while contrast adaptation is evident beginning in IC, it is necessary in ACtx for behavioral context related demands.

1.3 In Search of Circuit and Synaptic Mechanisms of Contrast Gain Control

While the neural input-output adaptation of CGC has been well described, the circuit and synaptic mechanisms that enable it remain elusive. Because of the input rescaling (gain change) that defines CGC, it is considered to be a divisive normalization computation (Carandini and Heeger, 2012; Rabinowitz et al., 2012). This computation is considered canonical because it is evident across species (Cooke et al., 2018; Rabinowitz et al., 2011), across brain regions (Lohse et al., 2020), and across multiple sensory systems including vision (Carandini et al., 1997; Wilson et al., 2012), and olfaction (Olsen et al., 2010). Thus, the same computation may be implemented with different components and cellular architecture associated with different species and brain regions. Highlighting this, is the finding that CGC in visual cortex relies upon parvalbumin expressing inhibitory interneurons (PV cells) (Wilson et al., 2012), while CGC in ACtx does not (Cooke et al., 2020). Furthermore, CGC adaptation time differs along the auditory pathway and baseline rate contrast invariance is solely evident in ACtx (Lohse et al., 2020), suggesting that

CGC relies upon additional, if not unique mechanisms that are not simply inherited from subcortical nuclei.

While CGC in ACtx relies upon different circuit mechanisms than those in visual cortex, what can be gleaned of synaptic mechanisms of CGC in visual cortex (V1)? Short-term synaptic plasticity (STP), specifically short-term depression (STD) at thalamocortical synapses, explains CGC in V1 as STD builds with increasing presynaptic activity and thus contrast. Furthermore, in ACtx, STRF models of neuron firing-rates significantly improve with a non-linear synaptic depression component (David et al., 2009). However, when the nonlinear STP model was compared against a CGC model (Rabinowitz et al., 2012) using the same natural sound stimuli, the combined models resulted in better fits than either in isolation, suggesting that they uniquely contribute and are not equivalent (Pennington and David, 2020). A thalamocortical STD mechanism would explain a gradient of contrast strength along cortical layers, but in mouse primary ACtx (A1), CGC was instead observed to be stronger in layer 5/6 output layers when compared to the primary thalamorecipient layer 4 (Cooke et al., 2018; Harris and Shepherd, 2015). Thus the circuit and synaptic mechanisms of CGC in ACtx remain poorly understood despite its importance to CGC guided behavior (Angeloni et al., 2021).

1.4 Synaptic Zinc as a Candidate Neuromodulator of Contrast Dependent Gain Change in Auditory Cortex

With evidence against an inhibitory circuit mechanism (Cooke et al., 2020) and short of support for a short-term depression explanation (Pennington and David, 2020), we hypothesized that a neuromodulator of gain and excitability, specifically synaptic zinc (Anderson et al., 2017;

Vergnano et al., 2014), contributes to CGC in ACtx. This hypothesis was motivated by recent work using 2-photon calcium imaging in awake mice that reveals synaptic zinc as a key neuromodulator of cortical sound processing (Anderson et al., 2017; Kumar et al., 2019). Notably, synaptic zinc signaling modulates the gain of cortical sound-evoked responses (Anderson et al., 2017) and contributes to frequency selectivity in the primary auditory cortex (A1) (Kumar et al., 2019).

1.5 Zinc Background

Zinc is critical to life (McAllister and Dyck, 2017a; Prasad et al., 1961). It is commonly appreciated for its presence as a metalloprotein cofactor (Palmiter et al., 1996) serving functions such as metabolizing ethanol (Auld and Bergman, 2008) and enabling DNA binding (Leon and Roth, 2000). Our understanding of its role in the brain has been developing over the past two decades (McAllister and Dyck, 2017a, 2017b). Zinc is present throughout the cortex, but concentrated in layers 2/3, 5, and 6 (Brown and Dyck, 2003; McAllister and Dyck, 2017a). Zinc stored in synaptic vesicles, termed synaptic zinc, is regulated by the vesicular zinc transporter (ZnT3) (Cole et al., 1999; McAllister and Dyck, 2017a; Palmiter et al., 1996). Low micromolar concentrations of zinc modulate post-synaptic excitability (Paoletti et al., 2009, 1997) via allosteric inhibition of AMPA and NMDA receptors (Anderson et al., 2015; Kalappa et al., 2015; Krall et al., 2020; Paoletti et al., 2009; Vergnano et al., 2014) and via enhancement of GABAergic inhibitory post-synaptic currents (Kouvaros et al., 2020). Such neuromodulation by synaptic zinc is regulated in a context- (Kalappa and Tzounopoulos, 2017) and experience-dependent fashion (Brown and Dyck, 2005; Dyck et al., 2003; Nakashima and Dyck, 2008; Perez-Rosello et al., 2015, 2013; Vogler et al., 2020). In the absence of cortical synaptic zinc, mice lacking ZnT3 (ZnT3

knockout mice; ZnT3-KO) exhibit reduced acuity for detecting changes in sound frequency (Kumar et al., 2019). This together with its gain modulation of cortical sound-evoked responses highlight synaptic zinc as a fundamental and dynamic neuromodulator of synaptic transmission and cortical sound processing (Anderson et al., 2017).

1.6 Pupil-indexed Neural States and Sensory Processing

In an awake quiescent animal, there are fluctuations in cortical state measurable by spontaneous neural activity and membrane potential that correspond to the animal's responsiveness to sensory stimuli (McGinley et al., 2015b; Steriade et al., 2001; Vinck et al., 2015). Improved sensory dependent task performance coincides with states of increased stimulus responsiveness (Hasenstaub et al., 2007). Under consistent lighting intensity (constant luminance), these states may be indexed by the animal's pupil diameter (PD) (McGinley et al., 2015a; Reimer et al., 2014). This is one of the reasons PD is considered an index of 'arousal' (McGinley et al., 2015b). As PD linearly increases from small and constricted to large and dilated, cortical state follows a U shape and stimulus sensitivity inversely follows an inverted U, or intersection symbol (\cap), shape (Aston-Jones and Cohen, 2005; McGinley et al., 2015a; Yerkes and Dodson, 1908). For example, sound detection task performance is low at small PD, maximal at intermediate PD size, and low again at large PDs (McGinley et al., 2015a). When the pupil is small, cortical neurons predominantly exhibit rhythmic low-frequency activity (1 – 10 Hz). As pupil increases into the intermediate size range, membrane potential reaches its most hyperpolarized and least variable state, thus membrane potential fluctuations decrease and coincide with decreased spontaneous activity and a suppression of low-frequency rhythms. At this intermediate state, sensory encoding

is optimal: stimulus responses are largest in magnitude; sensory evoked activity to spontaneous activity, or signal-to-noise ratio, is largest; and trial-to-trial variability in responses is reduced. As pupil enters its most dilated range, there is an increase in brief and small dilations and constrictions. In this range, cortical neuron membrane potentials begin to exhibit high frequency fluctuations as they become more depolarized (McGinley et al., 2015b). Upon a transition from quiescence to locomotion, the pupil enters this large, dilated range. Interestingly, locomotion onset is preceded by both an increase in PD and a decrease in rhythmic low-frequency cortical activity (Vinck et al., 2015). Importantly for this dissertation, pupil tracks ACtx excitability (Schwartz et al., 2019) and intermediate pupil sizes correspond to increased auditory stimulus response gain (McGinley et al., 2015a).

1.7 Pupil Size and ‘Arousal’

Cortical activity and sensory encoding follow similar U- and \cap -shaped relationships (respectively) with a linear increase in locus coeruleus (LC) norepinephrine (NE) activity (Aston-Jones and Cohen, 2005; McGinley et al., 2015b; Sara, 2009). Owing to this and LC inhibition of sleep promoting nuclei as well as direct excitatory effects on cortex (Saper et al., 2001), LC-NE activity is also considered a marker of ‘arousal’ (Satpute et al., 2019). Because of the equivalence between linear increases in pupil size and LC-NE activity with regard to cortical state and sensory encoding as well as direct LC-NE influence on wakefulness, pupil size has been used as a proxy for ‘arousal’ as it relates to LC-NE activity (Gilzenrat et al., 2010; Joshi, 2021; Privitera et al., 2020). Although PD does closely track LC-NE activity (Joshi et al., 2016), and LC stimulation causes pupil dilation (Privitera et al., 2020), the specific circuit driving pupil dilation/constriction

from LC has yet to be established (Joshi and Gold, 2020). Establishing this link is challenging due to the interconnectedness and extensive innervation of the multiple nuclei that directly affect PD (Joshi and Gold, 2020).

Pupil size indexes (varies with) several task-associated factors that are also considered measures of ‘arousal’ (McGinley et al., 2015b). However, arousal is a broad psychological construct that may be simplified into three categories: wakeful arousal, a wakefulness gradient from sleep to being awake; autonomic arousal, consisting of peripheral autonomic responses and heart rate; and finally affective arousal, meaning affective engagement with stimuli (Satpute et al., 2019). Task-associated factors, such as listening effort, may reflect one of these categories of ‘arousal’, but it is not the same as other categories of arousal including factors such as heart rate. Similarly, LC-NE activity may mechanistically explain one or multiple categories, but it does not account for all.

With regard to hearing, PD is reflective of listening effort (Borghini and Hazan, 2018; Winn et al., 2015; Zekveld et al., 2010); cognitive load as measured by speech perception in noise (Zekveld et al., 2014, 2011), and hearing loss (Kuchinsky et al., 2016). Although pupil tracks task engagement, pupil and task associated neural activity may be resolved into distinct neural populations in the inferior colliculus (IC) and ACtx by comparing responses to task related sounds between task and passive conditions (Saderi et al., 2021). In the midbrain (IC), a greater proportion of neurons were pupil associated compared to primary ACtx (A1) where more neurons were associated with task engagement (Saderi et al., 2021).

1.8 Pupil and Neuromodulators

Pupil size tracks other neuromodulators in addition to LC-NE activity (Reimer et al., 2016). Recordings of acetylcholine (ACh) and NE projections in layer 1 of mouse cortex during pupillometry reveal that both ACh and NE correlate with PD, albeit on different time scales, and that both pupil and projection activity increased prior to locomotion onset (Reimer et al., 2016). Furthermore, vagus nerve stimulation, which is associated with both cortical ACh release and LC-NE activation, drives pupil dilation (Mridha et al., 2021). Stimulation of the dorsal raphe nucleus (DRN), which drives neuromodulatory serotonin release throughout cortex, drives pupil dilation and the extent of stimulus evoked PD changes depend on task related uncertainty (Cazettes et al., 2020). Importantly, using a linear mixed-effects model, Cazettes et al., 2020 found no interaction effects between DRN stimulation and baseline pupil state on stimulus evoked PD changes. Although the pupil does tend to constrict when at relatively dilated states (Gee et al., 2014; Mridha et al., 2021), and stimulus evoked pupil responses are negatively correlated with pre-stimulus PD (Joshi and Gold, 2020; see also Figure 3-4), Cazettes show that DRN stimulus evoked PD changes associated with task related uncertainty do not depend on baseline (stimulus-independent) pupil state. This suggests that stimulus evoked PD changes with task-related neuromodulation may be dissociated from PD variation with stimulus independent behavioral/'arousal' state (Cazettes et al., 2020; Joshi, 2021). Chapter 2 of this thesis approaches a similar concept, instead regarding auditory stimulus related neuromodulation.

1.9 Sound Evoked Pupil Responses

So far pupil size has been discussed here in terms of an index of cortical state, whether it be reflective of wakefulness, task engagement, or locomotion. Discussion of pupil changes in this context is to understand how aspects of sensory processing, such as CGC as explored in Chapter 2, are affected by behavioral state and to explore how neuromodulatory factors that may be involved in regulating such behavioral states relate to pupil size. Now we inversely ask: how does sensory processing influence pupil size? In Chapter 2 we explore how cortical sensory adaptations, CGC, and/or associated neuromodulatory zincergic activity influence sound stimulus-dependent pupil responses. Numerous sound stimulus factors influence pupil responses: loudness, deviance from regularity, complexity, and signal-to-noise to name a few (Montes-Lourido et al., 2021; Zekveld et al., 2018). When stimulus factors are kept consistent, changes to sound evoked pupil responses are instead indicative of physiological factors, both clinically relevant and not, such as: age, hearing loss, cognitive ability, musical expertise, fatigue, dementia, and schizophrenia (Zekveld et al., 2018). Thus changes to sound evoked pupil responses may be used as a clinical marker (Montes-Lourido et al., 2021). The more that is known about the cortical mechanisms involved in processing the auditory stimulus, the more that can be gleaned from the stimulus-dependent pupil response. Chapter 2 reveals a zincergic neuromodulatory mechanism in auditory cortex that enables sound contrast-dependent changes to pupil responses. Thus, disrupted contrast-dependent pupil responses are indicative of disrupted zincergic neuromodulatory signaling in ACtx.

1.10 Dissertation Aims

Upon a transition from an environment with a narrow range of sound levels, such as a laundromat, to another with a wider range of sound levels but same average sound level, such as a crowded bar, the brain must adapt in dynamic range. For processing innumerable, but probabilistic sound contexts, the brain handles this by efficiently adapting the neurons to sound context statistics, in this case an increase in sound level contrast. By this sensory adaptation process termed contrast gain control, neurons decrease the slope of their sound level input to firing-rate output relationship so that they may encode a wider range of inputs, but at the cost of reduced sensitivity to subtle sound level differences (Angeloni et al., 2021; Lohse et al., 2020). This gain adaptation to sound level contrast has been modeled and described in detail in multiple species and at multiple stages of the auditory pathway (Cooke et al., 2018; Lohse et al., 2020; Rabinowitz et al., 2011). Despite this, circuit, synaptic, and neuromodulatory mechanisms that enable this adaptation remain unknown. Given recent work from the Tzounopoulos lab showing that synaptic zinc signaling modulates the response gain of cortical neurons (Anderson et al., 2017), we looked towards zinc signaling for a potential neuromodulatory mechanism for contrast gain control in auditory cortex (Chapter 1).

Does adaptation to sound environments depend upon brain state? Given that responsiveness to sensory stimuli and neural excitability change with pupil size, an index of cortical brain state (McGinley et al., 2015b, 2015a; Schwartz et al., 2019), we ask if contrast gain control compensates for contrast to the same extent regardless brain state. To answer this question, in Chapter 2 we pair pupil size measurements, pupillometry, with an assay for contrast gain control.

Sound evokes pupil dilations and changing sound features result in changes to these evoked pupil responses. Pupil responses to the same sound can change depending on age, hearing loss,

dementia, and schizophrenia (Zekveld et al., 2018). Thus, stimulus-dependent pupil responses can be reflective of brain physiology in a clinical setting. Given our understanding of zingergic neuromodulatory contribution to contrast gain control, what can sound contrast-dependent changes in pupil responses tell us about activity in auditory cortex? We explore this in the latter part of Chapter 2.

1.11 Dissertation Overview

In Chapter 1 we explore both neuromodulatory synaptic zinc signaling and cell type specific mechanisms of adaptation to sound level contrast. To accommodate pharmacological manipulation of zinc with cell type specificity we adapted an electrophysiological measure of contrast gain control (CGC) (Cooke et al., 2020; Rabinowitz et al., 2011) to a measure using awake in vivo 2-photon calcium imaging (2PCI). Due to the decrease in gain (shallower input-output slope) corresponding with increased contrast, neuron responses to a given sound in high contrast are lower than neuron responses to the same sound in low contrast (Cooke et al., 2020; Rabinowitz et al., 2011). We observe the same result while imaging neuron responses with 2PCI. Despite this gain change in neuron input-output functions, baseline firing-rates do not change with contrast in ACtx (Lohse et al., 2020). We observe an equivalent phenomenon of this contrast invariance using 2PCI. Thus, in Chapter 1, using 2PCI we recapitulate two phenomena of adaptation to sound contrast, CGC, and contrast invariance.

In the rest of Chapter 1, we combined this 2PCI assay for cortical CGC with pharmacological and transgenic approaches to explore both the involvement of neuromodulatory zinc signaling, and whether this involvement is specific to certain cell types. We found that

synaptic zinc is required for dampened sound responses in high contrast specifically in principal neurons of primary ACtx (A1). We found that zinc did not affect sound responses in low contrast, nor did it have any contrast specific effects on parvalbumin (PV) expressing or somatostatin expressing inhibitory interneurons. We did, however observe higher average PV-cell activity in high contrast sound. We thus concluded that PV cells may contribute to the cortical contrast invariance phenomenon of contrast adaptation. Importantly, we found that synaptic zinc is engaged in a contrast specific manner to enable CGC in A1.

In the first part of Chapter 2 we paired pupillometry with the 2PCI assay for CGC to ask whether CGC magnitude depends upon pupil-indexed brain state. We find that while CGC is on average apparent across the entire range of pupil-indexed states, it is maximal at intermediate pupil sizes. Given CGC magnitude dependence on stimulus-independent pupil-indexed state, we next asked if stimulus-dependent pupil responses also affect CGC. We found that CGC solely depended on pre-stimulus pupil-indexed state and thus confirmed that the 2PCI measure of CGC is not simply a measure of contrast-dependent pupil response effects on cell responses.

In the latter part of Chapter 2 we explored the inverse, pupil response dependence on sound processing rather than sound processing dependence on pupil-indexed brain state. We combined the 2PCI assay for CGC and pupillometry along with pharmacological and transgenic approaches to address whether pupil response changes with contrast are indicative of contrast-dependent zincergic (zinc signaling specific) activity in auditory cortex. We found that pupil responses increase in high contrast sound and that this increase depends upon synaptic zincergic neuromodulation in ACtx. Thus, neuromodulatory synaptic zinc effects on both A1 principal cells and pupil responses are specific to high contrast contrasts. This mirroring of state specific effects suggests that contrast specific pupil responses are linked to cortical responses via zinc signaling.

Thus, pupil responses to contrast could serve as a clinical measure for disrupted zinc signaling and possibly CGC in auditory cortex.

2.0 Chapter 1: Neuromodulatory Mechanisms Underlying Contrast Gain Control in Mouse Auditory Cortex

2.1 Overview

Neural adaptation enables the brain to efficiently process sensory signals despite large changes in background noise. Previous studies have established that recent background spectro- or spatio-temporal statistics scale neural responses to sensory stimuli via a canonical normalization computation, which is conserved among species and sensory domains. In the auditory pathway, this adaptation presents as decreasing instantaneous firing-rate gain with increasing spectrotemporal contrast, termed contrast gain control. Despite this gain rescaling, mean firing-rates in auditory cortex become invariant to sound level contrast, termed contrast invariance. The underlying neuromodulatory mechanisms of these two phenomena remain unknown. To study these mechanisms, we used a 2-photon calcium imaging preparation, pharmacological and genetic knockout approaches in layer 2/3 neurons of mouse primary auditory cortex (A1). We found that neuromodulatory cortical synaptic zinc signaling is necessary for contrast gain control but not contrast invariance in mouse A1.

2.2 Introduction

Neural adaptation enables the brain to efficiently process sensory signals amid changing environments (Carandini and Heeger, 2012; Schwartz and Simoncelli, 2001; Wen et al., 2012). In

the visual system, stimulus-response functions shift with respect to average light intensity to ensure neurons are most sensitive along the relevant light range (Carandini and Heeger, 2012). In the auditory system, when the mean and variance of sound levels change over time, the neuronal sound input level-response functions adapt accordingly to maintain dynamic range across the most relevant sound levels (Dean et al., 2005; Wen et al., 2009). In more complex environments increases in the stimulus variance (contrast) induce a decrease in the slope of the neural input-output relationship, a gain reduction, to efficiently to maintain stimulus discriminability (King and Walker, 2020). This gain control is achieved via a canonical neural computation, normalization (Carandini and Heeger, 2012), which is conserved among species (Cooke et al., 2018; Lohse et al., 2020; Rabinowitz et al., 2011) and sensory domains (Carandini and Heeger, 2012; Olsen et al., 2010; Rabinowitz et al., 2011; Schwartz and Simoncelli, 2001). As such, normalization relies on diverse circuits and mechanisms, and different brain regions or different species may implement it with different available components. In the auditory pathway, this adaptation, termed sound contrast gain control, is evident as early as the inferior colliculus (IC), and continues in comparable strength to thalamus and finally into auditory cortex (ACtx) (Lohse et al., 2020). Along this hierarchy, differences in the underlying cellular architecture, adaptation time, and response properties suggest unique contrast adaptation mechanisms along the auditory pathway (Lohse et al., 2020) that are not simply inherited from subcortical nuclei. The normalization associated with contrast gain control depends upon parvalbumin expressing (PV) neurons in visual (Wilson et al., 2012), but not in auditory cortex (Cooke et al., 2020), supporting the idea that normalization is not the outcome of a canonical circuit or mechanism. Moreover, uniquely in the ACtx, additional mechanisms contribute to cortical sound contrast adaptation, as the mean firing-rates during sustained sound remain invariant to contrast (Lohse et al., 2020), termed contrast invariance.

Importantly, sound contrast adaptations account for changes in perceptual judgements in humans (Lohse et al., 2020) and mice (Angeloni et al., 2021), however, the underlying neuromodulatory mechanisms remain poorly understood.

Recent work using 2-photon calcium imaging in awake mice has established synaptic zinc as a key neuromodulator of cortical sound processing (Anderson et al., 2017; Kumar et al., 2019). Critical to the current study, synaptic zinc signaling modulates the gain of cortical sound-evoked responses (Anderson et al., 2017) and contributes to frequency selectivity in the primary auditory cortex (A1) (Kumar et al., 2019). These effects are eliminated in ZnT3 knockout (ZnT3KO) mice that lack the vesicular zinc transporter (ZnT3), which loads zinc into synaptic vesicles (Anderson et al., 2017; Cole et al., 1999; McAllister and Dyck, 2017a; Palmiter et al., 1996). In the absence of cortical synaptic zinc, ZnT3 knockout mice exhibit reduced acuity for detecting changes in sound frequency (Kumar et al., 2019). At the level of synaptic transmission and neuromodulation, vesicular (synaptic) zinc is released with glutamate and GABA to inhibit GluN2A-containing NMDA and AMPA receptors (Rs) and potentiate GABARs (Anderson et al., 2015; Kalappa et al., 2015; Kouvaros et al., 2020; Krall et al., 2020; Paoletti et al., 2009; Vergnano et al., 2014). Together, these results have unmasked a fundamental role of zinc signaling in the fields of synaptic transmission and A1 sound processing.

Here, we probed the influence of zincergic neuromodulation on the two phenomena of cortical sound contrast adaptation, contrast gain control and contrast invariance. To study these phenomena, we used an awake 2-photon calcium imaging (2PCI) preparation to assay principal (excitatory projection), PV, and somatostatin-expressing (SOM) cell response properties with respect to low and high spectrotemporal sound level contrast. To determine the dependence of these adaptations on synaptic zinc, we used a combined pharmacological (Pan et al., 2011) and

genetic knockout approach (Cole et al., 1999). Our results support that A1 contrast gain control is under the neuromodulatory control of synaptic zinc signaling.

2.3 Results

2.3.1 2-Photon Calcium Imaging (2PCI) Assay for Adaptation to Sound Level Contrast in A1 L2/3 Principal Neurons

To interrogate neuromodulatory and cellular signaling mechanisms underlying contrast adaptation in A1 L2/3 principal neurons we devised an *in vivo* awake 2-photon calcium imaging (2PCI) assay in mice. Our non-parametric approach is based upon previous electrophysiological analyses that do not rely upon a parametric firing-rate model (Cooke et al., 2020; Rabinowitz et al., 2011). We used 2PCI to record sound evoked calcium fluorescence transients from single principal cells in awake head-fixed mice that express the GCaMP6f calcium indicator. For these experiments, we injected ACtx with an adeno-associated virus (AAV) that drives GCaMP6f expression under control of the calcium/calmodulin-dependent protein kinase 2 (CaMKII) promoter. For each recording, we first localized A1 using wide-field 4X epifluorescence calcium imaging by comparing the response to a 5 – 6 kHz pure tone at 50 – 60 dB SPL with established tonotopic maps of mouse ACtx (Anderson et al., 2017; Linden et al., 2003; Romero et al., 2019). We then mapped single cell frequency response areas (FRAs) for a single field of cells within A1 L2/3 under 2PCI at 40X. Then, to identify the pure tone frequency with the maximum response, we averaged the FRAs across these cells. To assess contrast adaptation, we presented this pure tone at 70 dB SPL following 2 s of dynamic random chords (DRCs) having either low or high

spectrotemporal sound level contrast (Figure 2-1a). Sound level varied across both frequency and time (Figure 2-1a-b), at ± 5 dB ($\sigma \approx 2.9$ dB) for low- and ± 15 dB ($\sigma \approx 8.7$ dB) for high-contrast DRCs, but both DRC stimuli had the same mean sound level of 55 dB (see **Methods: DRC stimuli**). Figure 2-1c shows the time course of the 2PCI assay and illustrates cell averages of fluorescence response traces during high and low contrast stimuli, covering from 1.2 s before the DRC onset until the end of the 8 s DRC stimulus ($n = 125$ cells, 7 mice). Traces were baseline (F_0) subtracted and normalized, $\Delta F/F = (F-F_0)/F_0$, where F_0 is the mean fluorescence prior to DRC onset (-1.2 – 0 s). We used this assay to assess two phenomena of contrast adaptation: contrast gain control and contrast invariance (Figure 2-1c, gray boxes). First, we assessed contrast gain control by comparing responses to pure tones preceded by low vs. high contrast (Figure 2-1c: left gray box, Figure 2-1d-e). Second, we assessed contrast invariance by comparing mean fluorescence responses during sustained low- vs. high-contrast DRC segments (Figure 2-1c: right gray box at 6 – 8 s, Figure 2-1i).

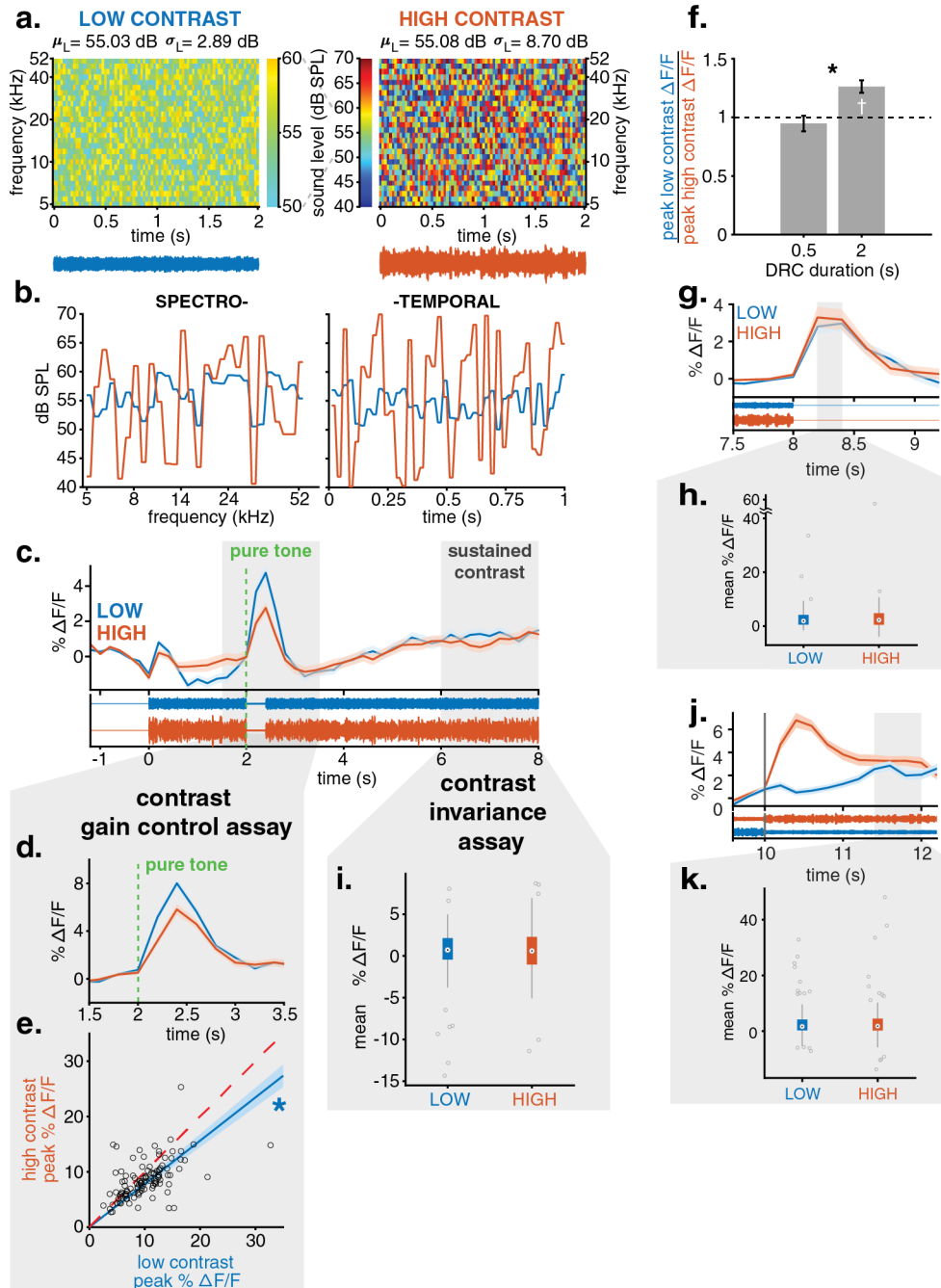


Figure 2-1: 2-photon calcium imaging (2PCDI) assay for A1 adaptation to spectrotemporal sound level contrast
(a) Spectrogram (top) and sound voltage signal (bottom) of a representative 2 s epoch from low- (left; blue) and high (right; red) contrast DRC stimuli. For each 25 ms time bin column in the spectrogram, sound levels for each frequency (depicted by color) are sampled from a narrow (low contrast; ± 5 dB; left colorbar) or wide (high contrast; ± 15 dB; right colorbar) uniform distribution with the same 55 dB SPL mean. **(b)** Sound level (dB SPL) plotted against frequency (left) and time (right) to depict low (blue) and high (red) spectro- and

temporal- contrast, respectively, of the DRC stimuli. (c) Mean \pm SEM of % $\Delta F/F$ traces from A1 principal cells (top) during low (blue) and high (red) contrast stimuli with a 400 ms pure tone occurring at 2 s after the initiation of the DRC stimulus. Baseline, F_0 , for % $\Delta F/F$ calculated prior to DRC onset at -1.2 – 0 s. Bottom: representative sound voltage signals. (d) Mean \pm SEM of % $\Delta F/F$ traces during the pure tone epoch calculated with F_0 at 1 – 2 s. (e) Scatterplot of each cell's mean peak % $\Delta F/F$ pure tone response in low vs high contrast. Significance ($p = 5.64e-3$, permutation test) denoted by blue asterisk (*). Direction of contrast effect denoted by blue coloring of fitted regression line and 95% confidence interval (slope 95% CI: 0.72 – 0.84). (f) Mean \pm SEM of contrast scaling factors from 2PCI assay with a pure tone occurring 0.5 s or 2 s after contrast DRC onset. Asterisk (*) denotes $p = 1.30e-4$ via permutation test and cross (†) denotes $p = 3.53e-8$ via Wilcoxon signed-rank test. (g) Mean \pm SEM of % $\Delta F/F$ traces (top) in low and high contrast at end of DRC stimulus (DRC offset at 8 s) using a baseline, F_0 , calculated prior to DRC offset at 7 – 8 s. Bottom: representative sound voltage signals. (h) Boxplot of temporal averages of % $\Delta F/F$ responses following DRC offset at 8.2 – 8.4 s for low and high contrast. (i) Boxplot of temporal averages of % $\Delta F/F$ responses during the sustained contrast epoch at 6 – 8 s for low (blue) and high (red) contrast. (j) Mean \pm SEM of % $\Delta F/F$ traces (top) during a change in sound level contrast from low to high (red) and high to low (blue). Baseline, F_0 , calculated before contrast change at 7 – 10 s. Bottom: representative sound voltage signals. (k) Boxplot of temporal averages of % $\Delta F/F$ responses during 11.4 – 12 s DRC segment of low or high contrast.

Consistent with previous studies assessing contrast gain control (Cooke et al., 2020; Rabinowitz et al., 2011), neural responses to pure tones in high contrast are reduced compared to responses in low contrast (Figure 2-1c: left gray box). To assess peak fluorescence responses to the pure tone, we calculated baseline subtracted fluorescence traces normalized to a baseline 1 s prior to pure tone onset (Figure 2-1d; F_0 is mean fluorescence intensity at 1 – 2 s). We plotted each cell's average peak pure tone response following 2 s of low contrast against its response following 2 s of high contrast (Figure 2-1e) and found that responses were significantly greater when preceded by low contrast ($p = 5.64e-3$, permutation test; blue fitted regression line and 95% confidence interval: slope 95% CI: 0.72 – 0.84; $n = 110$ cells, 7 mice). Note that the regression line and 95% confidence interval in Figure 2-1e and subsequent scatterplots is only used for depictive purposes; coloration other than gray denotes the direction of a significant effect of contrast as measured by a permutation test. To assess whether the effect of contrast is dependent on the duration of the contrast sound prior to the pure tone, we also performed the same assay but with pure tones occurring 0.5 s after low or high contrast sound (Figure 2-1f). To quantify contrast gain control, we calculated the contrast scaling factor, defined as the population mean of individual cell average peak responses in low- divided by average peak responses in high contrast. We determined contrast gain control to be evident if the contrast scaling factor is significantly greater than 1. We found that the contrast scaling factor was significantly greater when pure tones were preceded by 2 s of contrast DRC as opposed to 0.5 s ($p = 1.30e-4$, permutation test). With our assay, 0.5 s of contrast sound was not sufficient to observe a significant effect of contrast ($p = 0.227$; $n = 77$); solely 2 s of contrast DRC resulted in a contrast scaling factor significantly greater than 1 ($p = 3.53e-8$, $n = 125$; Wilcoxon signed-rank tests, 7 mice).

To control for a potential offset response contribution to the pure tone epoch due to the cessation of the DRCs during the 400 ms pure tone, we plotted % $\Delta F/F$ traces at DRC offset (8 s) that were followed by silence instead of a pure tone (Figure 2-1g; baseline, F_0 , calculated prior to DRC offset at 7 – 8 s). We did not observe a significant effect of contrast on offset responses (8.2 – 8.4 s; Figure 2-1h, boxplot; $p = 0.62$, permutation test; $n = 125$ cells, 7 mice), and thus conclude that the effect of contrast on responses during the pure tone epoch is not attributable to the cessation of the DRCs during the 400 ms pure tone. Taken together, using a 2PCI assay, we measure contrast gain control that is consistent with previous electrophysiological studies (Cooke et al., 2020, 2018; Rabinowitz et al., 2011). Moreover, the pure tone response epoch of our 2PCI assay reveals a duration-dependent effect of preceding context contrast that is also consistent with previous electrophysiology studies (Rabinowitz et al., 2011).

We next determined whether our assay recapitulates a second phenomenon of contrast adaptation, cortical contrast invariance. We hypothesized that mean % $\Delta F/F$ activity during the sustained contrast DRC segment (Figure 2-1c: right gray box at 6 – 8 s) would not differ with respect to contrast, as seen with mean A1 firing-rates in previous electrophysiological studies (Lohse et al., 2020). To assess contrast invariance with our assay, we isolated % $\Delta F/F$ activity during sustained DRC presentation within a 2 s epoch that sufficiently follows pure tone response decay (6 – 8 s). Average cell % $\Delta F/F$ traces were calculated with an F_0 at -1.2 – 0 s (as in Figure 2-1c) and comprise the 6 – 8 s epoch from both 2 s and 0.5 s pure tone onset conditions. Temporal averages of responses during this sustained contrast epoch do not differ with respect to contrast (Figure 2-1i, boxplot, $p = 0.66$, permutation test; $n = 125$ cells, 7 mice). While this DRC segment recapitulates contrast invariance, it does not clearly reveal the time course of response adaptation to comparable levels after a change in contrast, as observed in previous electrophysiological

studies (Lohse et al., 2020). To account for this, we performed additional experiments in which we recorded % $\Delta F/F$ activity after a change in contrast from low to high and from high to low, as done in previous studies (Cooke et al., 2018; Lohse et al., 2020) (Figure 2-1j; F_0 calculated before contrast change at 7 – 10 s). The change from low to high contrast (at 10 s) results in initially larger responses that fully adapt and return to low contrast response levels within 1.4 s (as seen with the 11.4 – 12 s temporal average in Figure 2-1k, boxplot; $p = 0.11$, permutation test; $n = 210$ cells, 5 mice). Consistent with Figure 2-1c (right gray box) and Figure 2-1i, mean responses during sustained DRC segments remain invariant to contrast. Despite the longer adaptation time that is likely due to the calcium imaging signal, our results are consistent with electrophysiology data (Lohse et al., 2020). Thus, the second epoch of our 2PCI assay during sustained contrast DRCs (Figure 2-1c: right gray box and Figure 2-1i) reproduces a second phenomenon of contrast adaptation, cortical contrast invariance. Taken together, we established a 2PCI assay that measures two phenomena of cortical contrast adaptation: contrast gain control and contrast invariance. We will employ this assay to explore the neuromodulatory mechanisms of cortical adaptation to sound level contrast.

Because neurons are most sensitive to changes in contrast within the frequency bandwidth at which they are most responsive (Rabinowitz et al., 2012), we explored the frequency dependence of contrast gain control with our 2PCI assay. For each recorded field of cells, a given cell's best frequency (BF), the frequency that elicited the maximum response across an average of presented sound levels, is at some octave difference from the pure tone frequency used to assess contrast gain control (Figure 2-2a, top, representative cell FRA in terms of cell BF octaves from pure tone in assay). We asked whether contrast gain control depends upon the distance of the pure tone frequency from cell BFs. We plotted contrast scaling factors with respect to whether the pure

tone stimulus occurred within ($n = 55$ cells) or outside 1 octave ($n = 55$ cells) of cell BF (Figure 2-2a boxplot; 7 mice). Contrast scaling factors did not significantly differ between the two conditions (Figure 2-2a, boxplot; $p = 0.425$, permutation test) and were significantly greater than 1 in both conditions (Figure 2-2a boxplot; within: $p = 2.90e-5$; outside: $2.27e-4$; Wilcoxon signed-rank tests). This result suggests that sound level contrast scales L2/3 A1 principal cell responses to pure tones regardless of the distance of the pure tone from the cell's BF.

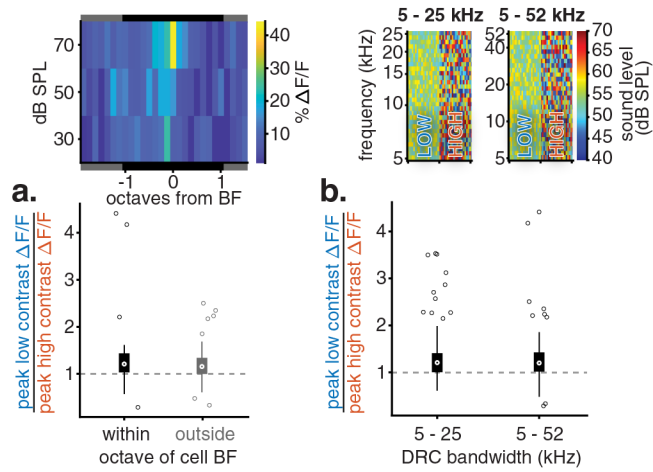


Figure 2-2: Frequency dependence of 2PCI assay for contrast gain control in A1 principal cells

(a) Top: Frequency response area (FRA) from a representative A1 principal cell with frequency on x-axis labeled with respect to octaves from cell best frequency (BF) at 18340 Hz. Color denotes mean peak % $\Delta F/F$ pure tone response amplitude. (a) Bottom: Boxplot of contrast scaling factors from cells with BF's within (black) or outside (gray) 1 octave of the pure tone used in the 2PCI assay. (b) Top: Representative low and high contrast DRC stimuli with bandwidths of 5 – 25 kHz (left) 5 – 52 kHz (right). (b) Bottom: Boxplot of contrast scaling factors from 5 – 25 kHz and 5 – 52 kHz DRC bandwidth conditions.

To further examine the frequency dependence of our 2PCI contrast gain control assay, we tested whether pure tone scaling by contrast depends upon the frequency bandwidth of the DRC stimuli. To address this question, we performed the same assay as in Figure 2-1c, but we used a narrower 5 – 25 kHz frequency bandwidth for both low- and high-contrast DRC (Figure 2-2b, top: representative 0.5 s epochs of low and high contrast from each DRC bandwidth condition). We found that the contrast scaling factors did not significantly differ between the two conditions (Figure 2-2b boxplot; $p = 0.50$, permutation test; 5 – 25 kHz: $n = 152$ cells, 8 mice; 5 – 52 kHz: $n = 110$ cells, 7 mice) and were significantly greater than 1 in both conditions (Figure 2-2b boxplot; 5 – 25 kHz: $p = 3.42e-15$; 5 – 52 kHz: $p = 3.53e-8$; Wilcoxon signed-rank tests). As we observe comparable contrast gain control in both bandwidth conditions, we include data from both conditions in subsequent analyses. This result supports that the scaling effect of contrast on L2/3 A1 principal cell responses to pure tones is robust to a more than halving of the contrast DRC bandwidth.

2.3.2 Contrast Gain Control in Primary Auditory Cortex Depends Upon Neuromodulatory Zinc Signaling

Given the lack of knowledge on synaptic neuromodulatory mechanisms underlying contrast gain control, we next investigated the involvement of synaptic zinc, a neuromodulator capable of cell-specific scaling of sound evoked responses (Anderson et al., 2017). To determine whether synaptic zinc contributes to contrast gain control, we measured contrast gain control as in Figure 2-1d-e (Figure 2-3a-c; 9 mice). We assessed contrast gain control before (CTRL, Figure 2-3b left; lighter shade) and after injecting into ACTx (Anderson et al., 2017, 2015; Kumar et al., 2019) a fast extracellular high-affinity zinc-specific chelator (Pan et al., 2011), ZX1 (100 μ M,

Figure 2-3b, right; darker shade), to inhibit endogenous extracellular zinc signaling (Anderson et al., 2017, 2015; Kumar et al., 2019). The effect of contrast on pure tone responses observed in CTRL (Figure 2-3b-c left; $n = 171$, $p = 1.99e-5$, permutation test, regression slope 95% CI: 0.73 – 0.81) is no longer evident after ZX1 treatment (Figure 2-3b-c right; $n = 174$, $p = 0.52$, permutation test, lack of significance denoted by black/gray coloring of fitted regression line and 95% confidence interval, slope 95% CI: 0.90 – 0.99). ZX1 did not, however, affect contrast invariance (Figure 2-3a: right grey box, Figure 2-3d). Specifically, mean % $\Delta F/F$ activity during the sustained contrast DRC segment (Figure 2-3a: right gray box at 6 – 8 s), remained invariant to contrast after ZX1 injection (Figure 2-3d boxplot). As in Figure 2-1i, mean % $\Delta F/F$ responses did not differ between low and high contrast ($p = 0.59$, permutation test; $n = 182$ cells, 9 mice). To directly assess the effect of ZX1 on contrast gain control, we plotted the contrast scaling factor from the same cells before and after ZX1 injection (Figure 2-3e, $n = 167$ cells, 9 mice). We observed a significant decrease in the contrast scaling factor following ZX1 injection ($p = 9.99e-6$, permutation test), and the contrast scaling factor no longer significantly differed from 1 in the presence of ZX1 ($p = 0.21$, Wilcoxon signed-rank test). To control for a potential effect of the injection pipette and the injection of a solution volume in cortex, we performed the same assay before and after injection of the vehicle: 50 μM AlexaFluor 594 in ACSF. The contrast scaling factor was significantly greater than 1 both before ($p = 7.71e-9$) and after vehicle injection ($p = 1.62e-7$, Wilcoxon signed-rank tests) and did not significantly differ post-injection (Figure 2-3f; $p = 0.73$, permutation test; $n = 82$ cells, 6 mice). Together, these results suggest that zinc signaling is necessary for cortical contrast gain control, but not for contrast invariance.

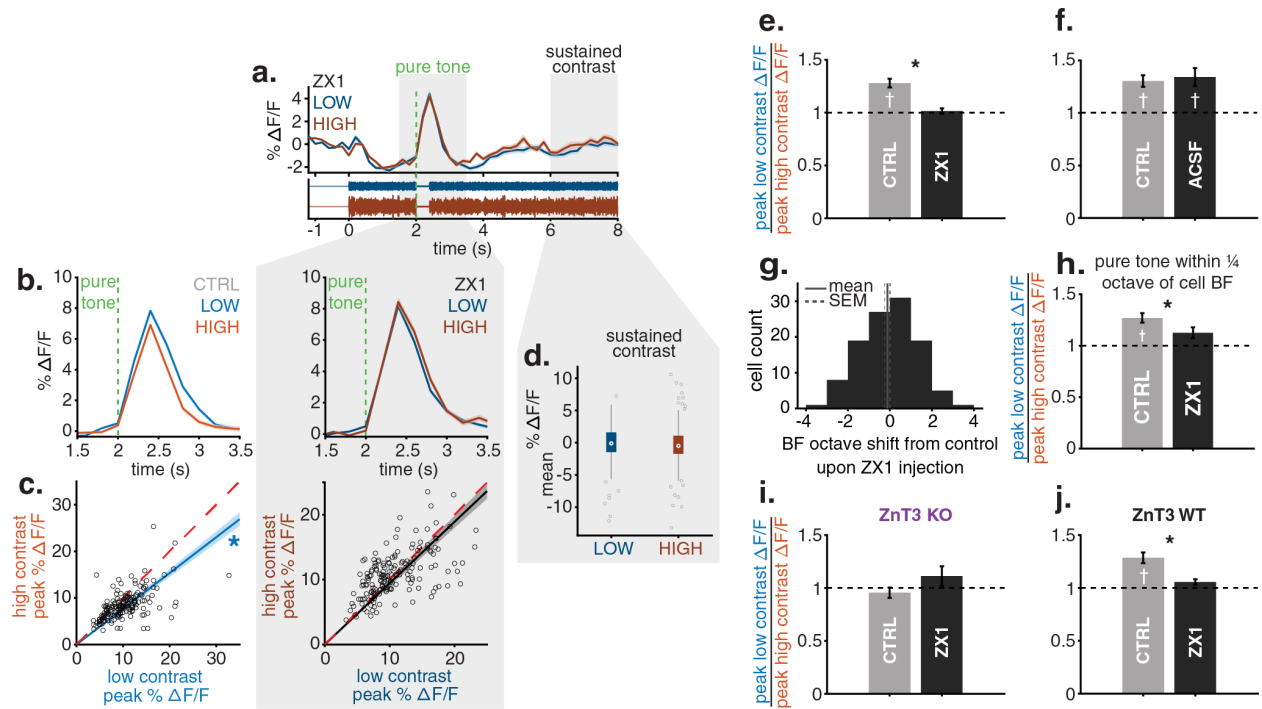


Figure 2-3: Contrast gain control in A1 depends upon cortical ZnT3-dependent synaptic zinc signaling

(a) Mean \pm SEM of $\% \Delta F/F$ traces from A1 principal cells after ZX1 treatment during low (blue) and high (red) contrast stimuli with a 400 ms pure tone occurring at 2 s after the initiation of the DRC stimulus. Baseline, F₀, for $\% \Delta F/F$ calculated prior to DRC onset at -1.2 – 0 s. Bottom: representative sound voltage signals. (b) Mean \pm SEM of $\% \Delta F/F$ traces during the pure tone epoch before (CTRL; left) and after ZX1 treatment (right) calculated with F₀ at 1 – 2 s. (c) Scatterplots of each cell's mean peak $\% \Delta F/F$ pure tone response in low vs high contrast before (CTRL; left) and after ZX1 treatment (right). In CTRL, significance ($p = 1.99e-5$, permutation test) denoted by blue asterisk (*) and direction of contrast effect denoted by blue coloring of fitted regression line and 95% confidence interval (slope 95% CI: 0.73 – 0.81). Black/gray coloring of ZX1 regression line and 95% confidence interval denote no significant effect of contrast (slope 95% CI: 0.90 – 0.99). (d) Boxplot of temporal averages of $\% \Delta F/F$ responses during the sustained contrast epoch at 6 – 8 s after ZX1 treatment for low (blue) and high (red) contrast. (e-f) Contrast scaling factors before (CTRL; gray) and after (black) ZX1 (e) or ACSF (f) treatment. (g) Histogram representing cell counts for bins of cell BF octave shifts after ZX1 treatment. (h) Mean \pm SEM of contrast scaling factors before (gray, CTRL) and after (black) ZX1 treatment limited to responses from pure tones occurring within 0.25 octave of cell BF calculated from FRAs both before and after ZX1 treatment. Asterisk (*) denotes $p = 4.39e-2$ via permutation test and cross (†) denotes $p = 3.78e-$

7 via Wilcoxon signed-rank test. (i-j) Contrast scaling factors before (CTRL; gray) and after ZX1 (black) treatment in ZnT3-KO (i) and ZnT3-WT (j) mice. Black asterisks (*) denote $p < 0.001$ via permutation test and cross (†) denotes $p < 0.001$ via Wilcoxon signed-rank test.

To test for potential ZX1 effects on cell FRA (Kumar et al., 2019) that could explain the ZX1 effects on contrast gain control, we mapped cell FRAs both before and after ZX1 injection in 5 out of 9 mice. We first measured the effect of ZX1 on BF and found that it did not affect BF across the cell population average (Figure 2-3g, $t(110) = -0.9184$, $p = 3.60e-1$, one sample t-test), suggesting that ZX1 effects on contrast gain control are not due to ZX1 effects on cell FRA. Because principal neuron pure tone responses in silence are scaled by synaptic zinc depending on pure tone distance from cell BF (Kumar et al., 2019), we next limited our analysis to responses from pure tones occurring within $\frac{1}{4}$ octave of cell BF in both control and ZX1 conditions (Figure 2-3h; $n = 63$ cells, 5 mice). We observed that the ZX1 effect on the contrast scaling factor persisted ($p = 4.39e-2$, permutation test) and was not different from that of the entire population average (in Figure 2-3e). Together, these two analyses suggest that the contribution of endogenous zinc signaling to contrast gain control is unlikely to be attributable to zinc effects on cell tuning.

The effect of endogenous zinc signaling may be attributable to synaptically released ZnT3-dependent vesicular zinc (Anderson et al., 2017; Cole et al., 1999), tonic zinc (Anderson et al., 2015; Perez-Rosello et al., 2015), or both (Krall et al., 2020). To ascertain the source of zinc signaling, we assessed contrast gain control before and after intracortical ZX1 injection (as in Figure 2-3e) in wild type mice (ZnT3-WT) and knock out (ZnT3-KO) mice that lacked ZnT3, and thus synaptic zinc (Cole et al., 1999). We found that contrast gain control was eliminated in ZnT3 KO mice (Figure 2-3i; the contrast scaling factors do not significantly differ from 1; ZnT3-KO: $p = 0.09$; ZnT3-WT: $p = 0.69$; Wilcoxon signed-rank tests), and furthermore, that ZX1 did not have any effect on ZnT3-KO mice ($p = 0.10$, permutation test; $n = 42$ cells, 4 mice). This suggests the

critical involvement of ZnT3-dependent zinc in contrast gain control and that ZX1 does not have any non-ZnT3-dependent effects on contrast gain control. In littermate controls, ZnT3-WT mice, ZX1 treatment caused a similar reduction in the contrast scaling factor (Figure 2-3j) as in Figure 2-3e ($p = 5.99e-5$, permutation test; $n = 47$ cells, 4 mice). Together, these results suggest that ZnT3-dependent synaptic zinc is needed for contrast gain control in principal neurons of mouse L2/3 primary auditory cortex.

2.3.3 Zinc Signaling Does Not Have Any Contrast-dependent Effects on Either PV or SOM Cells

Because zinc signaling affects the sound-evoked responses of PV and SOM interneurons (Anderson et al., 2017), we next explored whether zinc signaling affects potential contrast adaptations in these interneurons. To do so, we performed the same assay as in Figure 2-1c, but in PV and SOM cells before and after injection of ZX1 into ACtx. To isolate GCaMP6f expression to PV or SOM cells, we injected the ACtx of mice expressing Cre recombinase in PV or SOM cells, PV- or SOM-Cre mice, with a Cre-dependent GCaMP6f AAV. We found that PV cell pure tone responses are not scaled by contrast (Figure 2-4c, $p = 0.96$, permutation test; $n = 36$ cells, 7 mice). Thus, our results are consistent with previous findings (Cooke et al., 2020) suggesting that PV cells do not contribute to contrast gain control of A1 principal neurons. We did, however, observe significantly greater PV activity during sustained high contrast DRCs (Figure 2-4a: right grey box, Figure 2-4d boxplot, $p = 2.56e-2$, permutation test; $n = 38$ cells, 7 mice), which is contrary to previous reports (Cooke et al., 2020) using electrophysiology (see **Discussion**). Nonetheless, this result points towards a potential contribution of PV cells to contrast invariance in A1 principal cells. Importantly, in the presence of ZX1, PV activity during sustained contrast

DRCs remained significantly greater (Figure 2-4b: right grey box, Figure 2-4f boxplot; $p = 2.10 \times 10^{-2}$, permutation test; $n = 35$ cells, 7 mice) and the contrast gain control assay was unaffected (Figure 2-4e; $p = 0.52$, permutation test; $n = 31$ cells, 7 mice). In SOM cells, we did not observe any significant contrast-dependent effect before or after ZX1 injection, suggesting that the A1 SOM cell population does not contribute to contrast adaptation of L2/3 A1 principal neurons (Figure 2-4g-l; $p > 0.05$, permutation test; $n = 22$ cells, 7 mice). Together, these results suggest that zinc signaling does not have any contrast-dependent effects in either PV or SOM cells.

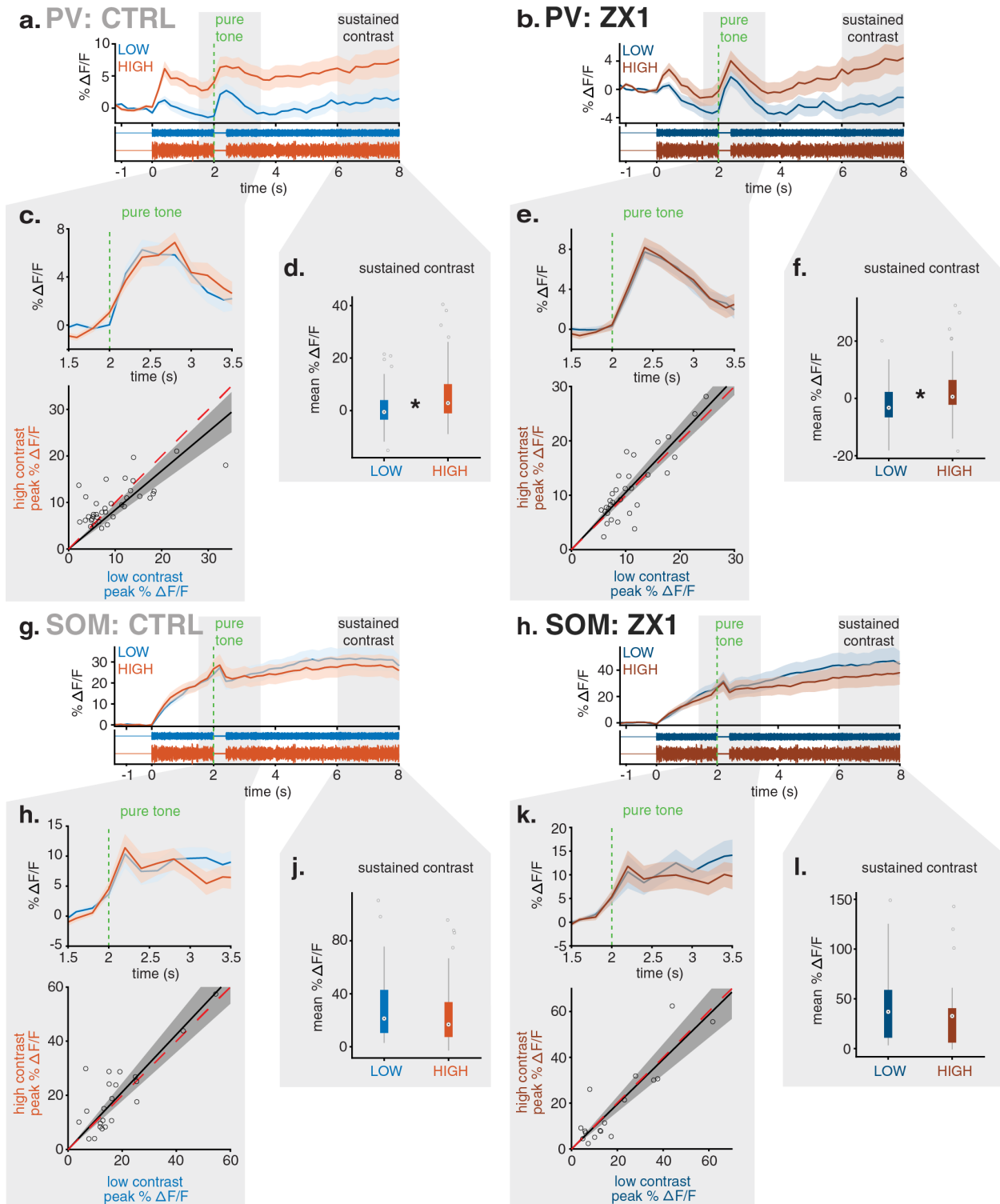


Figure 2-4: Zinc signaling does not have any contrast-dependent effects on either A1 PV or SOM cells

(a-b) Mean \pm SEM of % $\Delta F/F$ traces from PV cells before **(a)** and after ZX1 treatment **(b)** during low (blue) and high (red) contrast stimuli with a 400 ms pure tone occurring at 2 s. Baseline, F0, for % $\Delta F/F$ calculated

prior to DRC onset at -1.2 – 0 s. Bottom: representative sound voltage signals. (c,e) Top: Mean \pm SEM of % $\Delta F/F$ traces from PV cells during the pure tone epoch before (c, Top) and after (e, Top) ZX1 treatment calculated with F0 at 1 – 2 s. (c,e) Bottom: Scatterplot of each PV cell's mean peak % $\Delta F/F$ pure tone response in low vs high contrast before (c, Bottom) and after (e, Bottom) ZX1 treatment. (d,f) Boxplot of temporal averages of % $\Delta F/F$ responses from PV cells during the sustained contrast epoch at 6 – 8 s before (d) and after ZX1 treatment (f) for low (blue) and high (red) contrast. Asterisk (*) denotes $p < 0.05$ via permutation test. (g-l) Same as (a-f) but recorded in SOM cells. Black/gray coloring of regression lines and 95% confidence intervals denote no significant effect of contrast.

2.3.4 Zinc Signaling Suppresses Principal Neuron Responses Preceded by High, But Not Low, Sound Level Contrast

As our results show that zinc signaling is needed for the scaling of pure tone responses by sound level contrast, we further asked whether zinc contributes in a contrast-specific manner: is the effect of zinc signaling limited to responses following low contrast, high contrast, or both? To address this, we plotted average peak pure tone response amplitude across the principal cell population following low and high contrast DRCs before and after ZX1 injection (Figure 2-5a-c; 9 mice). Using a two-way ANOVA we compared the effect of the contrast and ZX1 factors on peak % $\Delta F/F$ responses. We observed significant main effects of both contrast ($F(1,166) = 28.74$, $p = 2.73e-7$) and ZX1 ($F(1,166) = 20.07$, $p = 1.39e-5$) with a significant interaction effect between the two ($F(1,166) = 31.04$, $p = 1.00e-7$). Bonferroni corrected post-hoc tests for multiple comparisons reveal that peak response amplitudes are significantly greater in low than in high contrast prior to (Figure 2-5a; $p = 1.22e-14$) but not after ZX1 injection (Figure 2-5a; $p = 0.31$). Importantly, ZX1 increased peak response amplitudes in high contrast (Figure 2-5a; $p = 1.12e-11$), but left amplitudes unaffected in low contrast (Figure 2-5a; $p = 0.58$). Scatterplots of peak pure

tone responses before vs. after ZX1 following low- (Figure 2-5b) or high (Figure 2-5c) contrast show that ZX1 did not affect peak responses in low contrast (Figure 2-5b; $p = 0.29$, $n = 176$, permutation test; slope 95% CI: 0.89 - 1.02) but increased peak responses in high contrast (Figure 2-5c; $p = 9.99\text{e-}6$, $n = 171$, permutation test; slope 95% CI: 1.09 – 1.25). To control for a potential effect of the injection pipette and the injection of a solution volume in cortex, we performed the same analysis before and after ACSF injection (Figure 2-5d; 6 mice). We solely observed a significant main effect of contrast ($F(1,81) = 32.47$, $p = 1.89\text{e-}7$) and no significant interaction effect between contrast and ACSF injection. Scatterplots of peak pure tone responses before vs. after ACSF injection following low- (Figure 2-5e; $n = 95$ cells) or high contrast (Figure 2-5f; $n = 84$ cells) showed that ACSF did not affect peak responses in either condition ($p > 0.05$, permutation tests). Together, these results suggest that zinc signaling suppresses pure tone responses specifically in high, but not low, contrast sound.

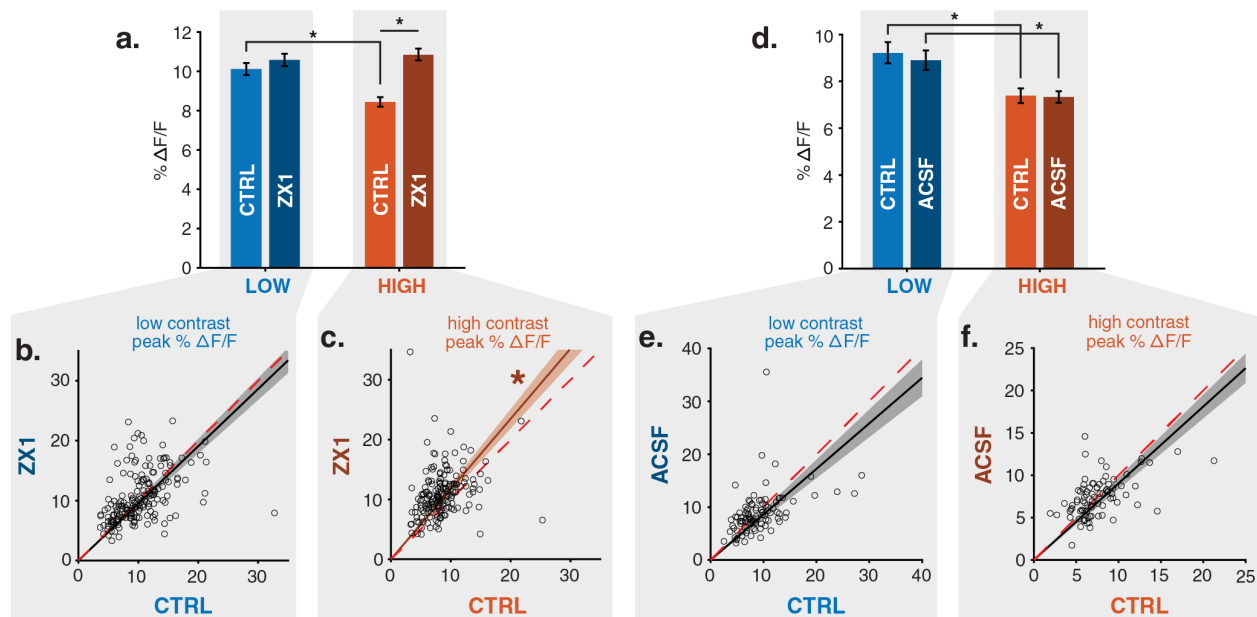


Figure 2-5: Zinc signaling suppresses A1 pure tone responses preceded by high- but not low sound level contrast

(a) Mean \pm SEM of principal cell peak pure tone $\% \Delta F/F$ responses preceded by 2 s of low (blue) and high (red) sound level contrast before (light shade; CTRL) and after (dark shade) ZX1 treatment. (b-c) Scatterplot of each cell's mean peak $\% \Delta F/F$ pure tone response before (CTRL, x-axis, light shade) vs after (y-axis, dark shade) ZX1 treatment in low (b) and high (c) contrast. Black/gray coloring of regression line and 95% confidence interval (on b) denote no significant effect of ZX1 treatment (slope 95% CI: 0.89 – 1.02). Significant ZX1 effect ($p = 1.12e-11$, permutation test) in (c) denoted by dark red asterisk (*) and fitted regression line with 95% confidence interval (slope 95% CI: 1.09 – 1.25). (d-f) Same as (a-c), but with ACSF treatment instead of ZX1. Black/gray coloring of regression lines and 95% confidence intervals (on e-f) denote no significant effect of ACSF treatment. Black asterisks (*) in (a,d) denote significant Bonferroni corrected post-hoc comparisons ($p < 0.001$).

2.4 Discussion

2.4.1 2-Photon Calcium Imaging Assay for Contrast Adaptation: Strengths and Limitations

To accommodate a 2-photon calcium imaging (2PCI) preparation we measured pure tone scaling by preceding contrast to assess contrast gain control. This approach is based upon an experiment in a seminal study using electrophysiology in ferret A1 reporting that responses to fixed test sounds within neurons' receptive fields are scaled by spectrotemporal contrast of a preceding sound context (Rabinowitz et al., 2011). Similarly, a more recent study from the same group revealed that, in single cells of mouse A1, excitatory post-synaptic potential evoked by broadband noise decreases when preceded by high contrast sound (Cooke et al., 2020). A calcium imaging approach allows for a large range of spatial scale thus enabling facile parcellation of auditory fields by tonotopy and anatomy on the mesoscale for A1 localization, as well as single cell resolution with cell-type specificity, via viral and transgenic targeting. These advantages come at the cost of temporal resolution. While the signal decay of the GCaMP6f calcium indicator (~1 s for one action potential) (Chen et al., 2013) may be resolved with spike deconvolution (Pachitariu et al., 2017), our recordings are still limited by a 5 Hz imaging frame rate, due to X-Y galvanometric laser scanning at 256 x 256 px. These constraints preclude the estimation of temporal kernels and accurate contrast adaptation time constants. We observed an effect of contrast on pure tone responses with a longer time scale than previously reported, >500 ms in Figure 2-1f vs. 86 – 157 ms (Rabinowitz et al., 2011). This discrepancy may be attributable to calcium signal decay from the DRC sound onset obscuring responses from earlier occurring pure tones.

Millisecond temporal resolution, as afforded by electrophysiology, allows for the simultaneous estimation of separable frequency and temporal kernels (Ahrens et al., 2008; Linden et al., 2003), as well as spectrotemporal contrast kernels, to evaluate temporal and spectral (frequency) regions within which a neuron is most sensitive to contrast changes (Rabinowitz et al., 2012). Our frame acquisition interval (200 ms) exceeds the reported temporal bandwidths of A1 neurons (Linden et al., 2003; Lohse et al., 2020), and thus precludes temporal kernel estimation. Assessing spectral contrast kernels with our 2PCI assay would require a separate stimulus trial for which contrast is low or high at individual frequency bins along the DRC bandwidth. For a given experiment, this would require a prohibitive number of trial repetitions for a sufficient frequency bin resolution. Thus, the analysis of frequency dependence in Figure 2-2 does not directly compare to spectral contrast kernels (Rabinowitz et al., 2012). Cell spectral contrast kernels correlate with cell frequency kernels; cells are most sensitive to changes in contrast, and thus show greater contrast gain control, along the frequency region at which they are most responsive (Rabinowitz et al., 2012). Here, because contrast extends across the full DRC bandwidth, we would expect to capture comparable contrast gain control among cells with different FRAs. Given this, our finding that contrast gain control is comparable between pure tone stimulus frequencies both near and away cell BFs Figure 2-2a is consistent with previous studies (Rabinowitz et al., 2012). Our results thus consider the frequency dependence between cell tuning and contrast effects on pure tone responses rather than frequency regions of the contrast bandwidth.

2.4.2 Heterogeneity in Scaling: Inclusion Criteria, Recording Depth, and Contrast Tuning

Despite the population effect of increased pure tone responses following low contrast, our results reveal heterogeneity in scaling: we observed cells that did not show contrast effects and

others showed increased pure tone responses following high contrast (Figure 2-1e and Figure 2-3c). This may be attributable to several factors such as inclusion criteria (see **Methods: 2PCI processing and analysis**), recording depth (Cooke et al., 2018), and potential tuning to contrast (Barbour and Wang, 2003). Previous studies that measured contrast gain control with either multi-unit (Cooke et al., 2020, 2018; Rabinowitz et al., 2011) or single-unit recordings (Lohse et al., 2020; Rabinowitz et al., 2012) included units based upon reliable firing-rate responses to the DRC stimuli (Rabinowitz et al., 2012). We include pure tone responses from single cells if they exhibit significant responses to pure tones when preceded by contrast. The dependence of our criterion to pure tone responses rather than strictly DRC responses could be excluding cells that exhibit contrast gain control not measurable by our non-parametric 2PCI assay. Our 2 SD significance criterion (see sections 2.5.8 and 2.5.10), for pure tone responses could also contribute to an underestimation of CGC. If gain reduces responses in high contrast below this threshold, the cell would not be included in analyses and thus measured CGC would be artificially lower. An underestimation of CGC could also result from saturation of the calcium imaging signal. Firing rates during the pure tone response in low contrast may saturate the fluorescence signal such that responses beyond the maximum fluorescence intensity of the imaging dynamic range within the 200 ms frame intervals would not be measurable. We would also expect a greater proportion of cells to exhibit pure tone response scaling by contrast if we extended our imaging plane below L2/3, due to both increases in tone evoked activity in layer 4 (Bowen et al., 2019) and increasing strength of contrast gain control in deeper cortical layers (Cooke et al., 2018). Furthermore, if the contrast tuning that is observed in marmoset ACtx (Barbour and Wang, 2003) extends to mouse ACtx, variability could also be explained by tuning to spectral contrast level, albeit not spectrotemporal. Additional experiments are needed to determine the presence of contrast tuning

in mouse ACtx and whether variability is captured by differences in auditory subfield (Barbour and Wang, 2003).

2.4.3 DRC Stimulus: Robustness and Comparison With Prior Studies

Contrast gain control in mouse ACtx is reliably elicited despite sound level and frequency differences in contrast DRC stimuli. Prior studies observed contrast gain control using DRC stimuli with average sound levels of 40 dB (Cooke et al., 2020; Lohse et al., 2020) and 80 dB (Cooke et al., 2018), both with a doubling of sound level range at high contrast (low Δ dB: 20, high Δ dB: 40). Our DRC stimuli are defined by a 55 dB mean, a tripling of sound level range from 10 dB in low to 30 dB in high, and narrower bandwidths, 5 – 52 or 5-25 kHz compared to 1 – 64 kHz, with narrower frequency intervals, $1/8^{\text{th}}$ and $1/12^{\text{th}}$ octave respectively vs. $1/4^{\text{th}}$ octave. Despite these differences, we observed significant response scaling by contrast (Figure 2-2b), further confirming the robustness of cortical contrast gain control.

2.4.4 PV Cells and A1 Sound Contrast Adaptation

Unique cell architecture and network dynamics (Litwin-Kumar et al., 2016; Sanzeni et al., 2020) in cortex likely necessitate additional adaptations to enable mean firing-rate invariance to contrast in principal cells (Lohse et al., 2020). Contrary to a recent study (Cooke et al., 2020), we observe a significant increase in mean PV population activity during high contrast DRC. With increasing contrast, elevated mean firing-rates in subcortical regions (Lohse et al., 2020) may become balanced at the cortical level by elevated PV activity. Upon a change from low to high contrast, initially elevated firing rates in ACtx become comparable to low contrast rates after a

~200 ms adaptation time (Lohse et al., 2020) (similarly shown in Figure 2-1j, but on a longer time scale). Cortical silencing leaves contrast gain control in IC and MGBv unaffected (Lohse et al., 2020), suggesting that contrast invariance serves cortical network stability rather than subcortical feedback. Without a cortical balancing mechanism, elevated firing rates in ACtx during high contrast could become exacerbated with recurrent excitation (Aponte et al., 2021; Reinhold et al., 2015), which is especially strong in superficial layers (Sadeh et al., 2017). Across sensory and motor areas, the inhibitory microcircuit architecture of cortex enables an inhibition stabilized network (ISN) regime (Kato et al., 2017; Litwin-Kumar et al., 2016; Sadeh et al., 2017; Sanzeni et al., 2020; Wehr and Zador, 2003) that may stabilize otherwise elevated activity during high contrast. The local inhibitory influence and peri-somatic principal cell innervation of PV cells compared to the broad influence and dendrite principal cell innervation of SOM cells (Kato et al., 2017) make PV cells well situated to modulate local excitation microcircuitry (Harris and Shepherd, 2015; Hu et al., 2014; Kato et al., 2017; Sanzeni et al., 2020). In anesthetized mice, Cooke et al. 2020 (Cooke et al., 2020) did not observe a population effect of contrast on mean putative PV firing rates; however, a third of recorded putative PV cells significantly increased firing rates during high contrast (Cooke et al., 2020). The discrepancy between those results and our observed population effect of contrast on PV cells may in part be explained by the suppressive effects of anesthesia on spike thresholds and spontaneous activity (Constantinople and Bruno, 2011; Sanzeni et al., 2020). The persistence of cortical firing-rate invariance to contrast despite anesthesia (Lohse et al., 2020) is consistent with ISN being robust to light anesthesia (Reinhold et al., 2015). If, however, PV activity in auditory cortex similarly follows principal cell activity with a threshold-linear function as has been shown in visual cortex (Atallah et al., 2012), lowered

principal cell firing-rates owing to anesthesia may not evoke sufficient PV activity for the population level effects of contrast.

2.4.5 Different Cellular and Neuromodulatory Mechanisms Underlie Cortical Contrast

Gain Control and Contrast Invariance

Our findings suggest that the two phenomena of contrast adaptation likely occur via separate mechanisms. Synaptic zinc solely affected contrast gain control, while leaving contrast invariance unaffected. Consistent with this and with recent findings negating inhibitory interneuron involvement in contrast gain control (Cooke et al., 2020), we observed no effect of contrast on pure tone responses from either PV or SOM interneurons. However, relating to contrast invariance, we observe sustained elevated mean PV activity during high contrast that persists in the absence of zinc signaling, which is necessary for cortical contrast gain control. Finally, in the IC, contrast gain control is present without contrast invariance (Lohse et al., 2020). Taken together, these points suggest that contrast gain control and contrast invariance are mediated by different mechanisms. Importantly, our findings reveal a zinc-dependent neuromodulatory mechanism for contrast gain control and point towards a PV-dependent and zinc-independent mechanism for contrast invariance in principal cells.

2.4.6 Zinc Signaling and Cell STRFs

Although we addressed the spectral tuning effects of ZX1 (Figure 2-3g-h), we were unable to estimate temporal kernels and thus complete spectrotemporal receptive fields (STRFs) due to the temporal resolution constraints of our calcium imaging acquisition rate (5 Hz). This precluded

an analysis of potential zinc effects on temporal tuning. Rabinowitz et. al. (2012) find that units are most sensitive to contrast within 50 – 100 ms of recent stimulation. In that study, the linear STRF, including the separable temporal kernel, is used for calculating the contrast kernel parameters of the non-linear input-output model. Thus, a change in temporal tuning could be pursuant to changes in temporal contrast tuning (Rabinowitz et al., 2012). However, given that the 2 second contrast context of our stimulus paradigm well exceeds both the temporal contrast kernel window and temporal bandwidth of A1 neurons, we would consider temporal tuning effects to be negligible using our 2PCI assay. Nonetheless, STRF estimations via cortical recordings with millisecond temporal resolution would provide a clearer picture of zinc's cell specific effects on spectrotemporal tuning.

2.4.7 Stimulus- and Context-dependent Effects of Zinc Signaling in Cortical Sound

Processing

Our results support that synaptic zinc signaling is necessary for contrast gain control in A1. The reported intracortical diffusion area of ZX1 is $2.1 \pm 0.1 \text{ mm}^2$, which was based on visualizing the spread of the extracellular red fluorescent dye Alexa-594, co-infused with ZX1 (Anderson et al., 2017). When this diffusion area is converted to radius ($0.8 \pm 0.2 \text{ mm}$), it suggests the spread of ZX1 is limited exclusively to cortex (Lein et al., 2007). The fact that this cortical zinc chelation eliminates contrast gain control in A1 supports that A1 sound contrast gain control is likely not simply inherited from the thalamus, but - importantly - even if inherited, it depends on cortical zinc for its implementation.

Zinc signaling decreases pure tone response amplitudes in principal cells specifically when they are preceded by high contrast DRC stimuli (Figure 2-5a,c). However, zinc signaling has no

effect on pure tones preceded by low contrast (Figure 2-5a,b). These results suggest a context-dependent effect of zinc signaling on cortical sound processing, likely due to context (experience)-dependent changes in synaptic zinc signaling. Sensory processing centers that express synaptic zinc (ZnT3) exhibit experience-dependent changes in vesicular zinc labeling, suggesting that the effects of synaptic zinc signaling can be activity-dependent (Brown and Dyck, 2005, 2002; Nakashima and Dyck, 2009). Indeed, we previously showed that synaptic zinc levels in DCN are decreased following exposure, and thus modulate glutamatergic neurotransmission in an experience-dependent manner (Kalappa et al., 2015; Vogler et al., 2020). Moreover, we discovered an mGluR-dependent mechanism underlying long-term synaptic zinc plasticity that is mediated by activity-dependent changes in zinc release upon different synaptic stimuli (Vogler et al., 2020). This synaptic zinc plasticity shapes long-term synaptic plasticity of glutamatergic neurotransmission in an activity-dependent manner (Vogler et al., 2020). Finally, synaptic zinc is a context-dependent modulator of short-term plasticity: at lower levels of activity, synaptic zinc reduces EPSC responses, but at higher levels, it inhibits responses during the first few stimuli, while enhancing responses during subsequent stimuli (Kalappa and Tzounopoulos, 2017). Together, these studies and the results presented here highlight that the effects of synaptic zinc signaling on neurotransmission and sound-evoked cortical responses are stimulus-, context- and activity-dependent.

Within this context, the zinc signaling effects on pure tone response amplitude shown here do not simply compare to our previous work (Anderson et al., 2017). For example, we previously showed that zinc signaling increases the response amplitude to 12 kHz pure tones in principal cells (Anderson et al., 2017), whereas here we show that zinc signaling decreases pure tone response amplitudes in high contrast sound. Similarly, with regard to PV and SOM cells, we previously

showed that zinc signaling decreases pure tone response amplitude (Anderson et al., 2017), whereas here we show that zinc signaling does not affect pure tone response amplitude in either PV or SOM cells (Figure 2-4c,e,h,k). The 12 kHz 0.5 s pure tones we used previously were preceded by silence (Anderson et al., 2017), whereas the pure tones used here were preceded by low or high contrast DRC stimuli lasting 0.5 – 2 s and consisting of a summation of 28 – 29 pure tone frequencies at varying sound level intensities. It is likely that the preceding sound context of low or high contrast DRC elicits activity-dependent changes in zinc signaling, including changes in the main targets of zinc signaling, such glutamatergic and GABAergic neurotransmission (Anderson et al., 2015; Kalappa et al., 2015; Kouvaros et al., 2020), or changes in zinc release (Vogler et al., 2020). For example, pharmacological blockade of glutamate NMDA receptors (NMDARs), changes the effect of zinc signaling on the amplitude of sound evoked responses in cortical principal neurons from excitatory to inhibitory (Anderson et al., 2017). Thus, it is possible that the inhibitory effect of zinc signaling on principal cell pure tone response amplitude in high contrast is attributable to differential NMDAR engagement during high vs. low contrast DRC stimuli. Thus, the ostensible incongruities of zinc signaling between this study and our previous ones are likely foremost explained by activity-dependent changes in zinc signaling induced by differences in the context within which the pure tone stimulus is delivered.

Regarding responses to the DRC sound onset, the lack of zinc effects on responses to the DRC sound onset compared to previously published effects zinc effects on pure tone stimuli (Anderson et al., 2017) may similarly be explained by stimulus-dependent changes in zinc signaling. The DRC stimulus persists for much longer than the isolated 12 kHz pure tone stimulus used in previous studies (Anderson et al., 2017) and includes multiple frequencies, and thus allows for adaptation and recruitment of a broader population of neurons and neural response properties.

Finally, the effect of zinc signaling on pure tone responses is sound level-dependent. In principal neurons, responses to pure tones at dB's below 70 are not affected by zinc signaling (Anderson et al., 2017). Here, the sound level of the DRC stimulus varies around a 55 dB mean at 25 ms intervals. Thus, the lack of a zinc signaling effect on responses to DRC sound onset is likely due to stimulus- and context-dependent effects of zinc signaling.

In our previous studies (Kumar et al., 2019), we found that the effect of zinc signaling on pure tone responses in principal cells depends upon the octave distance between the pure tone stimulus and the cell's best frequency (BF). Namely, zinc signaling increases pure tone response amplitude when tone frequencies are near cell BF, but decreases pure tone response amplitude when tone frequencies are away from cell BF. The low and high contrast DRC stimuli that preceded our pure tone stimuli consisted of a summation of 28 – 29 pure tone frequencies, both near to and away from cell BFs. Thus, one explanation for the observed inhibitory effect of zinc signaling in pure tone response amplitude in high contrast is that the effects of frequencies in the DRC that are away from cell BF may continue through to the pure tone onset and thus may influence cell responses to the pure tone stimulus. The high contrast dependence of this effect could be explained by the greater sound level deviations between frequencies in high contrast compared to low contrast (Figure 2-1b). Together, stimulus differences of context, frequency, level and duration preclude a 1:1 comparison with our prior studies, but highlight the stimulus and context dependent effects of zinc signaling in cortical sound processing. Given the importance of zinc signaling in cortical sound processing (Krall et al., 2021; McAllister and Dyck, 2017b) there is a need for further investigation on the various roles and mechanisms of stimulus-dependent zinc signaling on cortical processing, especially with the use of mouse lines that enable conditional knockout of synaptic zinc signaling in specific cortical cell types.

In summary, our results reveal that cortical synaptic zinc signaling is necessary for cortical sound contrast gain control, for specifically suppressing responses preceded by high contrast sound, while leaving responses preceded by low contrast sound unaffected. This study highlights the dynamic capacity for synaptic zinc to modulate cortical sound processing in a context-dependent manner. Cortical gain modulation serves various ends, including sensory adaptation (Rabinowitz et al., 2011), attention (Reynolds and Heeger, 2009), and compensation for hearing loss (Chambers et al., 2016). How synaptic zinc signaling contributes to each of these ends both in isolation and in combination significantly compels future studies.

2.5 Materials and Methods

2.5.1 Animals

Mice were handled, anesthetized, and sacrificed according to methods approved by the University of Pittsburgh Institutional Animal Care and Use Committees (IACUC). The approved IACUC protocol numbers that were employed for this study were: 17071036 and 17127808. We used 37 male and female mice for the experiments presented in the main figures and an additional 5 male and female mice for the experiment in Figure 2-1j. The genetic background of all mice was ICR/HaJ (Jackson Laboratory) for non-transgenic strains and C57BL/6J for all transgenic strains. Homozygous mice expressing Cre recombinase in parvalbumin (PV) or somatostatin (SOM) expressing cells (PV-Cre and SOM-Cre mice; Jackson Laboratory) were used for PV and SOM cell experiments (respectively). For Figure 2-3i-j, homozygous mice lacking the vesicular zinc transporter (ZnT3 (Cole et al., 1999); Jackson Laboratory), ZnT3-KO mice, were used along with

homozygous littermate controls, ZnT3-WT. Experiments using these mice were done blind to KO or WT designation. ZnT3-KO/WT mice were backcrossed with C57BL6/J mice at least 5 times from the founder line (Jackson Laboratory strain #005064) and thus considered congenic with C57BL6/J mice. Mice were injected between postnatal day (P) 24 and P30 for viral transduction of the GCaMP6f calcium indicator employed for *in vivo* non-anesthetized imaging experiments done at P38 – P49.

2.5.2 Stereotaxic AAV Injections

At P24 – P30 mice were induced to anesthesia with 3% isoflurane in oxygen, fastened on a stereotaxic frame (Kopf, Tujunga, CA), and maintained at 1.5% isoflurane for intracortical virus injections. A 30-gauge needle was used to bore a ~0.4 mm diameter craniotomy ~4 mm lateral to lambda above the right auditory cortex (ACtx). A pulled glass micropipette (1.2 mm OD, World Precision Instruments) was lowered 100 μ m below pia surface into cortex using a micromanipulator (Kopf) to deliver 600 nL of a GCaMP6f virus diluted in phosphate buffered saline (PBS). Putative principal cells expressing calcium/calmodulin-dependent protein kinase 2 (CaMKII) were targeted with AAV9.CaMKII.GCaMP6f.WPRE.SV40 (addgene 100834; 2-2.5 X 10¹³ GC/mL; diluted at 1:6 in PBS). Cre recombinase expressing cells in PV-Cre or SOM-Cre mice were targeted with AAV9.CAG.FLEX.GCaMP6f.WPRE.SV40 (addgene 100835; 2-2.5 X 10¹³ GC/mL; diluted 1:1 in PBS). The viral solution was delivered via tubing from a 5 μ L glass syringe (Hamilton, Reno, NV) backfilled with mineral oil and injected at a rate of 200 nL/min using a motorized syringe pump (World Precision Instruments, Sarasota, FL). The pipette was left in place for 1 min following injection. After retracting the pipette, the scalp surgical area was closed using cyanoacrylate adhesive and treated with triple antibiotic ointment. For analgesia, mice

were injected with 5 mg/kg carprofen intramuscularly following virus injection and 2 consecutive days post-surgery interperitoneally.

2.5.3 Acute Surgery Preparation For In Vivo Imaging

At P38 – P49 mice were induced to anesthesia with 3% isoflurane in oxygen then transferred to the imaging apparatus in a sound and light attenuating chamber and fitted into a head cone delivering 1.5% isoflurane in oxygen throughout surgical preparation. Body temperature was maintained at $\sim 37^{\circ}\text{C}$ via a heat pad with rectal thermistor. Ophthalmic ointment was applied to protect the eyes throughout anesthesia and 1% lidocaine was injected intramuscularly to numb the surgical site. The skull above the right temporal cortex was exposed with a ~ 1.5 cm incision in the scalp surrounding the right ear. The exposed skull was affixed to a custom imaging mount using cyanoacrylate adhesive and dental acrylic (Lang, Wheeling, IL) with the head at a 45° angle to the sagittal plane such that the pial surface of the right temporal cortex was perpendicular/transverse to the upright imaging optics. To minimize movement disturbance during imaging, the animal was positioned into a bottomless 50 mL tube (27 mm diameter). Dental acrylic around the affixed skull was formed into a reservoir centered around the imaging area to hold warmed artificial cerebrospinal fluid (ACSF). Contaminating zinc was removed during ACSF preparation by incubating with Chelex 100 resin (Biorad, Hercules, CA) for 1 hour. Chelex was removed by vacuum filtration and finally high purity calcium and magnesium salts were added (99.995% purity; Sigma-Aldrich, St. Louis, MO). The ACSF solution at pH 7.25 – 7.35 with an osmolarity of ~ 300 mOsm contained the following ingredients in millimolar concentration: 130 NaCl, 3 KCl, 2.4 CaCl₂, 1.3 MgCl₂, 20 NaHCO₃, 3 HEPES, 10 D-glucose.

2.5.4 Sound Stimulus Delivery

Sound was delivered from a calibrated free-field speaker (ES1, Tucker Davis) situated 10 cm from the animal's left ear. Speaker calibration was performed to create a flat speaker response across all frequencies comprising the dynamic random chord stimuli (see *DRC stimuli*). For calibration, microphones with attached pre-amps (1/8 in. 4138-A-015 and 1/4 in. 4954-B, Brüel and Kjær) were calibrated to a 1 kHz pure tone at 94 dB SPL from a reference sound calibrator (Type 4231, Brüel and Kjær) and positioned in the same location as the animal's left ear. Sound stimuli were generated and output voltage was scaled according to calibration data using custom MATLAB (MathWorks, Natick, MA) scripts employing the signalObject library for compatibility with the Ephus software (Suter et al., 2010) that was used for sound delivery and synchronized epifluorescence imaging. Digital sound signals were converted to analog output at 250 kHz (USB-6229, National Instruments) and sent to the ES1 speaker via an ED1 speaker driver (Tucker Davis).

2.5.5 Widefield Epifluorescence Imaging and Analysis for A1 Localization

After surgical preparation, transcranial sound evoked epifluorescence responses were recorded a minimum of 10 minutes following cessation of isoflurane delivery to localize ACtx and tentatively identify subfields by tonotopic gradients (Anderson et al., 2017; Linden et al., 2003) for mapping a craniotomy for 2-photon imaging. Mice were then re-anesthetized with isoflurane and a ~ 2 mm² craniotomy was made surrounding A1 by scoring the skull with an 18 G syringe needle. Again, at least 10 minutes following isoflurane cessation and with the skull above the 2-photon imaging area removed, A1 was more precisely localized using the same approach. For mapping tonotopic gradients we presented 5 – 6 kHz pure tones at 60 dB SPL while illuminating

the imaging area with a blue LED (nominal wavelength, 470 nm; M470L3, Thorlabs). We imaged GCaMP6f emission under a 4X objective (Olympus, Center Valley, PA) through a GFP filter (BrightLine GFP-A-Basic, Semrock) using a cooled CCD camera (Retiga 2000R, Q-imaging, Surrey, BC, Canada). Images were acquired with a 20 Hz frame rate at a resolution of 200 x 150 pixels using 8X spatial binning. Each pixel covered an area of 171.1 μm^2 .

For evaluating tone evoked epifluorescence responses, we calculated normalized fluorescence change from pre-stimulus baseline (F_0) at each pixel ($\Delta F/F = (F - F_0)/F_0$). Pre-stimulus baseline was calculated from a one second average of fluorescence intensity prior to pure tone onset (at 2-3 seconds during imaging). To assess sound responsive regions, we applied a two-dimensional 5 Hz low-pass 4th order Butterworth filter to 10 consecutive frames of % $\Delta F/F$ values following pure tone onset, then averaged frames across time. This post-stimulus (5 – 6 kHz pure tone) temporal average reveals two salient sound responsive regions corresponding to the low frequency tonotopic areas of A1 and the anterior auditory field (AAF) as well as smaller less responsive secondary areas ventral to A1 and AAF (Anderson et al., 2017; Linden et al., 2003).

2.5.6 DRC Stimuli

Dynamic random chord (DRC) stimuli were generated to have high or low spectrotemporal sound level contrast with the same mean sound level. DRCs consisted of 28 pure tone frequencies between 5 – 51.874 kHz at 1/8th octave intervals (all Figures) or 29 pure tone frequencies between 5 – 25 kHz at 1/12th octave intervals (Figure 2-2 onwards; see **Results**). For a single chord lasting 25 ms, sound levels for each frequency were sampled from a uniform distribution. Sound levels for low contrast DRC were sampled from a narrow uniform distribution between 50 to 60 dB SPL (± 5 dB; $\sigma_L \approx 2.9$ dB SPL), while sound levels for high contrast DRC were sampled from a wider

distribution between 40 to 70 dB SPL (± 15 dB; $\sigma_L \approx 8.7$ dB SPL). Both distributions had the same 55 dB SPL mean (Figure 2-1). Pure tones were scaled to output voltage with respect to sampled intensity via speaker response calibration data, then summed across frequency to result in a ‘chord’. Chord amplitude was enveloped with $1/4^{\text{th}}$ \sin^2 and \cos^2 ramps lasting 5 ms for onset and offset respectively. Chords were then concatenated across time to generate DRC sound stimuli lasting 8 s. At 0.5 s or 2 s chord amplitude was set to 0 V for 400 ms and instead a 70 dB SPL pure tone lasting 400 ms was inserted within this gap (Figure 2-1c: bottom). Four stimuli were generated for each pure tone frequency (5 – 51.874 kHz at $1/8^{\text{th}}$ octave intervals), contrast (low, high) and onset (0.5, 2 s) combination.

2.5.7 2-photon Calcium Imaging (2PCI)

We imaged sound evoked responses from single cells with 2PCI before (control; CTRL) and after injecting ZX1 (Pan et al., 2011) (a fast extracellular high-affinity zinc-specific chelator) solution or ACSF solution. Prior to imaging we inserted a pulled glass micropipette just below the pial surface at the edge of the craniotomy within ACtx. The pipette contained 100 μM ZX1 and 50 μM AlexaFluor 594 in ACSF (herein referred to as ‘ZX1 solution’) or just 50 μM AlexaFluor 594 in ACSF (herein referred to as ‘ACSF solution’) and was backfilled with mineral oil and connected to a 5 μL glass syringe mounted in a motorized syringe pump (World Precision Instruments). After a minimum of 20 minutes following cessation of isoflurane, we imaged neurons in L2/3 of A1 at a depth of 180 – 250 μm . We delivered mode-locked 940 nm infrared laser light (MaiTai HP, Newport) at 100 – 200 mW intensity through a 40X 0.8 NA objective (Olympus) using X-Y galvanometric scanning with a motorized moveable objective microscope (Sutter MOM, Novato, CA) focused on the craniotomy of the animal on a fixed stage. Green

fluorescence signal from GCaMP6f emission was amplified using a photomultiplier tube (PMT; Hamamatsu H10770PA-40) behind a green emission filter (FF03-525/50, Semrock) and dichroic splitter (Di02-R561, Semrock). PMT, galvanometric scanning, and shutter signals passed through a BNC-2090A breakout (National Instruments) to a PCI-6110 data acquisition card (DAQ; National Instruments) that was controlled with ScanImage 5.3 (Vidrio Technologies) software and synchronized via hard wire to the stimulus delivery DAQ using the NI-DAQmx driver with a MATLAB API. We collected 145 X 145 μm images at 256 X 256 pixel resolution at an effective frame rate of 5 Hz.

2.5.8 FRA Mapping

For each experiment we first mapped frequency response areas (FRAs) of the neurons in the imaging field. We presented pure tones (linearly ramped at 10 ms) comprising the dynamic random chord stimulus (5 – 51.874 kHz; see *DRC Stimuli*) lasting 400 ms at intensities of 30, 50, and 70 dB SPL, occurring at 0.6 s or 1 s within a 3 s inter-stimulus-interval window. We presented a minimum of 4 repetitions of each frequency/intensity combination across several 3 min imaging intervals separated by laser off periods lasting a minimum of 30 s. We then performed an *ad hoc* analysis to quickly determine a pure tone frequency that elicits the maximum $\Delta F/F$ response across an average of all cell FRAs collapsed across stimulus intensity. Using custom scripts written in MATLAB, ellipses were drawn around all non-overlapping cells in plane having a visible ‘doughnut’ shaped fluorescence signal. Normalized fluorescence change from pre-stimulus baseline ($\Delta F/F = (F - F_0)/F_0$) was calculated for each cell from mean fluorescence intensity signal within the ellipse bounds (F). Pre-stimulus baseline (F_0) was calculated as the average cell fluorescence signal (F) across a 600 ms baseline prior to pure tone onset. Significant peak $\Delta F/F$

responses were calculated as maximum $\Delta F/F$ values within an 800 ms window following pure tone onset that are greater than or equal to 2 standard deviations above F_0 . Significant peak $\Delta F/F$ responses for each cell were averaged across stimulus intensity then averaged across cells to determine the pure tone frequency eliciting the maximum response across cells. For the contrast adaptation assay, this pure tone frequency was then presented following 0.5 or 2 s of contrast DRC sound (see next section). For determining best frequency (BF) and final cell FRA, FRA mapping data were re-analyzed *post hoc* with non-rigid motion- and neuropil- correction (as were contrast assay data) as described in *2-photon calcium imaging: processing and analysis*. BF for a given cell was determined as the frequency eliciting the largest amplitude significant peak $\Delta F/F$ response averaged across the stimulus intensities.

2.5.9 Contrast Adaptation Assay

For each experiment, a given pure tone frequency (as determined during *ad hoc* FRA mapping; see previous section) was presented in each contrast (low, high) and onset (0.5 s, 2 s) combination in a pseudorandom fashion. For each imaging trace, the DRC sound stimulus was both preceded and followed by 4 s of silence. Traces were interleaved by laser off periods of pseudorandom duration lasting 25 – 35 seconds. A minimum of 8 repetitions of each parameter combination was presented both before and after intracortical injection of ZX1- or ACSF- solutions into ACtx. Solutions were infused at 30 nL/min to 600 nL for 20 minutes during which the microscope objective was periodically adjusted to maintain cell position. Post-injection recordings followed once solutions diffused within A1 and the syringe pump was adjusted to 9 nL/min. Following 2PCI, solution diffusion (containing AlexaFluor 594) was confirmed with 4X widefield epifluorescence imaging of the craniotomy using a green LED (nominal wavelength,

530 nm; M530L3, Thorlabs) and Texas Red filter (BrightLine TxRed-A-Basic, Semrock). Mice were then sacrificed and tails from transgenic mice were saved for genotype confirmation.

2.5.10 2-Photon Calcium Imaging (2PCI): Processing and Analysis

For a given experiment, 2PCI frames were concatenated for all traces across time and aligned using non-rigid motion correction via the NoRMCorre MATLAB toolbox (Pnevmatikakis and Giovannucci, 2017). Ellipses were manually drawn around cells (as described in *FRA mapping*) and contamination from surrounding neuropil (in the form of time varying fluorescence intensity) obtained using the FISSA Python toolbox (Keemink et al., 2018) was scaled by 0.8 (Chen et al., 2020; Kerlin et al., 2010) and removed to obtain motion- and neuropil- corrected average fluorescence intensity across time for each cell. Solely non-overlapping cells deemed tone responsive were included for further analysis. We used a tone sensitivity index, d-prime (d'), to identify tone responsive cells ($d' \geq 0$) as described in Romero et al 2020 (Romero et al., 2019). Briefly, for a given cell FRA, we calculated average response amplitude from responses at and immediately adjacent to the frequency/level combination eliciting the maximum response (average of 5 values if maximum response at dB < 70, 4 values if not). We then averaged the same number of values selected at random frequency/level locations of the FRA. We took the difference of these averages and iterated this process 1000 times. The tone sensitivity index, d-prime (d'), was calculated as the average of the iterated differences. Normalized baseline subtracted fluorescence traces ($\Delta F/F = (F-F_0)/F_0$) were calculated for each stimulus parameter combination for each stimulus epoch (DRC onset, pure tone onset, DRC offset) using a corresponding fluorescence baseline (F_0) as discussed later in the corresponding **Results** section. Solely significant peak $\Delta F/F$ pure tone responses, as calculated in *FRA mapping*, were included in pure tone response analyses.

2.5.11 Statistical Analysis

All statistical analyses were performed in MATLAB. Contrast scaling factors and % $\Delta F/F$ data are presented as mean \pm SEM, except where a boxplot is noted. For a given analysis, an Anderson-Darling test was first performed to determine whether data arose from a normal distribution. Data that failed to reject the null hypothesis were considered normally distributed. In this case, one sample t-tests were used to determine significance in single samples. For two sample comparisons, paired and unpaired t-tests were used for within- or between- subject data respectively. All t-tests were two-tailed. For comparison between multiple groups having within-subject factors (Figure 2-5a,d), a repeated-measures two-way analysis of variance (ANOVA) test was used. Bonferroni corrections were used in the case of multiple two-sample *post hoc* comparisons among a group of samples; the significance level ($\alpha = 0.05$) of the test was corrected via scaling by the reciprocal of the number of comparisons. Non-parametric comparisons were used on data for which the Anderson-Darling null hypothesis was rejected. The Wilcoxon signed-rank test was used for one-sample comparisons. A permutation test (Wasserman, 2004) was used for two sample comparisons. Samples for which fewer than 5,000 out of 100,000 random permutations of the data resulted in mean differences greater than the observed difference in sample means were considered significant ($p < 0.05$).

3.0 Chapter 2: Pupil-indexed State Effects on Cortical Adaptation to Sound Contrast and Cortical Neuromodulatory Effects on Sound Contrast-dependent Changes in Pupil Size

3.1 Overview

In consistent lighting, changes in pupil size can reveal inner states such as emotion and cognitive effort. Such states comprise a complex interaction of internally generated and externally driven factors that both influence and are shaped by sensory processing. Pupil size fluctuations in the absence of sensory stimuli (stimulus-independent), such as with wakefulness, are associated with spontaneous changes in internal brain state. Cortical states at intermediate pupil sizes are optimal for sensory encoding (McGinley et al., 2015a, 2015b). Within this range, sound response gain and cell excitability are maximal in auditory cortex. It is unknown how such changes to sensory processing at these pupil-indexed internal states interact with sensory adaptation to sound contexts. Here we show that the strength of adaptation to increased sound level variance across time and frequency, sound level contrast, is similarly maximal at intermediate pupil sizes. This adaptation to contrast involves a well described decrease in neural response gain termed contrast gain control. Although present subcortically, auditory cortex is necessary for contrast gain control dependent behavior. Further, our recent work shows that synaptic zinc neuromodulatory signaling is necessary for cortical contrast gain control. Here, we show that increased sound contrast evokes larger pupil responses and that this difference in stimulus-dependent pupil responses, like contrast gain control, relies upon cortical zinc signaling. Together, these results suggest that pupillometry can be used to predict internal brain states that are optimal for sensory adaptation, and importantly, may serve as a non-invasive clinical marker for disrupted zinc dependent sensory processing.

3.2 Introduction

Large dilations and constrictions of the pupil act as an aperture in adjusting to light intensity. In consistent lighting, however, pupil size still fluctuates in smaller degrees and can reveal changes in emotion, task engagement and cognitive effort (Joshi and Gold, 2020; Kuchinsky et al., 2016; Saderi et al., 2021; van der Wel and van Steenbergen, 2018; Winn et al., 2015; Zekveld et al., 2011). These states reflect a complex intersection of internally generated and externally driven factors that both influence and are shaped by sensory processing. Spontaneous changes in internal brain state, such as with wakefulness, may be indexed by stimulus- and task- independent changes to baseline pupil diameter (PD) when measured in consistent lighting. Within the intermediate baseline pupil size range, cortical membrane potential and spontaneous activity are most permissive to sensory encoding. For example, in the auditory cortex (ACtx), at this range, sound response gain and cell excitability are maximal (McGinley et al., 2015a, 2015b; Saderi et al., 2021). However, it is unknown how pupil-indexed changes in brain state and concomitant changes to sensory encoding interact with sound contexts and neural adaptation to those contexts.

Pupil size increases in response to external sound stimuli. Stimulus changes such as an increase in sound loudness, complexity, or salience, and resultant changes in sensory processing, yield evoked pupil responses (Liao et al., 2016; Montes-Lourido et al., 2021; Warda and Pandey, 2020; Zekveld et al., 2018). However, it is unclear which stages of the ascending auditory pathway contribute to these evoked pupil response differences. If instead sound stimuli are kept consistent, but neural physiology and sensory processing is altered, such as with schizophrenia and dementia, sound evoked pupil responses are also altered (Zekveld et al., 2018). This serves as further evidence of sensory processing driven changes to pupil size, and importantly highlights pupil as a marker for disrupted sensory processing (Montes-Lourido et al., 2021).

The auditory sensory system adapts to sound contexts efficiently by adjusting neural response properties to the probability of sound levels in the context, the sound level statistics. Adaptation to increasing variance of sound levels across frequency and time (contrast) is achieved by a decrease in the slope (gain) of the sensory input to neural output relationship (King and Walker, 2020; Rabinowitz et al., 2011). The change in gain maintains dynamic range across a broader range of sound levels at the cost of sensitivity to sound level differences (Angeloni et al., 2021; Lohse et al., 2020). This sensory adaptation, termed contrast gain control (CGC), is evident in the ascending auditory pathway from IC, to thalamus, and into ACtx (Lohse et al., 2020). ACtx is required for behavior that relies upon CGC (Angeloni et al., 2021). Additionally, our group recently found that CGC in ACtx depends upon cortical synaptic zinc neuromodulation using a combined pharmacological and transgenic approach to inhibit zinc signaling (*Chapter 1*, section 2.0). Given this understanding of the cortical sensory processing involved in a specific form of sensory adaptation, we are better able to study how such processing relates to changes in pupil size.

To study the contribution of stimulus-independent changes in pupil-indexed brain state to sensory adaptation we paired pupillometry with a 2-photon imaging assay of CGC in ACtx. We then used the same preparation but disrupted cortical CGC by manipulating synaptic zinc to explore cortical sensory processing driven changes to sound stimulus-dependent pupil responses. Our results support that adaptation to sound contrast is strongest at an intermediate pupil range where sound responses are maximal. Importantly, our data suggest that cortical neural adaptations and cortical synaptic zinc signaling influence changes in PD in response to changing sound contrast.

3.3 Results

3.3.1 Contrast Gain Control is Greatest at Intermediate Pupil Diameter

Because cortical gain is associated with pupil diameter (PD) (McGinley et al., 2015a; Schwartz et al., 2019), we investigated whether contrast gain control (CGC) (Angeloni et al., 2021; Lohse et al., 2020; Rabinowitz et al., 2011), similarly varies in strength with PD. To address this, we recorded PD during a 2-photon calcium imaging (2PCI) assay for CGC. Specifically, we asked if PD prior to sound onset (Figure 3-1a-c, gray box) is associated with CGC magnitude (Figure 3-1b; representative animal). Briefly, we presented low (± 5 dB; blue) and high (± 15 dB; red) contrast sound with a 70 dB pure tone occurring at 2s (Figure 3-1a) while recording single cell fluorescence responses with 2PCI (Figure 3-1b) and PD (Figure 3-1c). Previous studies show that pure tone responses depend on PD (Lin et al., 2019; McGinley et al., 2015a). Our stimuli differ, in that pure tones are instead preceded by 2 s of DRC sound. Thus, we first plotted peak pure tone response amplitude regardless of contrast (Figure 3-1d) to determine whether pupil-indexed state effects are similar despite the added 2 s of DRC sound. Comparable with previous studies (Lin et al., 2019; McGinley et al., 2015a), responses are largest at pre-stimulus PDs within the intermediate range of an animal's PD (relative to maximum animal PD; $p = 2.30e-11$, Kruskal-Wallace one-way ANOVA, 344 cells from 10 animals). In further agreement with prior studies, increased trial-to-trial consistency in cell temporal response profiles, reliability, coincides with increased response amplitudes at intermediate PD (Figure 3-1e; reliability calculated as average zero lag trial-to-trial cross correlation between all pairs of pure tone response $\Delta F/F$ traces at 2 – 3.2 s; $p = 4.95e-13$, Kruskal-Wallace one-way ANOVA). Thus, despite 2 s of DRC sound preceding the pure tone (Figure 3-1a), our assay replicates previously observed the effects of pre-

stimulus PD on cell pure tone response amplitude and reliability (Lin et al., 2019; McGinley et al., 2015a).

We next probed pre-stimulus PD effects on CGC magnitude. We assessed CGC as described in *Chapter 1*, Section 2.3.1 and shown in Figure 2-1d: the contrast scaling factor is defined as the population mean of individual cell average peak responses in low- divided by average peak responses in high contrast. Plotting contrast scaling factors across the same pupil measure reveals that the magnitude of CGC is similarly largest at intermediate pre-stimulus PD (Figure 3-1f; $p = 5.94e-4$, Kruskal-Wallis one-way ANOVA). That CGC magnitude changes with pre-stimulus PD (Figure 3-1f) suggests that the pre-stimulus effects of PD on pure tone response amplitude (seen in Figure 3-1d) differ between low and high contrast. To explore such contrast-dependent effects of PD, we plotted peak pure tone $\Delta F/F$ responses with regard to contrast across pre-stimulus PD (Figure 3-1g) and performed a 2-way ANOVA. We again observed a significant effect of pre-stimulus PD on response amplitude (Figure 3-1g; $F(6,1815) = 22.80$, $p = 4.76e-26$). Consistent with CGC we observed a significant effect of contrast ($F(2,1815) = 8.18$, $p = 4.3e-3$) on pure tone response amplitude. Notably, we found a significant interaction between contrast and pre-stimulus PD range ($F(6,1815) = 3.41$, $p = 2.4e-3$). Consistent with Figure 3-1f, the effect of pre-stimulus PD on pure tone response amplitude depends on sound contrast. Thus, contrast-dependent effects of pre-stimulus PD on pure tone response amplitude may in part explain the change in CGC magnitude with pre-stimulus PD (Figure 3-1f).

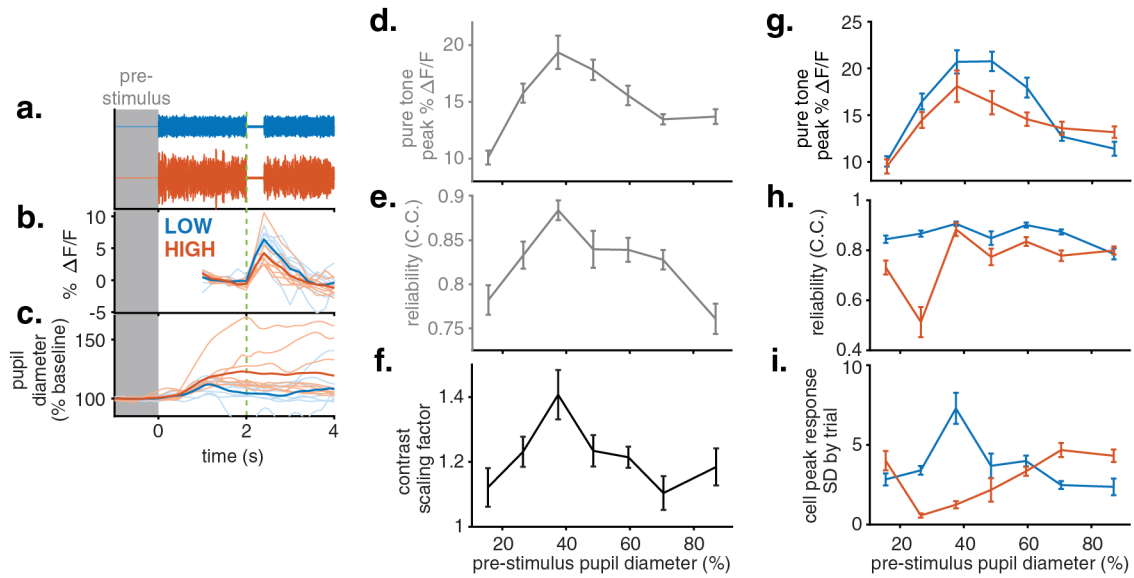


Figure 3-1: Contrast dependent pupil-indexed cortical state effects on A1 principal cell response properties

(a) Representative sound voltage signals of low (blue) and high (red) contrast DRC stimuli with a 400 ms pure tone occurring at 2 s. Gray box denotes pre-stimulus epoch. **(b-c)** Representative 2PCI and pupil traces from the same animal and stimuli. Thick lines are the mean of the thin line traces. **(b)** Pure tone % $\Delta F/F$ responses from a representative cell calculated with F_0 at 1 – 2 s. **(c)** Sound evoked pupil responses as percentage of average pupil diameter (PD) during pre-stimulus epoch (gray). **(d-i)** A1 principal cell response properties binned by the pre-stimulus PD at which responses occurred. Pre-stimulus PD is calculated by animal as mean pre-stimulus PD percentage of max animal PD across entire experimnt. **(d)** Mean \pm SEM of peak pure tone % $\Delta F/F$ responses from combined contrast conditions. **(e)** Mean \pm SEM of cell reliability (trial-to-trial cross correlation of pure-tone % $\Delta F/F$ response). **(f)** Mean \pm SEM of contrast scaling factors. **(g-h)** same as **(d-e)**, but with regard to contrast condition. **(i)** Mean \pm SEM of standard deviation of cell peak % $\Delta F/F$ pure tone responses with regard to contrast.

However, at the pre-stimulus PD range at which CGC is maximal (Figure 3-1f, at pre-stimulus PD of 32 – 43%, 3rd data point from the left), pure tone response amplitudes do not significantly differ between low and high contrast (Figure 3-1g, at pre-stimulus PD of 32 – 43%, 3rd data points from the left), as would have been expected. The contrast scaling factor measure of CGC (Figure 3-1f) is calculated from each cell's average peak response in low contrast divided by its peak response in high contrast, whereas responses in Figure 3-1g are not paired ratios by cell. The discrepancy between Figure 3-1f and g may thus be partly attributable to response variability between cells. We further explored cell response variability between contrast conditions in terms of reliability (Figure 3-1h): trial-to-trial consistency in temporal response profiles; and in terms of peak response variation: standard deviation (SD) cell peak $\Delta F/F$ response between trials (Figure 3-1i).

Pure tone response reliability does not differ between contrast within the PD range at which CGC is maximal (Figure 3-1f and h). Both contrast conditions have comparably consistent temporal response profiles between trials (reliability). However, we did observe overall significant effects of both PD and contrast ($F(6,1181) = 13.97$, $p = 2.12e-15$; $F(1,1181) = 68.46$, $p = 3.45e-16$) on response reliability (Figure 3-1h) and a significant interaction between the two factors ($F(6,1181) = 10.35$, $p = 3.36e-11$). Thus, although pre-stimulus PD has contrast-dependent effects on reliability overall, these effects are not associated with increased CGC magnitude.

The pre-stimulus PD range at which CGC is maximal (Figure 3-1f) coincides with the largest difference in pure tone response amplitude variability (peak response SD) between low and high contrast (Figure 3-1i) ($p = 8.86e-17$, Bonferroni corrected post-hoc pairwise test; PD effect: $F(6,1815) = 4.02$, $p = 5.19e-4$; contrast: $F(1,1815) = 9.65$, $p = 1.9e-3$; interaction: $F(6,1815) = 17.92$, $p = 2.76e-20$). Taken together, these results suggest that contrast-dependent effects of pre-

stimulus PD on pure tone response variability contribute to the maximal CGC observed at an intermediate PD range.

3.3.2 Contrast Gain Control Does Not Depend on Stimulus-dependent Pupil Responses to Contrast Sound

Having explored stimulus-*independent* (pre-stimulus) PD effects on CGC magnitude (Figure 3-1), we next explored whether stimulus-*dependent* changes in PD affect CGC magnitude. The contrast DRC sound stimulus results in an increase in PD upon stimulus onset at 0 s (Figure 3-2a). PD responses to high contrast sound are significantly larger than those in low contrast across a temporal average of the DRC stimulus (0 – 8 s; Wilcoxon rank sum test, $p = 0.0086$) (Figure 3-2b). Thus, we asked if PD responses to contrast DRC significantly affect pure tone response amplitude. To evaluate this we used a linear mixed-effects approach to model cell pure tone responses as a function of pre-stimulus pupil diameter (pre-stimulus_PD), sound evoked pupil responses (average PD at 1 – 2 s during the DRC sound stimulus; pupil_at_1-2s), and their interaction with sound contrast (Figure 3-3). We fit a linear mixed-effects model to peak pure tone responses with a fixed effect of contrast and random-intercept effects of subject, pre-stimulus PD, and average PD at 1 – 2 s during the DRC sound stimulus (Figure 3-3a). The model in Wilkinson notation is as follows: $\text{peakPureToneResponse} \sim \text{pre-stimulus_PD} + \text{contrast} * \text{pupil_at_1-2s} + (1 | \text{subject}) + (1 | \text{pre-stimulus_PD}) + (1 | \text{pupil_at_1-2s})$. We analyzed the contribution of these input factors using a coefficient test to test whether they significantly contribute to predicting cell pure tone responses (Figure 3-3b). Pre-stimulus pupil size was the only model coefficient that significantly differed from zero and thus pre-stimulus pupil size contributed to cell responses ($F(1,213.44) = 10.132$; $p = 0.00168$). Neither sound evoked pupil responses ($F(1,379.68) = 0.672$;

$p = 0.413$), nor their interaction with contrast ($F(1,282.32) = 0.0769$; $p = 0.781$) contributed to predicting cell pure tone responses. To further validate this, using a likelihood ratio test, we compared the full aforementioned model with a null model that solely includes pre-stimulus PD as a predictor (Figure 3-3c). The null model in Wilkinson notation is as follows: $\text{peakPureToneResponse} \sim \text{pre-stimulus_PD} + (1 | \text{subject}) + (1 | \text{pre-stimulus_PD})$. The fuller model including sound evoked pupil responses and their interaction with contrast did not significantly improve cell pure tone response prediction ($p = 0.333$). Thus, although PD responses to DRC sound are contrast-dependent, these data suggest CGC is not linked to stimulus-dependent changes in PD.

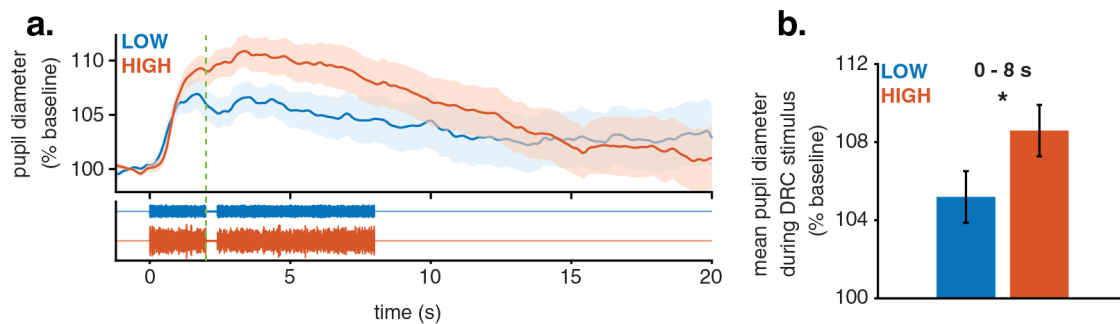


Figure 3-2: High sound contrast evokes larger pupil responses that return to baseline after sound offset

(a) Mean \pm SEM of contrast DRC sound evoked pupil traces as percentage of average pupil diameter (PD) during pre-stimulus epoch. Pure tone (400 ms) onset denoted by dotted green line. (b) Mean \pm SEM of average PD across duration of DRC stimulus (0 – 8 s) in each contrast condition. Asterisk (*) denotes $p < 0.05$.

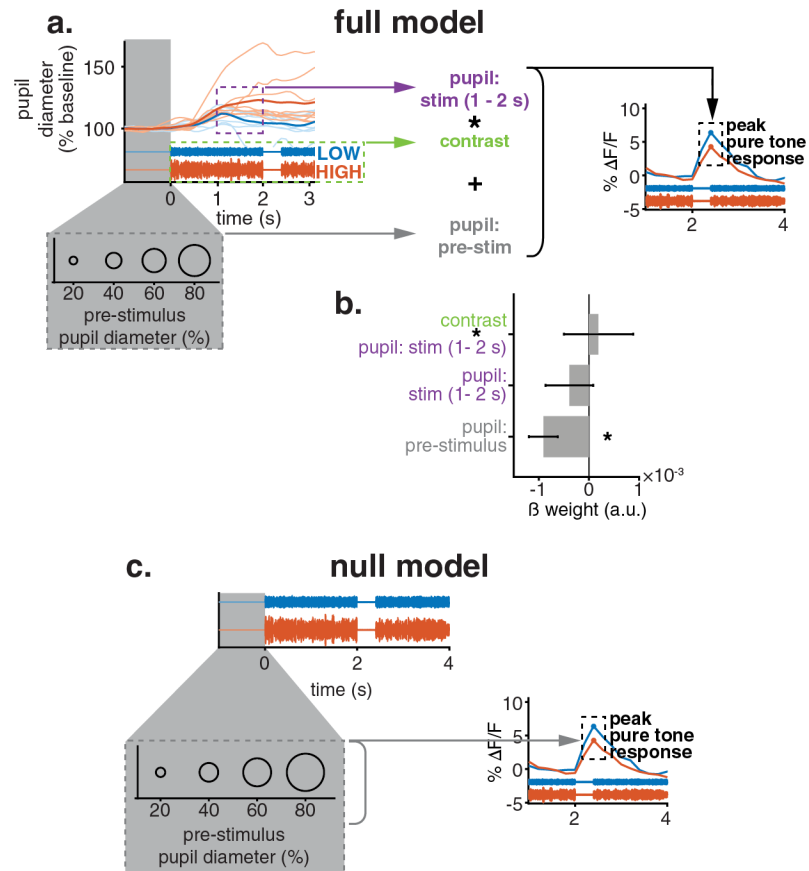


Figure 3-3: Contrast-dependent changes in PD do not contribute to contrast gain control

(a) Depiction of full linear mixed-effects model input factors (left) for assessing contribution to prediction of cell peak pure tone response output (right). (b) Coefficient weights of full model factors depicted in (a). (c) Depiction of null linear mixed-effects model consisting solely of pre-stimulus pupil size factor for comparison to full model via likelihood ratio test.

3.3.3 Synaptic Zinc Signaling Contributes to Increased Pupil Responses in High Contrast Sound

We observed larger evoked pupil responses to high contrast DRC stimuli beginning at 1 s and continuing throughout the DRC stimulus (Figure 3-2, also Figure 3-1c) that returned to low contrast pupil levels upon stimulus cessation (Figure 3-2). Recent work shows that cortex is necessary for sound detection in low and high contrast backgrounds (Angeloni et al., 2021). We thus, asked whether cortical CGC contributes to contrast-dependent changes in PD. While Figure 3-1 shows that CGC depends upon pre-stimulus pupil-indexed state, we are now exploring the reverse direction, whether contrast-dependent changes in sound evoked pupil responses are associated with A1 CGC. Previously, we reported that A1 principal cell response adaptation to high contrast sound depends upon synaptic zinc. We thus tested if synaptic zinc dependent CGC in A1 contributes to sound contrast effects on PD.

To assess the contribution of cortical zinc signaling to contrast effects on evoked pupil responses, we recorded evoked pupil responses to low and high contrast DRC stimuli before (Figure 3-3a, control) and after intracortical injection of ZX1, an extracellular high affinity zinc-specific chelator, into AC (Figure 3-3a, ZX1). To control for the gap in the DRC stimulus containing the pure tone (Figure 3-2a, bottom), we recorded PD using DRC stimuli without a pure tone (Figure 3a, bottom). To quantify the effect of contrast and ZX1 on PD, we fit a linear mixed-effects model using growth curve analysis (GCA; Figure 3-3b) (Mirman, 2016; Montes-Lourido et al., 2021). We assessed separate fixed interaction effects of contrast and ZX1 on first and second order orthogonal time polynomials fitted to pupil responses as fixed effects and included random subject-level intercept effects. We observed significant effects of both contrast and ZX1 treatment on intercept (contrast: $F(1,8003.6) = 65.66$, $p = 6.14e-16$; ZX1: $F(1,8011.3) = 10.38$, $p = 1.28e-$

3) and on the slope coefficient of the first order (linear) time polynomial (Figure 3-3c; contrast: $F(1,8002) = 60.95$, $p = 6.60e-15$; ZX1: $F(1,8002) = 30.07$, $p = 4.29e-8$). Thus, contrast and ZX1 significantly affect both evoked PD across the entire temporal response average (intercept) and PD rate of change (first order time polynomial, slope). Importantly, there was a significant interaction between contrast and ZX1 treatment ($F(1,8002.9) = 16.68$, $p = 4.48e-5$). A pairwise post-hoc Tukey test revealed that pupil responses to high contrast significantly decreased after ZX1 treatment ($p < 0.0001$), while low contrast responses did not. This high contrast specific effect of ZX1 on evoked pupil responses mirrors the high contrast specific effect of ZX1 on A1 principal neurons responses suggesting a link between A1 CGC and contrast-dependent effects on PD. Thus, context-dependent cortical zincergic signaling contributes to contrast-dependent changes in sound evoked pupil responses. This is an important finding suggesting that sound evoked pupil responses depend upon zincergic signaling in ACtx.

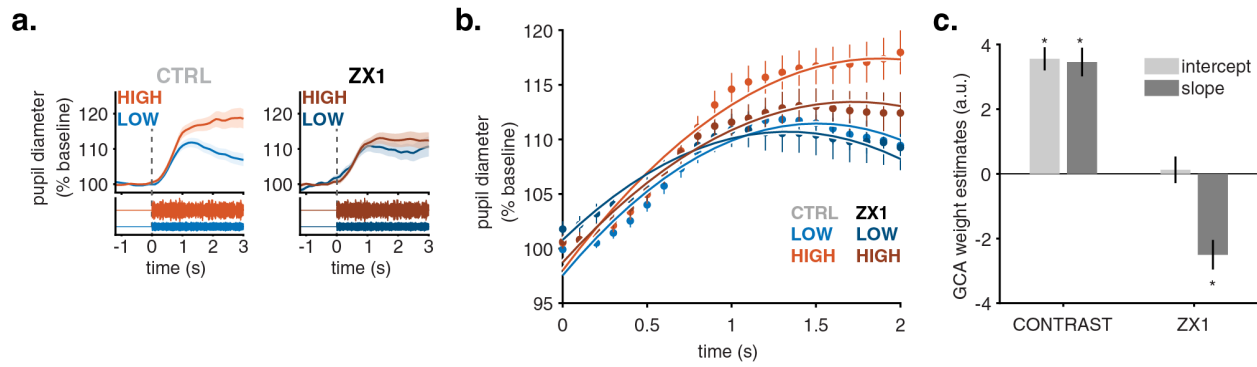


Figure 3-4: Cortical zinc signaling contributes to an increase in pupil response magnitude to high contrast sound

(a) Mean \pm SEM of sound evoked pupil responses to low (blue) and high (red) contrast DRC stimuli without a pure tone at 2 s. Responses shown before (left, CTRL), and after injection of ZX1 (right, ZX1) into auditory cortex. (b) Same responses in (a) limited to 0 – 2 s into DRC onset with fitted polynomials from growth curve analysis (GCA). (c) GCA model weight estimates for contrast and ZX1 model factors (linear mixed-effects model intercept and 1st order orthogonal polynomial coefficient).

We observed a significant increase in pre-stimulus PD across recording duration of ZX1 treatment experiments (Figure 3-4a; slope 95% CI = [0.0798,0.183], $p = 1.26e-6$). However, as aforementioned, we limited our pupil response analyses to the 50th percentile of pre-stimulus PD at which there was no significant correlation between pre-stimulus PD and sound evoked pupil response. Nonetheless, as a control for the effect of recording duration coincident with ZX1 treatment, we performed the same experiment instead with a vehicle injection of ACSF. Pre-stimulus PD similarly increased across recording duration during ACSF experiments (Figure 3-4a; slope 95% CI = [0.0159,0.279], $p = 0.0282$). Furthermore, unlike after ZX1 treatment, there was a significant effect of contrast on the intercept and fitted slope coefficient of the first order time polynomial following ACSF injection (Figure 3-4b; intercept: $F(1,2558.3) = 46.22$, $p = 1.31e-11$; slope: $F(1,2558) = 15.076$, $p = 1.10e-4$). This, in combination with the contrast specific effects of ZX1 (Figure 3-3), suggest that ZX1 effects on evoked pupil responses are not attributable to non-specific effects of ZX1 on pre-stimulus PD.

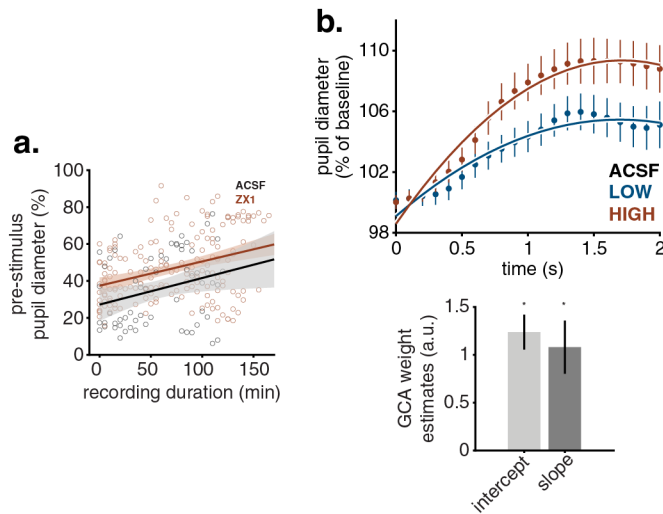


Figure 3-5: Pre-stimulus pupil diameter increases throughout experiment duration, but contrast effect on pupil responses persists upon ACSF control injection

(a) Open circles: mean pre-stimulus pupil diameter (PD) plotted against experiment recording duration during ACSF (black) and ZX1 (red) experiments. Black and red lines with shading: fitted ACSF and ZX1 (respectively) regression lines and 95% confidence intervals. Slope 95% CI ACSF: [0.0159,0.279], $p = 0.0282$ ZX1: [0.0798,0.183], $p = 1.26e-6$. (b) Top: mean \pm SEM of sound evoked pupil responses to low (blue) and high (red) contrast DRC stimuli after ACSF injection with fitted GCA polynomials. Bottom: GCA model weight estimates.

The zincergic signaling contributing to larger pupil responses in high contrast sound may arise from synaptically released ZnT3-dependent vesicular zinc (Anderson et al., 2017; Cole et al., 1999), tonic ZnT3-independent zinc (Anderson et al., 2015; Perez-Rosello et al., 2015), or both (Krall et al., 2020). To isolate the source of zinc involved we recorded pupil responses to contrast sound before and after ZX1 (as in Figure 3-3a-b) in wild-type mice (ZnT3-WT; Figure 3-5a) and knock-out mice (ZnT3-KO; Figure 3-5b) that lack ZnT3 and thus synaptic zinc (Cole et al., 1999). In ZnT3-WT mice we observed the same results as in Figure 3-3b: a significant effect of both contrast and ZX1 on both intercept and the first order polynomial coefficient (slope), with a significant interaction between contrast and ZX1 treatment (contrast intercept and slope: $F(1,7921.6) = 19.48$, $p = 1.03e-5$; $F(1,7918.8) = 26.54$, $p = 2.64e-7$; ZX1 intercept and slope: $F(1,7926.3) = 4.47$, $p = 0.0344$; $F(1,7918.8) = 40.45$, $p = 2.13e-10$; contrast and ZX1 interaction: $F(1,7921.6) = 24.2$, $p = 8.85e-7$). Pairwise post-hoc Tukey tests revealed a significant effect of contrast before ($p < 0.0001$), but not after ZX1 treatment, and solely a significant effect of ZX1 on high contrast responses ($p < 0.0001$). In ZnT3-KO mice (Figure 3-5b), we did not observe a significant effect of either contrast or ZX1 treatment on pupil responses (contrast: $F(1,4500.8) = 1.30$, $p = 0.255$; ZX1: $F(1,4502.5) = 2.10$, $p = 0.147$), nor a significant interaction between the two ($F(1,4500.2) = 0.292$, $p = 0.589$). The lack of an effect of ZX1 in ZnT3-KO mice suggests that the effect of ZX1 in Figure 3a-b and in Figure 3-5a (ZnT3-WT) is largely attributable to ZnT3 dependent vesicular zinc signaling and not tonic zinc. As an additional control for effects of recording duration, we used a linear mixed-effects GCM model to compare high contrast pupil responses between genotype (ZnT3-WT vs ZnT3-KO) prior to ZX1 injection (Figure 3-5c). We observed a significant effect of genotype on the slope coefficient of the first order (linear) time polynomial ($F(1,3869) = 22.37$, $p = 2.33e-6$). Thus, the effect of contrast on pupil responses in

ZnT3-WT mice is absent in ZnT3-KO mice across the same recording duration (prior to ZX1 treatment). Taken together these results reveal that cortical synaptic zinc signaling is necessary for increases in PD associated with adaptation to high contrast sound.

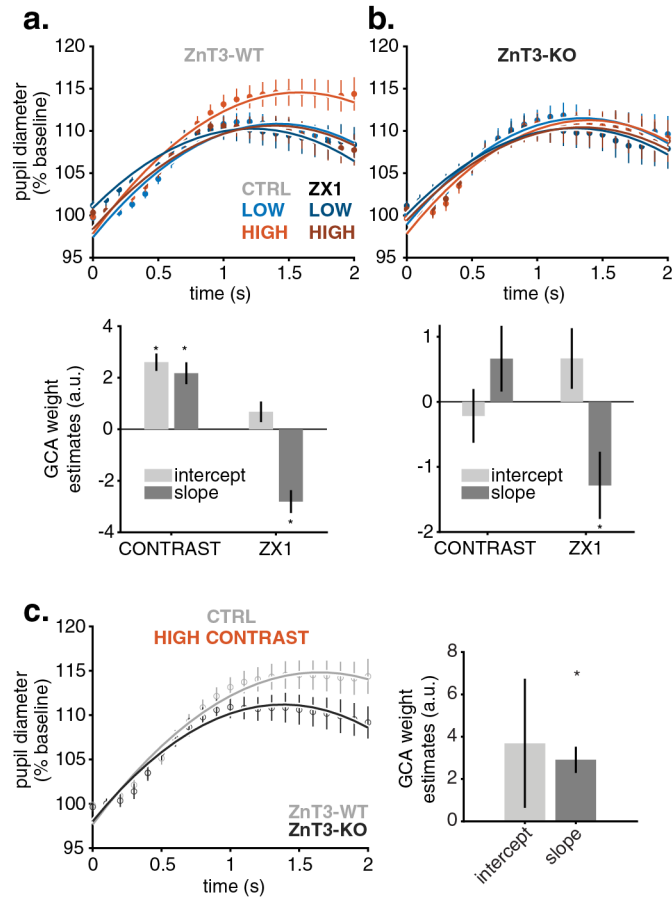


Figure 3-6: Synaptic zinc signaling enables larger pupil responses to high contrast sound

(a-b) Top: mean \pm SEM of sound evoked pupil responses to low (blue) and high (red) contrast DRC stimuli with fitted GCA polynomials before and after ZX1 injection into auditory cortex recorded from ZnT3-WT (a) and ZnT3-KO (b) mice. Bottom: GCA model weight estimates. (c) Left: pupil responses to high contrast sound before ZX1 injection (CTRL) from ZnT3-WT (gray) and ZnT3-KO (black) mice with fitted GCA polynomials (light red shaded responses in (a) and (b)). Right: GCA model weight estimates.

3.4 Discussion

3.4.1 Exploring the Contrast-dependent Effects of Pupil-indexed Cortical State on A1

Principal Neuron Response Properties

In this study we reveal that stimulus-independent internal brain state, as indexed by pupil size, affects adaptation sound CGC in A1. Specifically, pre-stimulus PD has a significant effect on CGC magnitude (Figure 3-1f). This is likely attributable to a contrast-dependent effect of pre-stimulus PD on a combination of A1 principal neuron response properties (Figure 3-1g-i). While we did not measure movement (as could be done with a piezoelectric sensor (Montes-Lourido et al., 2021)), the PD effects we observe are unlikely due to locomotion effects on cortical activity (Vinck et al., 2015), as the change in CGC strength is in a PD range well below PDs associated with locomotion (McGinley et al., 2015a). Momentary fluctuations in membrane potential associated with micro-dilations are also likely excluded as a factor owing to the 4 s duration over which pre-stimulus PD is averaged and the 2 s of DRC contrast sound that precedes the CGC measurement (Reimer et al., 2014). Although sound contrast itself has been shown to have no effect on peak excitatory post synaptic potential variability (Cooke et al., 2020), we observe contrast-dependent effects of pre-stimulus PD on pure tone response amplitude variability (Figure 3-1i). Thus, the cortical activity tracked by pre-stimulus PD is sensitive to sound contrast changes and this impacts CGC. Because CGC is evident along the auditory pathway from IC, to thalamus (ventral medial geniculate), and into ACtx (Lohse et al., 2020), and neural activity in these areas is tracked by pupil size (McGinley et al., 2015a; Schwartz et al., 2019), future studies are needed to address which regions are susceptible to sensory adaptation effects of pupil-indexed brain state.

3.4.2 Exploring the Pupil-indexed Cortical State Factors That Impact Contrast Gain

Control

A prevailing theory is that fluctuations in pupil size during quiet wakefulness are attributable to activity in the locus coeruleus (LC) with which they covary on both short (< 1 s) and long timescales (>10 s) (Joshi and Gold, 2020; McGinley et al., 2015b). This theory is supported by equivalence of LC mediated norepinephrine (NE) effects and pupil effects on cortical sensory coding (McGinley et al., 2015; Sara, 2009). Partly due to this equivalence and LC inhibition of sleep promoting nuclei and direct excitatory effects on cortex (Saper et al., 2001), pupil fluctuations during quiet wakefulness are considered an index of arousal. However, the exact direct pathway between PD and LC has yet to be established and is further complicated by the interconnectedness and extensive innervation of the multiple nuclei that directly affect PD (Joshi and Gold, 2020). Nonetheless, within this framework and our observation of pre-stimulus PD effects on CGC, it is thus surprising that previous studies find CGC is not affected by ketamine anesthesia (Lohse et al., 2020; Rabinowitz et al., 2011). Although ketamine is foremost recognized as an NMDA antagonist, ketamine's effects on LC-NE are considered to mediate its desired analgesic effects during anesthesia (Gitlin et al., 2020). Further, ketamine directly affects NE neurotransmission via noncompetitive inhibition of the NE transporter (Hara et al., 1998), and has broad effects on LC activity (Liebe et al., 2018). Can insight into the factor that modulates CGC and varies with PD be drawn from the resilience of CGC to ketamine anesthesia? If CGC variation with PD is modulated by LC-NE, then it does not act in IC, as CGC strength in IC is equivalent between awake and anesthetized states (Lohse et al., 2020). Additionally, the measurement of CGC in ACtx of an awake versus ketamine anesthetized ferret would have been at PD states with comparable CGC strength (Rabinowitz et al., 2011).

3.4.3 Neural Activity Indexed by Pre-stimulus Pupil Size Versus That Associated With Sound Evoked Pupil Responses

Is the internal cortical state during sound evoked increases in pupil size the same as the pre-stimulus pupil-indexed cortical state at a similar absolute pupil size? In other words, does sound contrast change the internal cortical states that are measured by pre-stimulus PD, or are sound evoked pupil responses associated with separate neural activity? Several lines of evidence suggest pre-stimulus PD indexes different neural activity than that associated with sensory evoked pupil responses (aside from ambient light levels/in consistent lighting). First, pupil-indexed cortical states are considered to be reflective of fluctuations in cortical membrane potential variability and spontaneous activity that impact responsiveness to sensory stimuli (McGinley et al., 2015b, 2015a). Sound contrast itself, however, does not affect cortical membrane potential variability (Cooke et al., 2020). Second, we did not observe an effect of evoked pupil responses on CGC (as described with Figure 3-2), whereas pre-stimulus PD does affect CGC (Figure 3-1f). Finally, optogenetic activation of serotonergic neurons in the dorsal raphe nucleus causes pupil dilation, but the change in pupil size does not depend on baseline pupil size (Cazettes et al., 2020). Together, these findings suggest that stimulus evoked pupil responses track different neural activity than that associated with pre-stimulus pupil-indexed cortical state.

3.4.4 The Role of Neuromodulatory Zinc Signaling in Contrast Adaptation

In the opposite direction of pre-stimulus pupil state effects on adaptation to contrast, we find that increased sound contrast evokes larger pupil responses and that pupil sensitivity to this

contrast difference relies upon synaptic zinc signaling in ACtx. Our previous work shows that cortical CGC also relies upon synaptic zinc signaling. Furthermore, the high contrast state specific effects of zinc on evoked pupil responses mirror the high contrast specific effects on A1 principal neuron responses, suggesting a mechanistic link between CGC and evoked pupil responses. However, as PD has been shown to track neuromodulatory activity (Cazettes et al., 2020), including in cortex (Reimer et al., 2016), the zinc signaling effect on pupil responses (Figure 3-3 and Figure 3-5) could be interpreted instead as pupil tracking cortical neuromodulatory zincergic activity. The zinc effect on pupil responses is nonetheless significant as it corroborates a contrast specific contribution of synaptic zinc signaling to cortical activity; another example of context specific zincergic activity (Kalappa and Tzounopoulos, 2017; Nakashima and Dyck, 2010). Taken together, we reveal a neuromodulatory mechanism of sensory processing in primary auditory cortex that enables sound stimulus-dependent changes in PD.

What do the effects of zinc signaling on sound contrast evoked pupil responses suggest for zinc's role in cortical CGC? Why does zinc contribute to cortical CGC if CGC is already present in the midbrain (Lohse et al., 2020) where zincergic innervation is nominal compared to ACtx (McAllister and Dyck, 2017a)? While the pathway from ACtx to nuclei controlling PD is unknown, it is likely to span several synapses. That zinc signaling in ACtx influences sound evoked pupil responses suggests a role of zinc signaling in long-range coordination of neural activity for specific sensory contexts. Regardless of its purpose, its importance to contrast-dependent effects on pupil responses suggests that pupillometry may serve as a clinical marker for disorders involving potentially disrupted cortical zinc signaling and sensory adaptation to sound level variability (contrast) (Montes-Lourido et al., 2021).

3.5 Materials and Methods

3.5.1 Animals

We used 24 male and female mice for the experiments presented in the main figures and an additional 4 mice for the experiments in supplemental figures. The genetic background of all mice was C57BL/6J. For Figure 3-5 homozygous mice lacking the vesicular zinc transporter (ZnT3 (Cole et al., 1999); Jackson Laboratory), ZnT3-KO mice, were used along with homozygous littermate controls, ZnT3-WT. Experiments using these mice were done blind to KO or WT designation. Mice were handled, anesthetized, and sacrificed according to methods approved by the University of Pittsburgh Institutional Animal Care and Use Committees (IACUC). The approved IACUC protocol numbers that were employed for this study were: 17071036 and 17127808.

3.5.2 Stereotaxic AAV Injection

At P24 – P30 mice were injected with an AAV virus (AAV9.CaMKII.GCaMP6f.WPRE.SV40 (addgene 100834; 2.5×10^{13} GC/mL; diluted at 1:6 in PBS) into right auditory cortex (ACtx) to drive GCaMP6f expression in putative principal cells expressing calcium/calmodulin-dependent protein kinase 2 (CaMKII) as described previously (*Chapter 1*, section 2.5.2) in preparation for calcium imaging.

3.5.3 Acute Surgery Preparation For In Vivo Imaging

At P38 – P49 mice underwent craniotomy surgery and were secured to the microscope apparatus for imaging experiments as described previously (*Chapter 1*, section 2.5.3). Mice were situated on the microscope stage such that the right pupil was visible to the pupillometry camera (see *Chapter 2*, section 3.5.8), and the left pupil was in view of the UV LED light for maintaining constant pupil size.

3.5.4 Sound Stimulus Delivery

Sound stimuli were delivered from a calibrated free-field speaker as described in *Chapter 1*, section 2.5.4.

3.5.5 Widefield Epifluorescence Imaging and Analysis for A1 Localization

Widefield epifluorescence imaging was used to localize A1 for 2PCI as described in *Chapter 1*, section 2.5.5.

3.5.6 DRC Stimuli

Low and high sound level contrast dynamic random chord (DRC) stimuli were generated with the same mean sound level. DRCs consisted of 28 pure tone frequencies between 5 – 51.874 kHz at 1/8th octave intervals. Sound levels for low contrast DRC were sampled from a narrow uniform distribution between 50 to 60 dB SPL (± 5 dB; $\sigma_L \approx 2.9$ dB SPL), while sound levels for

high contrast DRC were sampled from a wider distribution between 40 to 70 dB SPL (± 15 dB; $\sigma_L \approx 8.7$ dB SPL). Both distributions had the same 55 dB SPL mean. For contrast gain control analyses DRC stimuli included a 70 dB pure tone at 2 s. In this case DRC amplitude was set to 0 V for 400 ms and a 70 dB SPL pure tone lasting 400 ms was inserted within this gap. For sound evoked pupil response analyses, DRC stimuli did not include a pure tone.

3.5.7 2-Photon Calcium Imaging (2PCI)

Sound evoked responses from putative principal cells expressing CaMKII in ACTx were imaged with 2-photon calcium imaging (2PCI) as described in *Chapter 1*, section 2.5.10. We collected 145 X 145 μm images at 256 X 256 pixel resolution at an effective frame rate of 5 Hz.

3.5.8 Pupillometry: Acquisition

Video of animal's pupil was recorded 4 s prior to sound onset and continued for the duration of each 2PCI imaging trace. A UV LED (375 nm, 2.5 mW, ThorLabs) maintained the animal's pupil at mid-size range in the dark recording chamber to optimize dynamic range for stimulus independent state and auditory stimulus dependent changes. After this UV intensity was set with an LEDD1B driver (ThorLabs) via a voltage divider circuit (470 Ohm rated at 25 W, Mouser) it was kept at constant luminance throughout the duration of the experiment. UV light was shielded from the 2PCI objective to avoid interference with the 2P PMTs. Spillover from the 2P laser through the animal's brain and into the pupil provided sufficient illumination for pupil imaging. Video frames were captured with a monochrome CMOS USB camera (ThorLabs) behind a 1X telecentric lens and 380 nm cut-on UV filter (Edmund Optics). Frames were captured at 10

Hz, synchronized with 2P frame acquisition using an NI-DAQ board counter output channel, and time stamped using a custom written MATLAB function for ScanImage with a .NET camera API library (ThorLabs).

Sound evoked pupil responses were recorded before (control: CTRL) and after injecting ZX1 (Pan et al., 2011) (a fast extracellular high-affinity zinc-specific chelator) solution or ACSF solution. Prior to imaging we inserted a pulled glass micropipette just below the pial surface at the edge of the craniotomy within ACtx. The pipette contained 100 μ M ZX1 and 50 μ M AlexaFluor 594 in ACSF (herein referred to as ‘ZX1 solution’) or just 50 μ M AlexaFluor 594 in ACSF (herein referred to as ‘ACSF solution’) and was backfilled with mineral oil and connected to a 5 μ L glass syringe mounted in a motorized syringe pump (World Precision Instruments). After a minimum of 20 minutes following cessation of isoflurane, we recorded sound evoked pupil responses.

3.5.9 FRA Mapping

For each 2PCI experiment we mapped frequency response areas (FRAs) of the neurons in the imaging field as described in *Chapter 1*, section 2.5.8 to determine the pure tone frequency to be used in the contrast gain control assay.

3.5.10 Contrast Gain Control Assay

For each experiment, a given pure tone frequency (as determined during *ad hoc* FRA mapping; see previous section) was presented in each contrast (low, high) combination in a pseudorandom fashion. For each imaging trace, the DRC sound stimulus was both preceded and

followed by 4 s of silence. Traces were interleaved by laser off periods of pseudorandom duration lasting 25 – 35 seconds. A minimum of 8 repetitions of each contrast was presented.

3.5.11 2PCI Processing and Analysis

For a given experiment, 2PCI frames were concatenated for all traces across time and aligned using non-rigid motion correction via the NoRMCorre MATLAB toolbox (Pnevmatikakis and Giovannucci, 2017). Ellipses were manually drawn around cells (as described in *FRA mapping*) and contamination from surrounding neuropil (in the form of time varying fluorescence intensity) obtained using the FISSA Python toolbox (Keemink et al., 2018) was scaled by 0.8 (Chen et al., 2020; Kerlin et al., 2010) and removed to obtain motion- and neuropil- corrected average fluorescence intensity across time for each cell. Solely non-overlapping cells deemed tone responsive were included for further analysis. To assess peak fluorescence responses to the pure tone, we calculated baseline subtracted fluorescence traces ($\Delta F/F = (F-F_0)/F_0$) normalized to a baseline 1 s prior to pure tone onset (F_0 is mean fluorescence intensity at 1 – 2 s). Solely significant peak $\Delta F/F$ pure tone responses, as calculated in *FRA mapping*, were included in pure tone response analyses. Cells were grouped by animal in pre-stimulus pupil diameter bins to maintain pairing by contrast condition. To quantify contrast gain control, we calculated the contrast scaling factor, defined as the population mean of individual cell average peak responses in low- divided by average peak responses in high contrast. Reliability was calculated as the average trial-to-trial 0 lag cross-correlation of peak pure tone response traces (at 2 – 3.2 s) for all responses for a given cell and was presented as a population average.

3.5.12 Pupillometry: Analysis

Pupil diameter (PD) was obtained from pupil videos using a least squares circle fit to dots fitted to pupil perimeter using a DeepLabCut convolutional neural network model (Mathis et al., 2018; Nath et al., 2019) along with custom written MATLAB and Python scripts. Pupil videos with dropped frames were realigned to frame time stamps. Using DeepLabCut, we trained a 101-layer Resnet model with default augmentation on 11 videos from different experiments that were labeled with 8 dots around the pupil perimeter (Mathis et al., 2018). For each frame from model analyzed videos, a minimum of 3 dots at >0.9 likelihood were needed to fit a circle via least squares else the frame was discarded. Pupil (circle) diameter traces were processed sequentially by first removing >6 SD outlier frames from the first derivative, next linearly interpolating missing time points with the previous 2 and following 2 adjacent time points, and finally filtering the trace with a 3rd order 3 Hz low-pass Butterworth filter (Mridha et al., 2021).

Evoked pupil responses are presented as percent pre-stimulus baseline: for each PD trace, PD was divided by average PD prior to sound onset (-4 – 0 s) then multiplied by 100. For responses binned by percent pre-stimulus PD, PD traces for each animal were first calculated as a percentage of the animal's maximum PD during the experiment. These traces were then averaged across the pre-stimulus epoch (-4 – 0 s), then grouped in 7 bins. The last bin ($>76\%$) was wider to accommodate fewer samples in that pupil range. 2PCI data in each of these bins correspond to an average of cell average traces occurring at a given pupil bin.

We limited sound evoked pupil response analyses in Figure 3-3 - Figure 3-5 to responses with a pre-stimulus PD at less than 50 % of animal max PD (50th percentile) for several reasons. First, at relatively dilated states, the pupil tends to constrict (Gee et al., 2014; Mridha et al., 2021), and evoked pupil responses are significantly negatively correlated with pre-stimulus PD (Figure

3-6; $r(624) = -0.35$, $p = 1.20e-19$). At PDs less than 50 % of maximum animal PD, this correlation becomes much smaller and is no longer significant ($r(382) = -0.055$, $p = 0.285$). Additionally, because we are interested in the contribution of cortical CGC to pupil responses, we focused on the 50th percentile where CGC is strongest (Figure 3-1f).

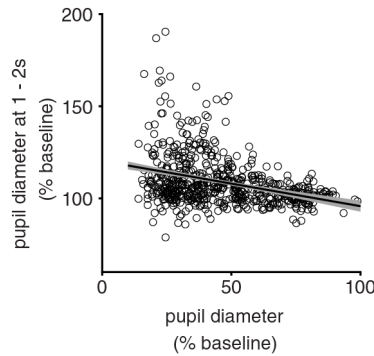


Figure 3-7: Sound contrast evoked pupil response magnitude correlates with pre-stimulus pupil diameter
Open circles: mean of evoked pupil responses 1 – 2 s into DRC stimulus across both contrast conditions
plotted against the pre-stimulus pupil diameter that preceded them. Pearson’s correlation coefficient: $r(624)$
= -0.35, $p = 1.20e-19$). Black line: fitted regression line with gray 95% confidence interval (slope 95% CI = [-
0.297, -0.194]).

We used growth curve analysis (GCA) (Mirman, 2016; Montes-Lourido et al., 2021) to quantitatively compare pupil responses between contrast and drug treatment conditions. This analysis precludes bias associated with choosing analysis windows and captures pupil evolution over time (slope) (Montes-Lourido et al., 2021). For this analysis we fit a linear mixed-effects (LME) model with separate fixed interaction effects of contrast and ZX1 treatment on first and second order orthogonal time polynomials fitted to pupil responses (sound onset to 2 s post onset) as fixed effects and included random subject-level intercept effects. This is the model in Wilkinson notation (Pinheiro and Bates, 2000; Wilkinson and Rogers, 1973): $\text{pupil} \sim (\text{tPoly1} + \text{tPoly2}) * \text{contrast} + (\text{tPoly1} + \text{tPoly2}) * \text{treatment} + (1 | \text{subject})$. For comparing control high contrast

responses between ZnT3-WT and ZnT3-KO genotypes we used a simpler LME model: $\text{pupil} \sim (\text{tPoly1} + \text{tPoly2}) * \text{genotype} + (1 | \text{subject})$. tPoly1 and tPoly2 are the first and second order orthogonal time polynomials; their coefficients correspond to slope and acceleration GCA weight estimates. The MATLAB ‘fitlme’ function was used to calculate coefficients and standard errors. These were confirmed with the ‘lmer’ function in R. Tukey adjusted pairwise comparisons were done using the ‘emmeans’ function in R with a Satterthwaite correction for large degrees of freedom.

3.5.13 Statistics

For grouped single factor data that rejects the Anderson-Darling null hypothesis test for normality we used a Kruskal-Wallis one-way ANOVA. We analyzed grouped two-factor cell response data with two-way ANOVAs. A linear mixed-effects model was used to analyze evoked pupil response effects on cell responses (as described in section 3.3.2). GCA was used to compare the initial rising phase (0 – 2 s) of evoked pupil responses between conditions (as described in *Pupil analyses*). Linear regression and the Pearson correlation coefficient were used to assess both the relationship between magnitude evoked pupil response and pre-stimulus pupil diameter as well as pre-stimulus pupil diameter across experiment duration.

4.0 Conclusion

4.1 Summary of Results

This work reveals that sensory adaptation to increased sound level variability, contrast, depends upon synaptic zinc neuromodulatory signaling in auditory cortex. Chapter 1 shows that zinc signaling is recruited in high sound contrast contexts to yield dampened sound responses that are reflective of contrast gain control (Rabinowitz et al., 2011). This finding is supported by recent studies showing zinc's dynamic and context-dependent synaptic actions (Kalappa and Tzounopoulos, 2017; Vogler et al., 2020) as well as studies of zinc's influence on cortical sensory processing relating to gain modulation (Anderson et al., 2017) and frequency discrimination (Kumar et al., 2019). This contrast dependent involvement of synaptic zinc is specific to principal neurons, consistent with the exclusion of parvalbumin expressing inhibitory neurons and shunting inhibition from contrast gain control mechanisms (Cooke et al., 2020). Angeloni et al 2021 find that inactivating auditory cortex with receptor agonist muscimol impedes contrast gain control dependent behavioral performance, but has comparable effects in both low and high sound contrast (Angeloni et al., 2021). This both highlights the contrast specific effects of synaptic zinc, and suggests cortex is necessary for behaviors relying upon contrast adaptation. However, contrast gain control is already implemented subcortically (Lohse et al., 2020) in areas with little to no zincergic innervation (McAllister and Dyck, 2017a). Why then would cortex involve different mechanisms? This is partly addressed by differences in contrast adaptation times and response properties as well as cellular architecture from midbrain nuclei to cortex (Lohse et al., 2020) that suggest additional mechanisms develop along the auditory pathway. This question is addressed

further in Chapter 2 using a combination of pharmacologic and transgenic zinc perturbations with pupillometry during a 2PCI assay for contrast gain control.

Chapter 2 presents two main findings regarding pupil size and sensory adaptation. First, it shows that the strength of contrast gain control changes with pre-stimulus pupil-indexed brain state. Second, it reveals that pupil responses to high contrast sound are larger than responses to low contrast sound. Importantly, this effect of contrast on pupil responses relies upon zincergic neuromodulation in auditory cortex. This result has two key implications. First, zinc signaling may serve as an indicator of sound context state to coordinate intracortical activity for more demanding high contrast sensory contexts. The combination of long range communication between cortical areas and hemispheres afforded by cortex (Harris and Shepherd, 2015) with zinc's ability to modulate multiple post-synaptic receptors (Anderson et al., 2015; Kalappa et al., 2015; Kouvaros et al., 2020; Krall et al., 2020; Paoletti et al., 2009; Vergnano et al., 2014; Wang et al., 2001), motivates a zinc dependent cortical mechanism of contrast adaptation. Furthermore, auditory processing demand and complexity are associated with larger pupil responses (Zekveld et al., 2018). The second key implication is that pupillometry may be used as a relatively simple (compared to EEG) non-invasive clinical marker for disrupted sensory processing in auditory cortex (Montes-Lourido et al., 2021). Changes in sound evoked pupil responses have been associated with schizophrenia, dementia, and hearing loss (Zekveld et al., 2018). While the mirroring of high contrast effects of zinc between pupil and cell responses suggests that cortical contrast gain control is linked to the contrast effect on pupil, future work is needed to address whether the zinc signaling that is required of contrast gain control is that which enables contrast dependent changes to pupil responses.

4.2 Future Directions

Without zinc signaling, cortical cell responses to sound do not adapt to an increase in contrast: responses in high contrast are not scaled down as would be the case of contrast gain control (CGC). This suggests that synaptic zinc signaling is required for cortical CGC, but it does not address whether zinc signaling is sufficient to generate this change in response properties. As broached in *Chapter 1*, section 2.4.7, zincergic neurons could be selectively engaged upon increased sound contrast, and/or AMPA, NMDA, or GABA receptor sensitivity to synaptic zinc may be selectively modulated by an increase in sound contrast. If zincergic engagement differs between contrast states, selective activation of zincergic neurons to mimic contrast stimuli would address whether synaptic zinc signaling is both necessary and sufficient for cortical contrast gain control in A1. Awake *in vivo* voltage clamp recordings to measure both excitatory and inhibitory post-synaptic potential (EPSC and IPSC) during contrast stimuli in combination with pharmacologic and zinc imaging approaches (Vogler et al., 2020) would enable further mechanistic definition and assessment of AMPA, NMDA, or GABA receptor sensitivity to synaptic zinc. Addressing these two possibilities, zincergic engagement and receptor sensitivity, would be the first step towards a deeper mechanistic understanding of zinc's role in CGC.

Novel transgenic mice expressing recombinases in ZnT3 expressing cells would enable both selective recording and activation of specifically zincergic cells. Recording ZnT3 expressing cells would address whether zincergic cells are uniquely activated with respect to sound contrast. If they are, this contrast specific activity could be artificially driven optogenetically, without contrast stimuli, and paired with electrophysiological recordings of A1. This would reveal whether selective zincergic activity is sufficient to decrease A1 principal neuron gain and thus drive cortical CGC. Pairing these same zincergic recording/activation approaches with pupillometry would

address whether increased pupil responses to high contrast, as described in *Chapter 2*, section 3.3.3, are attributable to the same zincergic activity contributing to CGC.

A behavioral paradigm, in which task performance depends upon the strength of CGC (Angeloni et al., 2021), would serve to further validate our results and address additional mechanistic questions. First, behavior combined with pharmacological and transgenic zinc signaling perturbations would address whether cortical CGC dependence on synaptic zinc is behaviorally relevant. Second, if combined with pupillometry and 2-photon calcium imaging (2PCI), a behavioral assay would address whether task performance is similarly maximal at pupil-indexed states with maximal CGC strength (described in *Chapter 2*, section 3.3.1). The findings discussed in *Chapter 1*, sections 2.3.3 and 2.4.4 suggest that parvalbumin expressing inhibitory interneurons (PV-cells) may be involved in the cortical contrast invariance phenomenon (discussed in *Chapter 1*, sections 2.4.4 and 2.4.5) of contrast adaptation. In agreement with this, Cooke et. al, 2020 observe contrast specific effects of PV inactivation on cortical multiunit activity (Cooke et al., 2020). Assaying task performance effects of selective optogenetic activation or inactivation of PV-cells would probe PV-cell contribution to contrast invariance if task performance depends upon contrast invariance.

Chapter 2, section 3.3.1 reveals that there is an optimal pupil-indexed cortical state range for CGC. In both the midbrain and cortex, CGC is, however, not impacted by ketamine anesthesia (Lohse et al., 2020; Rabinowitz et al., 2011), which disrupts locus coeruleus norepinephrine (NE) signaling (see *Chapter 2*, section 3.4) (Gitlin et al., 2020; Hara et al., 1998; Liebe et al., 2018). Additionally, CGC is measured 2 s after pre-stimulus pupil indexed cortical state. While both NE and acetylcholine (ACh) activity precede pupil dilations, NE activity exhibits shorter decay time than ACh, and ACh is more coherent with pupil than NE at slow frequencies (< 0.03 Hz) (Reimer

et al., 2016). Together, this points to ACh rather than NE mediated pupil-indexed cortical state effects on CGC. A combined 2PCI and viral approach for recording layer 1 ACh activity in auditory cortex with electrophysiology to record CGC in principal neurons of deeper layers would address this possibility.

Current behavioral assays of CGC solely reveal a performance cost and no benefit (as introduced in section 1.3). Increased contrast results in a decrease in the sensitivity to sound level differences (Angeloni et al., 2021; Lohse et al., 2020). With decreased gain, a shallower slope of the input-output function, and thus expanded dynamic range in high contrast, neural firing-rate output would continue to increase at larger sound levels rather than saturating, had gain not adapted. Thus, in a task that relies on the discrimination of high sound levels, one would expect improved performance in high contrast sound when CGC has decreased neural input-output gain. Additional behavioral paradigms, that incorporate such a feature, are needed to uncover the low-level behavioral benefits of contrast gain control.

The prevalent approach for electrophysiological assessment of CGC involves a change in contrast across the full stimulus frequency bandwidth (Angeloni et al., 2021; Cooke et al., 2020, 2018; Lohse et al., 2020; Rabinowitz et al., 2011). Thus, this method does not consider a neuron's sensitivity to contrast change in particular frequency bands and how this sensitivity relates to a neuron's frequency receptive field. This concept was broached in Rabinowitz, et. al., 2011 and more thoroughly explored in Rabinowitz, et. al., 2012 by estimating spectral contrast kernels that reveal frequency sensitivity to contrast change closely compares to a neuron's frequency selectivity (Rabinowitz et al., 2012, 2011). However, the Rabinowitz, et. al., 2012 study was limited to A1, while CGC has been described in IC and thalamus (Lohse et al., 2020). An earlier study that introduced IC adaptation to sound level variance considered solely temporal variance

and did not employ a model with a linear STRF passed through a sigmoid nonlinearity (Dean et al., 2005). Nonetheless, the functional consequence of the adaptation closely compares to CGC. This raises the question of whether the spectral contrast kernel may instead be the defining feature of CGC, and whether this feature arises in IC or is limited to cortex. This motivates both further electrophysiological study of subcortical spectral contrast kernels, and the influence of zinc on cortical spectral contrast kernels.

Bibliography

- Ahrens, M.B., Linden, J.F., Sahani, M., 2008. Nonlinearities and Contextual Influences in Auditory Cortical Responses Modeled with Multilinear Spectrotemporal Methods. *J. Neurosci.* 28, 1929–1942. <https://doi.org/10.1523/JNEUROSCI.3377-07.2008>
- Anderson, C.T., Kumar, M., Xiong, S., Tzounopoulos, T., 2017. Cell-specific gain modulation by synaptically released zinc in cortical circuits of audition. *eLife* 6, e29893. <https://doi.org/10.7554/eLife.29893>
- Anderson, C.T., Radford, R.J., Zastrow, M.L., Zhang, D.Y., Apfel, U.-P., Lippard, S.J., Tzounopoulos, T., 2015. Modulation of extrasynaptic NMDA receptors by synaptic and tonic zinc. *Proc. Natl. Acad. Sci.* 112, E2705–E2714. <https://doi.org/10.1073/pnas.1503348112>
- Angeloni, C.F., Mlynarski, W., Piasini, E., Williams, A.M., Wood, K.C., Garami, L., Hermundstad, A., Geffen, M.N., 2021. Cortical efficient coding dynamics shape behavioral performance. *bioRxiv* 2021.08.11.455845. <https://doi.org/10.1101/2021.08.11.455845>
- Aponte, D.A., Handy, G., Kline, A.M., Tsukano, H., Doiron, B., Kato, H.K., 2021. Recurrent network dynamics shape direction selectivity in primary auditory cortex. *Nat. Commun.* 12, 314. <https://doi.org/10.1038/s41467-020-20590-6>
- Aston-Jones, G., Cohen, J.D., 2005. An integrative theory of locus coeruleus-norepinephrine function: adaptive gain and optimal performance. *Annu. Rev. Neurosci.* 28, 403–450. <https://doi.org/10.1146/annurev.neuro.28.061604.135709>
- Atallah, B.V., Bruns, W., Carandini, M., Scanziani, M., 2012. Parvalbumin-Expressing Interneurons Linearly Transform Cortical Responses to Visual Stimuli. *Neuron* 73, 159–170. <https://doi.org/10.1016/j.neuron.2011.12.013>
- Auld, D.S., Bergman, T., 2008. Medium- and short-chain dehydrogenase/reductase gene and protein families: The role of zinc for alcohol dehydrogenase structure and function. *Cell. Mol. Life Sci. CMLS* 65, 3961–3970. <https://doi.org/10.1007/s00018-008-8593-1>
- Barbour, D.L., Wang, X., 2003. Contrast Tuning in Auditory Cortex. *Science* 299, 1073–1075. <https://doi.org/10.1126/science.1080425>
- Borghini, G., Hazan, V., 2018. Listening Effort During Sentence Processing Is Increased for Non-native Listeners: A Pupillometry Study. *Front. Neurosci.* 12, 152. <https://doi.org/10.3389/fnins.2018.00152>

- Bowen, Z., Winkowski, D.E., Seshadri, S., Plenz, D., Kanold, P.O., 2019. Neuronal Avalanches in Input and Associative Layers of Auditory Cortex. *Front. Syst. Neurosci.* 13. <https://doi.org/10.3389/fnsys.2019.00045>
- Brown, C.E., Dyck, R.H., 2005. Modulation of synaptic zinc in barrel cortex by whisker stimulation. *Neuroscience* 134, 355–359. <https://doi.org/10.1016/j.neuroscience.2005.05.011>
- Brown, C.E., Dyck, R.H., 2003. An improved method for visualizing the cell bodies of zincergic neurons. *J. Neurosci. Methods* 129, 41–47. [https://doi.org/10.1016/S0165-0270\(03\)00195-X](https://doi.org/10.1016/S0165-0270(03)00195-X)
- Brown, C.E., Dyck, R.H., 2002. Rapid, Experience-Dependent Changes in Levels of Synaptic Zinc in Primary Somatosensory Cortex of the Adult Mouse. *J. Neurosci.* 22, 2617–2625. <https://doi.org/10.1523/JNEUROSCI.22-07-02617.2002>
- Carandini, M., Heeger, D.J., 2012. Normalization as a canonical neural computation. *Nat. Rev. Neurosci.* 13, 51–62. <https://doi.org/10.1038/nrn3136>
- Carandini, M., Heeger, D.J., Movshon, J.A., 1997. Linearity and Normalization in Simple Cells of the Macaque Primary Visual Cortex. *J. Neurosci.* 17, 8621–8644. <https://doi.org/10.1523/JNEUROSCI.17-21-08621.1997>
- Cazettes, F., Reato, D., Morais, J.P., Renart, A., Mainen, Z.F., 2020. Phasic Activation of Dorsal Raphe Serotonergic Neurons Increases Pupil Size. *Curr. Biol.* <https://doi.org/10.1016/j.cub.2020.09.090>
- Chambers, A.R., Resnik, J., Yuan, Y., Whitton, J.P., Edge, A.S., Liberman, M.C., Polley, D.B., 2016. Central Gain Restores Auditory Processing following Near-Complete Cochlear Denervation. *Neuron* 89, 867–879. <https://doi.org/10.1016/j.neuron.2015.12.041>
- Chen, Q., Deister, C.A., Gao, X., Guo, B., Lynn-Jones, T., Chen, N., Wells, M.F., Liu, R., Goard, M.J., Dimidschstein, J., Feng, S., Shi, Y., Liao, W., Lu, Z., Fishell, G., Moore, C.I., Feng, G., 2020. Dysfunction of cortical GABAergic neurons leads to sensory hyper-reactivity in a Shank3 mouse model of ASD. *Nat. Neurosci.* 23, 520–532. <https://doi.org/10.1038/s41593-020-0598-6>
- Chen, T.-W., Wardill, T.J., Sun, Y., Pulver, S.R., Renninger, S.L., Baohan, A., Schreiter, E.R., Kerr, R.A., Orger, M.B., Jayaraman, V., Looger, L.L., Svoboda, K., Kim, D.S., 2013. Ultrasensitive fluorescent proteins for imaging neuronal activity. *Nature* 499, nature12354. <https://doi.org/10.1038/nature12354>
- Cody, P.A., Eles, J.R., Lagenaur, C.F., Kozai, T.D.Y., Cui, X.T., 2018. Unique electrophysiological and impedance signatures between encapsulation types: An analysis of biological Utah array failure and benefit of a biomimetic coating in a rat model. *Biomaterials* 161, 117–128. <https://doi.org/10.1016/j.biomaterials.2018.01.025>

- Cole, T.B., Wenzel, H.J., Kafer, K.E., Schwartzkroin, P.A., Palmiter, R.D., 1999. Elimination of zinc from synaptic vesicles in the intact mouse brain by disruption of the ZnT3 gene. *Proc. Natl. Acad. Sci.* 96, 1716–1721. <https://doi.org/10.1073/pnas.96.4.1716>
- Constantinople, C.M., Bruno, R.M., 2011. Effects and Mechanisms of Wakefulness on Local Cortical Networks. *Neuron* 69, 1061–1068. <https://doi.org/10.1016/j.neuron.2011.02.040>
- Cooke, J.E., Kahn, M.C., Mann, E.O., King, A.J., Schnupp, J.W.H., Willmore, B.D.B., 2020. Contrast gain control occurs independently of both parvalbumin-positive interneuron activity and shunting inhibition in auditory cortex. *J. Neurophysiol.* 123, 1536–1551. <https://doi.org/10.1152/jn.00587.2019>
- Cooke, J.E., King, A.J., Willmore, B.D.B., Schnupp, J.W.H., 2018. Contrast gain control in mouse auditory cortex. *J. Neurophysiol.* 120, 1872–1884. <https://doi.org/10.1152/jn.00847.2017>
- David, S.V., Mesgarani, N., Fritz, J.B., Shamma, S.A., 2009. Rapid Synaptic Depression Explains Nonlinear Modulation of Spectro-Temporal Tuning in Primary Auditory Cortex by Natural Stimuli. *J. Neurosci.* 29, 3374–3386. <https://doi.org/10.1523/JNEUROSCI.5249-08.2009>
- Dean, I., Harper, N.S., McAlpine, D., 2005. Neural population coding of sound level adapts to stimulus statistics. *Nat. Neurosci.* 8, 1684. <https://doi.org/10.1038/nn1541>
- Dyck, R.H., Chaudhuri, A., Cynader, M.S., 2003. Experience-dependent Regulation of the Zincergic Innervation of Visual Cortex in Adult Monkeys. *Cereb. Cortex* 13, 1094–1109. <https://doi.org/10.1093/cercor/13.10.1094>
- Evans, E.F., Palmer, A.R., 1980. Relationship between the dynamic range of cochlear nerve fibres and their spontaneous activity. *Exp. Brain Res.* 40, 115–118. <https://doi.org/10.1007/BF00236671>
- Gee, J.W. de, Knapen, T., Donner, T.H., 2014. Decision-related pupil dilation reflects upcoming choice and individual bias. *Proc. Natl. Acad. Sci.* 111, E618–E625. <https://doi.org/10.1073/pnas.1317557111>
- Gilzenrat, M.S., Nieuwenhuis, S., Jepma, M., Cohen, J.D., 2010. Pupil diameter tracks changes in control state predicted by the adaptive gain theory of locus coeruleus function. *Cogn. Affect. Behav. Neurosci.* 10, 252–269. <https://doi.org/10.3758/CABN.10.2.252>
- Gitlin, J., Chamadia, S., Locascio, J.J., Ethridge, B.R., Pedemonte, J.C., Hahm, E.Y., Ibala, R., Mekonnen, J., Colon, K.M., Qu, J., Akeju, O., 2020. Dissociative and Analgesic Properties of Ketamine Are Independent. *Anesthesiology* 133, 1021–1028. <https://doi.org/10.1097/ALN.0000000000003529>
- Hara, K., Yanagihara, N., Minami, K., Ueno, S., Toyohira, Y., Sata, T., Kawamura, M., Brüss, M., Bönisch, H., Shigematsu, A., Izumi, F., 1998. Ketamine interacts with the noradrenaline

- transporter at a site partly overlapping the desipramine binding site. *Naunyn-Schmiedeberg's Arch. Pharmacol.* 358, 328–333. <https://doi.org/10.1007/PL00005261>
- Harris, K.D., Shepherd, G.M.G., 2015. The neocortical circuit: themes and variations. *Nat. Neurosci.* 18, 170–181. <https://doi.org/10.1038/nn.3917>
- Hasenstaub, A., Sachdev, R.N.S., McCormick, D.A., 2007. State Changes Rapidly Modulate Cortical Neuronal Responsiveness. *J. Neurosci.* 27, 9607–9622. <https://doi.org/10.1523/JNEUROSCI.2184-07.2007>
- Hu, H., Gan, J., Jonas, P., 2014. Fast-spiking, parvalbumin+ GABAergic interneurons: From cellular design to microcircuit function. *Science* 345. <https://doi.org/10.1126/science.1255263>
- Joshi, S., 2021. Pupillometry: Arousal State or State of Mind? *Curr. Biol.* 31, R32–R34. <https://doi.org/10.1016/j.cub.2020.11.001>
- Joshi, S., Gold, J.I., 2020. Pupil Size as a Window on Neural Substrates of Cognition. *Trends Cogn. Sci.* 24, 466–480. <https://doi.org/10.1016/j.tics.2020.03.005>
- Joshi, S., Li, Y., Kalwani, R.M., Gold, J.I., 2016. Relationships between Pupil Diameter and Neuronal Activity in the Locus Coeruleus, Colliculi, and Cingulate Cortex. *Neuron* 89, 221–234. <https://doi.org/10.1016/j.neuron.2015.11.028>
- Kalappa, B.I., Anderson, C.T., Goldberg, J.M., Lippard, S.J., Tzounopoulos, T., 2015. AMPA receptor inhibition by synaptically released zinc. *Proc. Natl. Acad. Sci.* 112, 15749–15754. <https://doi.org/10.1073/pnas.1512296112>
- Kalappa, B.I., Tzounopoulos, T., 2017. Context-Dependent Modulation of Excitatory Synaptic Strength by Synaptically Released Zinc. *eNeuro* 4, ENEURO.0011-17.2017. <https://doi.org/10.1523/ENEURO.0011-17.2017>
- Kato, H.K., Asinof, S.K., Isaacson, J.S., 2017. Network-Level Control of Frequency Tuning in Auditory Cortex. *Neuron* 95, 412-423.e4. <https://doi.org/10.1016/j.neuron.2017.06.019>
- Keemink, S.W., Lowe, S.C., Pakan, J.M.P., Dylida, E., Rossum, M.C.W. van, Rochefort, N.L., 2018. FISSA: A neuropil decontamination toolbox for calcium imaging signals. *Sci. Rep.* 8, 3493. <https://doi.org/10.1038/s41598-018-21640-2>
- Kerlin, A.M., Andermann, M.L., Berezovskii, V.K., Reid, R.C., 2010. Broadly Tuned Response Properties of Diverse Inhibitory Neuron Subtypes in Mouse Visual Cortex. *Neuron* 67, 858–871. <https://doi.org/10.1016/j.neuron.2010.08.002>
- King, A.J., Walker, K.M., 2020. Listening in complex acoustic scenes. *Curr. Opin. Physiol.* 18, 63–72. <https://doi.org/10.1016/j.cophys.2020.09.001>

- Kouvaros, S., Kumar, M., Tzounopoulos, T., 2020. Synaptic Zinc Enhances Inhibition Mediated by Somatostatin, but not Parvalbumin, Cells in Mouse Auditory Cortex. *Cereb. Cortex* 30, 3895–3909. <https://doi.org/10.1093/cercor/bhaa005>
- Krall, R.F., Moutal, A., Phillips, M.B., Asraf, H., Johnson, J.W., Khanna, R., Hershinkel, M., Aizenman, E., Tzounopoulos, T., 2020. Synaptic zinc inhibition of NMDA receptors depends on the association of GluN2A with the zinc transporter ZnT1. *Sci. Adv.* 6, eabb1515. <https://doi.org/10.1126/sciadv.abb1515>
- Krall, R.F., Tzounopoulos, T., Aizenman, E., 2021. The Function and Regulation of Zinc in the Brain. *Neuroscience* 457, 235–258. <https://doi.org/10.1016/j.neuroscience.2021.01.010>
- Kuchinsky, S.E., Vaden, K.I., Ahlstrom, J.B., Cute, S.L., Humes, L.E., Dubno, J.R., Eckert, M.A., 2016. Task-Related Vigilance During Word Recognition in Noise for Older Adults with Hearing Loss. *Exp. Aging Res.* 42, 50–66. <https://doi.org/10.1080/0361073X.2016.1108712>
- Kumar, M., Xiong, S., Tzounopoulos, T., Anderson, C.T., 2019. Fine Control of Sound Frequency Tuning and Frequency Discrimination Acuity by Synaptic Zinc Signaling in Mouse Auditory Cortex. *J. Neurosci.* 39, 854–865. <https://doi.org/10.1523/JNEUROSCI.1339-18.2018>
- Lein, E.S. et al., 2007. Genome-wide atlas of gene expression in the adult mouse brain. *Nature* 445, 168–176. <https://doi.org/10.1038/nature05453>
- Leon, O., Roth, M., 2000. Zinc fingers: DNA binding and protein-protein interactions. *Biol. Res.* 33, 21–30. <https://doi.org/10.4067/s0716-97602000000100009>
- Liao, H.-I., Kidani, S., Yoneya, M., Kashino, M., Furukawa, S., 2016. Correspondences among pupillary dilation response, subjective salience of sounds, and loudness. *Psychon. Bull. Rev.* 23, 412–425. <https://doi.org/10.3758/s13423-015-0898-0>
- Liebe, T., Li, M., Colic, L., Munk, M.H.J., Sweeney-Reed, C.M., Woelfer, M., Kretschmar, M.A., Steiner, J., von Düring, F., Behnisch, G., Schott, B.H., Walter, M., 2018. Ketamine influences the locus coeruleus norepinephrine network, with a dependency on norepinephrine transporter genotype - a placebo controlled fMRI study. *NeuroImage Clin.* 20, 715–723. <https://doi.org/10.1016/j.nicl.2018.09.001>
- Lin, P.-A., Asinof, S.K., Edwards, N.J., Isaacson, J.S., 2019. Arousal regulates frequency tuning in primary auditory cortex. *Proc. Natl. Acad. Sci.* 116, 25304–25310. <https://doi.org/10.1073/pnas.1911383116>
- Linden, J.F., Liu, R.C., Sahani, M., Schreiner, C.E., Merzenich, M.M., 2003. Spectrotemporal Structure of Receptive Fields in Areas AI and AAF of Mouse Auditory Cortex. *J. Neurophysiol.* 90, 2660–2675. <https://doi.org/10.1152/jn.00751.2002>

- Litwin-Kumar, A., Rosenbaum, R., Doiron, B., 2016. Inhibitory stabilization and visual coding in cortical circuits with multiple interneuron subtypes. *J. Neurophysiol.* 115, 1399–1409. <https://doi.org/10.1152/jn.00732.2015>
- Lohse, M., Bajo, V.M., King, A.J., Willmore, B.D.B., 2020. Neural circuits underlying auditory contrast gain control and their perceptual implications. *Nat. Commun.* 11, 1–13. <https://doi.org/10.1038/s41467-019-14163-5>
- Mathis, A., Mamidanna, P., Cury, K.M., Abe, T., Murthy, V.N., Mathis, M.W., Bethge, M., 2018. DeepLabCut: markerless pose estimation of user-defined body parts with deep learning. *Nat. Neurosci.* 21, 1281–1289. <https://doi.org/10.1038/s41593-018-0209-y>
- McAllister, B.B., Dyck, R.H., 2017a. Zinc transporter 3 (ZnT3) and vesicular zinc in central nervous system function. *Neurosci. Biobehav. Rev.* 80, 329–350. <https://doi.org/10.1016/j.neubiorev.2017.06.006>
- McAllister, B.B., Dyck, R.H., 2017b. Sound Processing: A new role for zinc in the brain. *eLife* 6, e31816. <https://doi.org/10.7554/eLife.31816>
- McGinley, M.J., David, S.V., McCormick, D.A., 2015a. Cortical Membrane Potential Signature of Optimal States for Sensory Signal Detection. *Neuron* 87, 179–192. <https://doi.org/10.1016/j.neuron.2015.05.038>
- McGinley, M.J., Vinck, M., Reimer, J., Batista-Brito, R., Zaghera, E., Cadwell, C.R., Tolias, A.S., Cardin, J.A., McCormick, D.A., 2015b. Waking State: Rapid Variations Modulate Neural and Behavioral Responses. *Neuron* 87, 1143–1161. <https://doi.org/10.1016/j.neuron.2015.09.012>
- Mirman, D., 2016. Growth Curve Analysis and Visualization Using R. Chapman and Hall/CRC, Boca Raton. <https://doi.org/10.1201/9781315373218>
- Montes-Lourido, P., Kar, M., Kumbam, I., Sadagopan, S., 2021. Pupillometry as a reliable metric of auditory detection and discrimination across diverse stimulus paradigms in animal models. *Sci. Rep.* 11, 3108. <https://doi.org/10.1038/s41598-021-82340-y>
- Mridha, Z., de Gee, J.W., Shi, Y., Alkashgari, R., Williams, J., Suminski, A., Ward, M.P., Zhang, W., McGinley, M.J., 2021. Graded recruitment of pupil-linked neuromodulation by parametric stimulation of the vagus nerve. *Nat. Commun.* 12, 1539. <https://doi.org/10.1038/s41467-021-21730-2>
- Nakashima, A.S., Dyck, R.H., 2010. Dynamic, experience-dependent modulation of synaptic zinc within the excitatory synapses of the mouse barrel cortex. *Neuroscience* 170, 1015–1019. <https://doi.org/10.1016/j.neuroscience.2010.08.020>
- Nakashima, A.S., Dyck, R.H., 2009. Zinc and cortical plasticity. *Brain Res. Rev.* 59, 347–373. <https://doi.org/10.1016/j.brainresrev.2008.10.003>

- Nakashima, A.S., Dyck, R.H., 2008. Enhanced Plasticity in Zincergic, Cortical Circuits after Exposure to Enriched Environments. *J. Neurosci.* 28, 13995–13999. <https://doi.org/10.1523/JNEUROSCI.4645-08.2008>
- Nath, T., Mathis, A., Chen, A.C., Patel, A., Bethge, M., Mathis, M.W., 2019. Using DeepLabCut for 3D markerless pose estimation across species and behaviors. *Nat. Protoc.* 14, 2152–2176. <https://doi.org/10.1038/s41596-019-0176-0>
- Olsen, S.R., Bhandawat, V., Wilson, R.I., 2010. Divisive Normalization in Olfactory Population Codes. *Neuron* 66, 287–299. <https://doi.org/10.1016/j.neuron.2010.04.009>
- Pachitariu, M., Stringer, C., Dipoppa, M., Schröder, S., Rossi, L.F., Dagleish, H., Carandini, M., Harris, K.D., 2017. Suite2p: beyond 10,000 neurons with standard two-photon microscopy. *bioRxiv*. <https://doi.org/10.1101/061507>
- Palmiter, R.D., Cole, T.B., Quaife, C.J., Findley, S.D., 1996. ZnT-3, a putative transporter of zinc into synaptic vesicles. *Proc. Natl. Acad. Sci.* 93, 14934–14939. <https://doi.org/10.1073/pnas.93.25.14934>
- Pan, E., Zhang, X., Huang, Z., Krezel, A., Zhao, M., Tinberg, C.E., Lippard, S.J., McNamara, J.O., 2011. Vesicular Zinc Promotes Presynaptic and Inhibits Postsynaptic Long-Term Potentiation of Mossy Fiber-CA3 Synapse. *Neuron* 71, 1116–1126. <https://doi.org/10.1016/j.neuron.2011.07.019>
- Paoletti, P., Ascher, P., Neyton, J., 1997. High-Affinity Zinc Inhibition of NMDA NR1–NR2A Receptors. *J. Neurosci.* 17, 5711–5725. <https://doi.org/10.1523/JNEUROSCI.17-15-05711.1997>
- Paoletti, P., Vergnano, A.M., Barbour, B., Casado, M., 2009. Zinc at glutamatergic synapses. *Neuroscience, Protein trafficking, targeting, and interaction at the glutamate synapse* 158, 126–136. <https://doi.org/10.1016/j.neuroscience.2008.01.061>
- Pennington, J.R., David, S.V., 2020. Complementary Effects of Adaptation and Gain Control on Sound Encoding in Primary Auditory Cortex. *eNeuro* 7. <https://doi.org/10.1523/ENEURO.0205-20.2020>
- Perez-Rosello, T., Anderson, C.T., Ling, C., Lippard, S.J., Tzounopoulos, T., 2015. Tonic zinc inhibits spontaneous firing in dorsal cochlear nucleus principal neurons by enhancing glycinergic neurotransmission. *Neurobiol. Dis., Metals and Neurodegeneration* 81, 14–19. <https://doi.org/10.1016/j.nbd.2015.03.012>
- Perez-Rosello, T., Anderson, C.T., Schopfer, F.J., Zhao, Y., Gilad, D., Salvatore, S.R., Freeman, B.A., Hershfinkel, M., Aizenman, E., Tzounopoulos, T., 2013. Synaptic Zn²⁺ inhibits neurotransmitter release by promoting endocannabinoid synthesis. *J. Neurosci. Off. J. Soc. Neurosci.* 33, 9259–9272. <https://doi.org/10.1523/JNEUROSCI.0237-13.2013>

- Pinheiro, J.C., Bates, D.M. (Eds.), 2000. Extending the Basic Linear Mixed-Effects Model, in: *Mixed-Effects Models in S and S-PLUS, Statistics and Computing*. Springer, New York, NY, pp. 201–270. https://doi.org/10.1007/0-387-22747-4_5
- Pnevmatikakis, E.A., Giovannucci, A., 2017. NoRMCorre: An online algorithm for piecewise rigid motion correction of calcium imaging data. *J. Neurosci. Methods* 291, 83–94. <https://doi.org/10.1016/j.jneumeth.2017.07.031>
- Prasad, A.S., Halsted, J.A., Nadimi, M., 1961. Syndrome of iron deficiency anemia, hepatosplenomegaly, hypogonadism, dwarfism and geophagia. *Am. J. Med.* 31, 532–546. [https://doi.org/10.1016/0002-9343\(61\)90137-1](https://doi.org/10.1016/0002-9343(61)90137-1)
- Privitera, M., Ferrari, K.D., von Ziegler, L.M., Sturman, O., Duss, S.N., Floriou-Servou, A., Germain, P.-L., Vermeiren, Y., Wyss, M.T., De Deyn, P.P., Weber, B., Bohacek, J., 2020. A complete pupillometry toolbox for real-time monitoring of locus coeruleus activity in rodents. *Nat. Protoc.* 15, 2301–2320. <https://doi.org/10.1038/s41596-020-0324-6>
- Rabinowitz, N.C., Willmore, B.D.B., King, A.J., Schnupp, J.W.H., 2013. Constructing Noise-Invariant Representations of Sound in the Auditory Pathway. *PLOS Biol.* 11, e1001710. <https://doi.org/10.1371/journal.pbio.1001710>
- Rabinowitz, N.C., Willmore, B.D.B., Schnupp, J.W.H., King, A.J., 2012. Spectrotemporal Contrast Kernels for Neurons in Primary Auditory Cortex. *J. Neurosci.* 32, 11271–11284. <https://doi.org/10.1523/JNEUROSCI.1715-12.2012>
- Rabinowitz, N.C., Willmore, B.D.B., Schnupp, J.W.H., King, A.J., 2011. Contrast Gain Control in Auditory Cortex. *Neuron* 70, 1178–1191. <https://doi.org/10.1016/j.neuron.2011.04.030>
- Reimer, J., Froudarakis, E., Cadwell, C.R., Yatsenko, D., Denfield, G.H., Tolias, A.S., 2014. Pupil Fluctuations Track Fast Switching of Cortical States during Quiet Wakefulness. *Neuron* 84, 355–362. <https://doi.org/10.1016/j.neuron.2014.09.033>
- Reimer, J., McGinley, M.J., Liu, Y., Rodenkirch, C., Wang, Q., McCormick, D.A., Tolias, A.S., 2016. Pupil fluctuations track rapid changes in adrenergic and cholinergic activity in cortex. *Nat. Commun.* 7, 13289. <https://doi.org/10.1038/ncomms13289>
- Reinhold, K., Lien, A.D., Scanziani, M., 2015. Distinct recurrent versus afferent dynamics in cortical visual processing. *Nat. Neurosci.* 18, 1789–1797. <https://doi.org/10.1038/nn.4153>
- Reynolds, J.H., Heeger, D.J., 2009. The Normalization Model of Attention. *Neuron* 61, 168–185. <https://doi.org/10.1016/j.neuron.2009.01.002>
- Robinson, B.L., McAlpine, D., 2009. Gain control mechanisms in the auditory pathway. *Curr. Opin. Neurobiol., Sensory systems* 19, 402–407. <https://doi.org/10.1016/j.conb.2009.07.006>

- Romero, S., Hight, A.E., Clayton, K.K., Resnik, J., Williamson, R.S., Hancock, K.E., Polley, D.B., 2019. Cellular and Widefield Imaging of Sound Frequency Organization in Primary and Higher Order Fields of the Mouse Auditory Cortex. *Cereb. Cortex*. <https://doi.org/10.1093/cercor/bhz190>
- Sachs, M.B., Abbas, P.J., 1974. Rate versus level functions for auditory-nerve fibers in cats: tone-burst stimuli. *J. Acoust. Soc. Am.* 56, 1835–1847. <https://doi.org/10.1121/1.1903521>
- Sadeh, S., Silver, R.A., Mrsic-Flogel, T.D., Muir, D.R., 2017. Assessing the Role of Inhibition in Stabilizing Neocortical Networks Requires Large-Scale Perturbation of the Inhibitory Population. *J. Neurosci.* 37, 12050–12067. <https://doi.org/10.1523/JNEUROSCI.0963-17.2017>
- Saderi, D., Schwartz, Z.P., Heller, C.R., Pennington, J.R., David, S.V., 2021. Dissociation of task engagement and arousal effects in auditory cortex and midbrain. *eLife* 10, e60153. <https://doi.org/10.7554/eLife.60153>
- Sanzeni, A., Akitake, B., Goldbach, H.C., Leedy, C.E., Brunel, N., Histed, M.H., 2020. Inhibition stabilization is a widespread property of cortical networks. *eLife* 9, e54875. <https://doi.org/10.7554/eLife.54875>
- Saper, C.B., Chou, T.C., Scammell, T.E., 2001. The sleep switch: hypothalamic control of sleep and wakefulness. *Trends Neurosci.* 24, 726–731. [https://doi.org/10.1016/S0166-2236\(00\)02002-6](https://doi.org/10.1016/S0166-2236(00)02002-6)
- Sara, S.J., 2009. The locus coeruleus and noradrenergic modulation of cognition. *Nat. Rev. Neurosci.* 10, 211–223. <https://doi.org/10.1038/nrn2573>
- Satpute, A.B., Kragel, P.A., Barrett, L.F., Wager, T.D., Bianciardi, M., 2019. Deconstructing arousal into wakeful, autonomic and affective varieties. *Neurosci. Lett., Functional Neuroimaging of the Emotional Brain* 693, 19–28. <https://doi.org/10.1016/j.neulet.2018.01.042>
- Schwartz, O., Simoncelli, E.P., 2001. Natural signal statistics and sensory gain control. *Nat. Neurosci.* 4, 819. <https://doi.org/10.1038/90526>
- Schwartz, Z.P., Buran, B.N., David, S.V., 2019. Pupil-associated states modulate excitability but not stimulus selectivity in primary auditory cortex. *J. Neurophysiol.* 123, 191–208. <https://doi.org/10.1152/jn.00595.2019>
- Steriade, M., Timofeev, I., Grenier, F., 2001. Natural Waking and Sleep States: A View From Inside Neocortical Neurons. *J. Neurophysiol.* 85, 1969–1985. <https://doi.org/10.1152/jn.2001.85.5.1969>

- Suter, B.A., O'Connor, T., Iyer, V., Petreanu, L.T., Hooks, B.M., Kiritani, T., Svoboda, K., Shepherd, G.M.G., 2010. Ephus: multipurpose data acquisition software for neuroscience experiments. *Front. Neural Circuits* 4, 100. <https://doi.org/10.3389/fncir.2010.00100>
- van der Wel, P., van Steenbergen, H., 2018. Pupil dilation as an index of effort in cognitive control tasks: A review. *Psychon. Bull. Rev.* 25, 2005–2015. <https://doi.org/10.3758/s13423-018-1432-y>
- Vergnano, A.M., Rebola, N., Savtchenko, L.P., Pinheiro, P.S., Casado, M., Kieffer, B.L., Rusakov, D.A., Mulle, C., Paoletti, P., 2014. Zinc Dynamics and Action at Excitatory Synapses. *Neuron* 82, 1101–1114. <https://doi.org/10.1016/j.neuron.2014.04.034>
- Vinck, M., Batista-Brito, R., Knoblich, U., Cardin, J.A., 2015. Arousal and locomotion make distinct contributions to cortical activity patterns and visual encoding. *Neuron* 86, 740–754. <https://doi.org/10.1016/j.neuron.2015.03.028>
- Vogler, N.W., Betti, V.M., Goldberg, J.M., Tzounopoulos, T., 2020. Mechanisms Underlying Long-Term Synaptic Zinc Plasticity at Mouse Dorsal Cochlear Nucleus Glutamatergic Synapses. *J. Neurosci.* <https://doi.org/10.1523/JNEUROSCI.0175-20.2020>
- Wang, Z., Li, J.-Y., Dahlström, A., Danscher, G., 2001. Zinc-enriched GABAergic terminals in mouse spinal cord. *Brain Res.* 921, 165–172. [https://doi.org/10.1016/S0006-8993\(01\)03114-6](https://doi.org/10.1016/S0006-8993(01)03114-6)
- Warda, S., Pandey, S., 2020. Pupil tracks statistical regularities: Behavioral and neural implications. *J. Integr. Neurosci.* 19, 729–731. <https://doi.org/10.31083/J.JIN.2020.04.331>
- Wasserman, L., 2004. Hypothesis Testing and p-values, in: *All of Statistics: A Concise Course in Statistical Inference*. Springer, pp. 161–163.
- Watanabe, T., Thomas, E.C., Clark, L.F., Kiang, N., 1965. Discharge patterns of single fibers in the cat's auditory nerve. MIT Press 165.
- Wehr, M., Zador, A.M., 2003. Balanced inhibition underlies tuning and sharpens spike timing in auditory cortex. *Nature* 426, 442–446. <https://doi.org/10.1038/nature02116>
- Wen, B., Wang, G.I., Dean, I., Delgutte, B., 2012. Time course of dynamic range adaptation in the auditory nerve. *J. Neurophysiol.* 108, 69–82. <https://doi.org/10.1152/jn.00055.2012>
- Wen, B., Wang, G.I., Dean, I., Delgutte, B., 2009. Dynamic Range Adaptation to Sound Level Statistics in the Auditory Nerve. *J. Neurosci.* 29, 13797–13808. <https://doi.org/10.1523/JNEUROSCI.5610-08.2009>
- Wilkinson, G.N., Rogers, C.E., 1973. Symbolic Description of Factorial Models for Analysis of Variance. *J. R. Stat. Soc. Ser. C Appl. Stat.* 22, 392–399. <https://doi.org/10.2307/2346786>

- Willmore, B.D.B., Cooke, J.E., King, A.J., 2014. Hearing in noisy environments: noise invariance and contrast gain control. *J. Physiol.* 592, 3371–3381. <https://doi.org/10.1113/jphysiol.2014.274886>
- Wilson, N.R., Runyan, C.A., Wang, F.L., Sur, M., 2012. Division and subtraction by distinct cortical inhibitory networks in vivo. *Nature* 488, 343–348. <https://doi.org/10.1038/nature11347>
- Winn, M.B., Edwards, J.R., Litovsky, R.Y., 2015. The Impact of Auditory Spectral Resolution on Listening Effort Revealed by Pupil Dilation. *Ear Hear.* 36, e153. <https://doi.org/10.1097/AUD.0000000000000145>
- Yerkes, R.M., Dodson, J.D., 1908. The relation of strength of stimulus to rapidity of habit-formation. *J. Comp. Neurol. Psychol.* 18, 459–482.
- Zekveld, A.A., Heslenfeld, D.J., Johnsrude, I.S., Versfeld, N.J., Kramer, S.E., 2014. The eye as a window to the listening brain: Neural correlates of pupil size as a measure of cognitive listening load. *NeuroImage* 101, 76–86. <https://doi.org/10.1016/j.neuroimage.2014.06.069>
- Zekveld, A.A., Koelewijn, T., Kramer, S.E., 2018. The Pupil Dilation Response to Auditory Stimuli: Current State of Knowledge. *Trends Hear.* 22, 2331216518777174. <https://doi.org/10.1177/2331216518777174>
- Zekveld, A.A., Kramer, S.E., Festen, J.M., 2011. Cognitive load during speech perception in noise: the influence of age, hearing loss, and cognition on the pupil response. *Ear Hear.* 32, 498–510. <https://doi.org/10.1097/AUD.0b013e31820512bb>
- Zekveld, A.A., Kramer, S.E., Festen, J.M., 2010. Pupil response as an indication of effortful listening: the influence of sentence intelligibility. *Ear Hear.* 31, 480–490. <https://doi.org/10.1097/AUD.0b013e3181d4f251>